

ACTIVE NITROGEN DIAGNOSTICS AND DETECTION  
OF POLYNUCLEAR AROMATIC HYDROCARBONS BY  
ACTIVE NITROGEN-INDUCED CHEMILUMINESCENCE

By

HEATHER ANDREWS JURGENSEN

A DISSERTATION PRESENTED TO THE GRADUATE SCHOOL  
OF THE UNIVERSITY OF FLORIDA IN  
PARTIAL FULFILLMENT OF THE REQUIREMENTS  
FOR THE DEGREE OF DOCTOR OF PHILOSOPHY

UNIVERSITY OF FLORIDA

1983

I would like to dedicate this dissertation to the people  
dearest to me: my husband, Art, my children, Michael and  
Melanie, and my mother Ruth.

#### ACKNOWLEDGEMENTS

The author wishes to express her gratitude to Dr. James D. Winefordner for his continued guidance, support, encouragement and friendship. She would also like to thank Juan P. Frias for his invaluable assistance in the single channel studies and Tiing Yu for his help in the multichannel studies.

Abstract of Dissertation Presented to the Graduate  
Council of the University of Florida in Partial  
Fulfillment of the Requirements for the Degree  
of Doctor of Philosophy

ACTIVE NITROGEN DIAGNOSTICS AND DETECTION  
OF POLYNUCLEAR AROMATIC HYDROCARBONS BY  
ACTIVE NITROGEN-INDUCED CHEMILUMINESCENCE

By

Heather Andrews Jurgensen

December, 1983

Chairman: James D. Winefordner  
Major Department: Chemistry

A gentle molecular excitation source based upon energy transfer from metastable nitrogen molecules in a second positive system of nitrogen afterglow is presented. A dielectric discharge through flowing nitrogen is shown to generate a large population of metastable nitrogen molecules and very few nitrogen atoms. The dependence of emission intensity from the transition  $N_2(C^3\Pi_u) \rightarrow N_2(B^3\Pi_g)$  in the afterglow on voltage, distance from the dielectric discharge active nitrogen generator, and nitrogen flow rate is given. The average electronic temperature of the discharge and afterglow is found to be  $3280 \pm 132K$  and  $3090 \pm 70K$ , respectively. The effect of adding argon or helium to the afterglow is described. Chemiluminescence spectra of benzene, iodine, naphthalene and anthracene are presented. Limits of detection (LOD's) for numerous polynuclear aromatic hydrocarbons (PAH's) and hydrocarbons are listed for single and multichannel detection. Most LOD's with single channel detection are in the tenths of a nanogram range. Multichannel detection limits are 100 to 500 times worse. Results of a hydrocarbon and a PAH mixture separated on a gas chromatographic column with multichannel detection are presented.

# TABLE OF CONTENTS

	<u>Page</u>
ACKNOWLEDGEMENTS .....	iii
ABSTRACT .....	iv
CHAPTER	
I INTRODUCTION TO CHEMILUMINESCENCE .....	1
Introduction .....	1
Measurements in the Liquid Phase .....	2
Metals .....	4
Organic Compounds .....	4
Measurements in the Gas Phase .....	4
Nitrogen Oxides .....	7
Ozone .....	7
Sulfur Compounds .....	7
Hydrocarbons in Active Nitrogen .....	9
II ACTIVE NITROGEN SYSTEMS .....	10
Introduction .....	10
The First Positive System of $N_2$	
$B_2 (B^3\Pi_g) \rightarrow N_2 (A^3\Sigma_u^+)$ .....	11
The Pink Afterglow .....	19
The "Y" Bands $N_2 (B'^3\Sigma_u) \rightarrow N_2 (B^3\Sigma_g)$ .....	20
The Vegard-Kaplan System	
$N_2 (A^3\Sigma_u^+) \rightarrow N_2 (X^1\Sigma_g^+)$ .....	20
The Lyman-Birge-Hopfield System of $N_2$	
$N_2 (a^1\Pi_g) \rightarrow N_2 (X^1\Sigma_g^+)$ .....	21
The Second Positive System of $N_2$	
$N_2 (C^3\Pi_u) \rightarrow N_2 (B^3\Pi_g)$ .....	22
The Goldstein-Kaplan System of $N_2$	
$N_2 (b^1\Pi_u) \rightarrow N_2 (B^3\Pi_g)$ .....	30
The Birge-Hopfield Systems of $N_2$	
$N_2 (b^1\Sigma_u) \rightarrow N_2 (X^1\Sigma_g^+)$ ; $N_2 (b'^1\Sigma_u^+) \rightarrow N_2 (X^1\Sigma_g^+)$ ..	30
The First Negative System of $N^+$	
$N_2^+ (B^2\Sigma_u^+) \rightarrow N_2^+ (X^2\Sigma_g^+)$ .....	30
Emission from Atomic Nitrogen	
$N (^2D) \rightarrow N (^4S)$ ; $N (^2P) \rightarrow N (^4S)$ .....	31
Effect of Additive Gases .....	32
Analytical Studies with Active Nitrogen .....	32

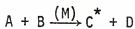
	<u>Page</u>
CHAPTER	
III INSTRUMENT DESIGN .....	49
Introduction .....	49
Active Nitrogen Generator .....	50
Light Trap .....	53
Reaction Chamber .....	56
Vacuum System .....	58
Emission Detection .....	58
Single Channel Detection .....	59
Multichannel Detection .....	60
IV METHODS OF ANALYSIS .....	65
Diagnostic Methods .....	65
Discharge Emission .....	65
Afterglow Emission .....	65
Temperature Determination .....	66
Nitrogen Atom Detection .....	68
Metastable Concentration .....	70
Effect of Additive Gases .....	71
Detection Methods .....	71
Benzene, Iodine and Naphthalene .....	71
Polynuclear Aromatic Hydrocarbons .....	72
Introduction .....	72
Single channel detection .....	73
Multichannel detection .....	75
V RESULTS AND DISCUSSION .....	78
Dielectric Discharge .....	78
Discharge Emission .....	78
Nitrogen Afterglow .....	81
Temperature Results .....	90
Estimate of Metastable Concentration .....	94
NO Titration .....	95
Molecular Species .....	100
Polynuclear Aromatic Hydrocarbons .....	103
VI CONCLUSIONS .....	125
REFERENCES .....	129
BIOGRAPHICAL SKETCH .....	138

CHAPTER I  
INTRODUCTION TO CHEMILUMINESCENCE

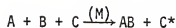
Introduction

Chemiluminescence is defined as the emission of light from chemical reactions (1). In a chemiluminescence reaction, a reaction intermediate or product is formed in an electronically excited state, and radiative decay of the excited state is the source of light (2). If the emission is from an excited singlet state, the radiative process is identical to fluorescence. If the excited state is a triplet, the emission is phosphorescence (3). In order for chemiluminescence to occur, three conditions must be fulfilled: (1) sufficient energy must be produced in the reaction to populate an excited energy state; (2) the reaction mechanism must favor the production of the excited state; (3) and the excited state formed must be able to emit a photon or transfer its energy to another molecule that can emit (4). Thus, chemiluminescence is a special case of chemiexcitation (5). Chemiexcitation is unusual since most chemical reactions follow a ground-state potential energy surface (6). Any excess energy is released as vibrational excitation of ground-state products and is detected as heat.

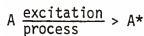
Direct chemiluminescence is defined as follows (7):



where M represents a third body and \* indicates an excited state. An example of indirect chemiluminescence may be written as (7):



Chemiluminescence can also result from metastable energy transfer (5):



The efficiency of chemiluminescence is given by the expression (4)

$$\phi_{CL} = \frac{(\text{number (or rate) of molecules going to the excited state})}{(\text{number (or rate) of molecules reacting})} \cdot \left( \frac{\text{number of photons emitted}}{\text{number of molecules in the excited state}} \right)$$

The first term represents the efficiency of excited state production, and the second term is the efficiency of emission.

The intensity of chemiluminescence ( $I_{CL}$ ) is related to the concentration of the analyte (c) as follows:

$$I_{CL}(t) \left( \frac{\text{photons}}{s} \right) = \phi_{CL} \frac{\text{photons emitted}}{\text{molecules reacting}} \cdot \frac{dc(t)}{dt} \frac{\text{molecules reacting}}{s}$$

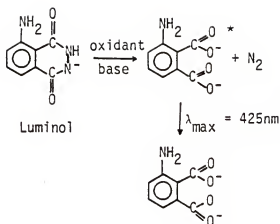
where  $dc(t)/dt$  is the reaction rate for the reactant producing an electronically excited state.

#### Measurements in the Liquid Phase

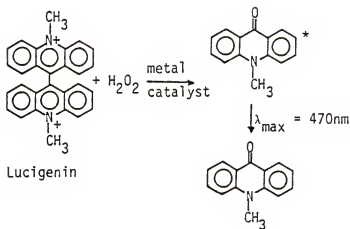
Most analytical applications of chemiluminescence reactions in the liquid phase involve luminol, lucigenin, and inorganic siloxenes (4).

Albrecht (8) was the first to report the chemiluminescence of luminol in 1928. The chemiluminescence reaction involves the oxidation of luminol (usually by  $H_2O_2$ ) and often occurs in the presence of a catalyst (such as  $Fe(CN)_6^{3-}$ ,  $Cu(II)$  and  $Co(II)$ ) (4). The light emission matches the fluorescence of the aminophthalate oxidation product:





The oxidation of lucigenin (N,N'-dimethyldiacridinium) by H<sub>2</sub>O<sub>2</sub> in basic solution is another widely used chemiluminescence reaction (9). The resulting blue-green emission is believed to be from N-methylacridone, and the quantum yield of the process is approximately 0.01 - 0.02 (10,11).



Siloxene and its derivatives are highly polymerized solids composed of silicon-6-rings (12,13). The siloxene unit is Si<sub>6</sub>H<sub>6</sub>O<sub>3</sub>. The Si-H and Si-Si bonds in siloxene are very reactive. Hence, siloxene can be oxidized rapidly by hydrogen peroxide or permanganate in acid solution

to produce intense chemiluminescence. The oxidizing agent and degree of oxidation determine the chemiluminescence color.

### Metals

Many chemiluminescence reactions are catalyzed by several metal ions resulting in an increase in intensity and duration of the chemiluminescence (14). Measurements of metal catalysts are performed at the optimal pH and concentration of each component in the reagent solution. Calibration curves consist of plots of chemiluminescence emission as a function of the metal catalyst concentration. Metals that can be determined by chemiluminescence are listed in Table 1-1 as well as the corresponding chemiluminescence system, action and limit of detection. The "action" entry is defined as follows: "Inh" refers to those metals which have been measured by determining their inhibiting effect on a chemiluminescence system catalyzed by some other metal ion; "Cat" indicates that the chemiluminescence reaction catalyzed by a metal ion has been activated by organic substances, e.g., a mixture of o-phenanthroline and sodium citrate.

### Organic Compounds

Measurements of organic compounds can be achieved by monitoring the effects of these compounds on chemiluminescence reactions. Some of the organic compounds that can be determined by this method are listed in Table 1-2. A substance is labelled "Inh" if it inhibits the chemiluminescence reaction and "Cat" if the substance catalyzes the reaction.

### Measurements in the Gas Phase

Chemiluminescence methods for measurements in the gas phase were developed primarily because of the need for determining atmospheric

Table 1-1 Analysis of Metals by Liquid Chemiluminescence

Metal	Date	System	Action	Limit of Detection	Reference
Ag	1968	Lucigenin-H <sub>2</sub> O <sub>2</sub>	Cat	0.1μg	15
As(As <sup>+3</sup> )	1973	Luminol-I <sub>2</sub>		2x10 <sup>-7</sup> M	16
Bi	1971	Lucigenin-H <sub>2</sub> O <sub>2</sub>	Cat	5μg	17
Ce	1962	Luminol-H <sub>2</sub> O <sub>2</sub> -Cu <sup>+2</sup>	Inh	0.1μg	18
Co	1963	Luminol-H <sub>2</sub> O <sub>2</sub>	Cat	2ng	19
Cr(Cr <sup>+3</sup> )	1972	Luminol-H <sub>2</sub> O <sub>2</sub>	Cat	30pg	20
Cu	1962	Luminol-H <sub>2</sub> O <sub>2</sub>	Cat	0.03μg	21
Fe	1970	Luminol-H <sub>2</sub> O <sub>2</sub> - diethylene triamine	Cat	0.2ng	22
Fe(Fe <sup>+2</sup> )	1972	Luminol-O <sub>2</sub>	Cat	5pg	23
Hg	1971	Luminol-H <sub>2</sub> O <sub>2</sub>	Cat	0.2μg	24
Mn	1971	Lucigenin-H <sub>2</sub> O <sub>2</sub>	Cat	1μg	25
Mn	1971	Lucigenin-H <sub>2</sub> O <sub>2</sub> - org. amine	Cat	0.1μg	26
Mn	1969	Luminol-H <sub>2</sub> O <sub>2</sub> - activator	Cat	80pg	27
Os(OsO <sub>4</sub> )	1963	Lucigenin-H <sub>2</sub> O <sub>2</sub>	Cat	1μg	28
Pb	1970	Lucigenin-H <sub>2</sub> O <sub>2</sub>	Cat	0.5μg	29
Th	1969	Luminol-H <sub>2</sub> O <sub>2</sub> -Cat	Inh	1μg	30
Tl	1971	Lucigenin-H <sub>2</sub> O <sub>2</sub>	Cat	-	31
V	1965	Luminol-H <sub>2</sub> O <sub>2</sub> - [Co(NH <sub>3</sub> ) <sub>4</sub> (NO <sub>2</sub> ) <sub>2</sub> ]Cl	Inh	0.4μg	32
Zr	1968	Luminol-H <sub>2</sub> O <sub>2</sub> -Cu <sup>+2</sup>	Inh	-	33

Table 1-2 Analysis of Organic Species by Liquid Chemiluminescence

Compound	Date	System	Action	Limit of Detection	Reference
Amino Acids:					
Glycine	1965	Luminol-H <sub>2</sub> O <sub>2</sub>	Cat	( $\mu$ g) 150	34
Cysteine	1965	Luminol-I <sub>2</sub>	Inh	0.01	35
Hematin Compounds:					
Ferritin	1965	Luminol-H <sub>2</sub> O <sub>2</sub>	Cat	2	36
Cytochromes	1965	Luminol-H <sub>2</sub> O <sub>2</sub>	Cat	0.025	36
Myoglobin	1965	Luminol-H <sub>2</sub> O <sub>2</sub>	Cat	0.0001	36
Hemoglobin	1965	Luminol-H <sub>2</sub> O <sub>2</sub>	Cat	0.00006	36
Catalase	1965	Luminol-H <sub>2</sub> O <sub>2</sub>	Cat	0.0001	36
Organic Phosphorus Compounds:					
Nerve gases, type Sarin	1957	Luminol-sodium perborate-Na <sub>3</sub> PO <sub>4</sub>		0.5	37
Insecticides, type Isopestox	1958	Luminol-H <sub>2</sub> O <sub>2</sub>	Cat	200	38
	1969		Cat		
Tabun (nerve gas)	1965	Lucigenin-sodium perborate	Cat	100	39
Benzene derivatives:					
Phenol	1964	Luminol-H <sub>2</sub> O <sub>2</sub> -Cu <sup>+2</sup> -NH <sub>4</sub> OH	Inh	400	40
Naphthols:					
1-nitroso-2-naphthol	1971	Luminol-H <sub>2</sub> O <sub>2</sub> -Co <sup>+2</sup>	Inh	20	41

pollutants (11). Several chemiluminescence methods are already in practical use. These methods are discussed in the following sections and are listed in Table 1-3.

### Nitrogen Oxides

Nitrogen oxides ( $\text{NO}_x$ ) are major pollutants produced by cars, trucks, and fossil fuel plants (5). The chemiluminescence system most frequently used to detect nitric oxide (NO) is the reaction between nitric oxide and ozone ( $\text{O}_3$ ) (5). To determine total nitrogen oxides, nitrogen dioxide ( $\text{NO}_2$ ) must be dissociated thermally to NO prior to detection (5,7). To prevent interference from ammonia, it should be removed from the analyte gas stream by oxidation with dichromate.

### Ozone

Nederbragt et al. (53) developed a homogeneous gas-phase chemiluminescence technique for the determination of ozone. This technique utilized the reaction between ozone and ethylene which yields chemiluminescence between 300-600nm. The linear dynamic range is 0.003-30ppm and no interferences have been reported (45). Chemiluminescence ozone monitors based on this technique are available commercially (54).

### Sulfur Compounds

The atmosphere contains a variety of sulfur compounds including  $\text{SO}_2$ ,  $\text{H}_2\text{S}$ , organic sulfides and mercaptans, sulfuric acid, and sulfates (7). The only chemiluminescence method now being applied is a flame method which detects gas-phase sulfur compounds as a class. Volatile sulfur compounds are burned in a hydrogen-rich flame, resulting in intense blue chemiluminescence (7). The emitting molecule is  $\text{S}_2$  ( $\text{B}^3\Sigma_u^-$ ) resulting from the recombination of sulfur

Table 1-3 Gas-Phase Chemiluminescence

Compound	Date	Chemiluminescence Reaction System	Limit of Detection	Reference
Sulfur Compounds	1971	$\text{SO}_2 + 2\text{H}_2 \rightarrow \text{S} + 2\text{H}_2\text{O}$ $\text{S} + \text{S} \rightarrow \text{S}_2^*$ $\text{S}_2^* \rightarrow \text{S}_2 + h\nu \text{ (300-425nm)}$	< 1 ppm quantities	42,43
Phosphorus Compounds	1966	burned in $\text{H}_2$ rich flame	< 1 ppm quantities	42
Sulfur Compounds	1969	$\text{O}\cdot + \text{O}\cdot + \text{SO}_2 \rightarrow \text{O}_2 + \text{SO}_2^*$ $\text{SO}_2^* \rightarrow \text{SO}_2 + h\nu \text{ (}\lambda_{\text{max}}=380\text{nm)}$	1 ppm	43,44
Ozone	1971	$\text{O}_3 + \text{C}_2\text{H}_4, h\nu \text{ (300-600nm)}^\dagger$	3 ppb	45,46
Nitrogen Compounds	1972	$\text{NO} + \text{O}_3 \rightarrow \text{NO}_2^* + \text{O}_2$ $\text{NO}_2^* \rightarrow \text{NO}_2 + h\nu \text{ (600-2800nm)}$	1 ppb	4,45 47-50
	1972	$\text{NO} + \text{O}\cdot \rightarrow \text{NO}_2^*$ $\text{NO}_2^* \rightarrow \text{NO}_2 + h\nu \text{ (450-1800nm)}$ $\text{NO}_2 + \text{O}\cdot \rightarrow \text{NO} + \text{O}_2$	< 1 ppb	48
	1972	$\text{H}\cdot + \text{NO}_2 \rightarrow \text{NO} + \cdot\text{OH}$ $\text{H}\cdot + \text{NO} + \text{M} \rightarrow \text{HNO}^* + \text{M}$ $\text{HNO}^* \rightarrow \text{HNO} + h\nu \text{ (650-760nm)}$	0.1 ppm	51
Na	1939	$\text{Na} + \text{Cl}_2 \rightarrow \text{NaCl} + \text{Cl}\cdot$ $\text{Cl}\cdot + \text{Na}_2 \rightarrow \text{NaCl} + \text{Na}^*$ (sodium chlorine cool flame)		52

<sup>†</sup>The chemiluminescing product is unknown, but may be an excited aldehyde linkage (45).

atoms. Detection limits are in the ppm range (54). Flame photometric detector-gas chromatographs are available commercially (54).

#### Hydrocarbons in Active Nitrogen

Very little research has been conducted to explore the chemiluminescence reactions of hydrocarbons in the gas phase. This research effort studies the chemiluminescence of organic molecules in an active nitrogen environment. This work is the first to report the feasibility of a second positive active nitrogen afterglow as a molecular excitation source.

Previous active nitrogen research has been confined primarily to first positive system nitrogen afterglows. Analytical studies employing active nitrogen are reviewed in Chapter II. Because the utilization of a second positive system is a new research topic, several diagnostic experiments are presented in this dissertation. It is also shown that the energy available,  $\sim 6\text{eV}$  is enough to excite a wide range of molecules without fragmentation. Limits of detection are reported for several small hydrocarbons as well as numerous polyaromatic compounds.

This dissertation examines the feasibility of using active nitrogen as a chemiluminescence detector for gas chromatography of organic species. Single channel and multichannel detection of the analyte luminescence are explored. Single channel detection is shown to be more sensitive, but multichannel detection offers greater selectivity.

## CHAPTER II ACTIVE NITROGEN SYSTEMS

### Introduction

Evidence that a chemically active form of nitrogen ( $N_2$ ) could be produced by passing an electric discharge through nitrogen ( $N_2$ ) was first obtained in early studies in electrochemistry (55). In 1792, Lavoisier discovered that various oxides of nitrogen could be produced when a spark passed through air (56). In 1869, Berthelot reported that sparking a mixture of nitrogen and hydrocarbons produced hydrogen cyanide (57,58). The persistent luminescence in nitrogen at low pressures following an electrical discharge was first reported by Warburg in 1865 (59). Later, Warburg found that when he subjected air to an electric discharge in a static system, it emitted a bright, peach-colored glow that changed to a rich yellow which persisted for several seconds after the discharge was discontinued (60). In 1900, E.P. Lewis performed the first systematic study of the nitrogen afterglow (61-63) and in 1911 the Hon. R.J. Strutt (later, the third Lord Rayleigh) labelled this glowing gas "active nitrogen." Lord Rayleigh clearly showed in a series of outstanding papers, that a chemically active modification of nitrogen was present in the afterglow (64-67). Strutt felt that many of the properties of active nitrogen were attributable to the presence of atomic nitrogen. His theory was not accepted widely until it was incorporated into Spomer's explanation of the afterglow in 1925 (68). Quantitative studies of the rates of nitrogen atom reactions have been performed successfully



only recently. Despite the vast number of investigations, the fundamental mechanisms governing the nitrogen afterglow are not yet elucidated completely (64,69-70), although Mitra (1965) (71) and Wright and Winkler (1968) (55) have summarized the majority of their research concerning active nitrogen.

The states and transitions of  $N_2$  and  $N_2^+$  that have been observed in various nitrogen afterglows are illustrated in Fig. 2-1 and listed in Table 2-1. In Fig. 2-1, the systems are numbered in order of increasing electronic energy of the emitting state. The positions of the energy levels relative to the energy available by recombination of ground state or excited nitrogen atoms may also be seen. Note that the energy required for emissions of these molecular systems is available from the recombination of ground state  $N(^4S)$  atoms, with the exceptions of the second positive system of  $N_2$ , the Goldstein-Kaplan and Birge-Hopfield systems of  $N_2$ , and the first negative system of  $N_2^+$ .

The radiative lifetimes of the principal emitting species in the nitrogen afterglow are listed in Table 2-2. For reference, note that the collision frequency of ground state nitrogen molecules is  $6 \times 10^6 \text{ s}^{-1}$  at 1 torr and 300°K (72,73), and that collisions involving excited and ground state nitrogen molecules are expected to occur at a higher frequency (74-76).

#### The First Positive System of $N_2$ $N_2(B^3\Pi_g) \rightarrow N_2(A^3\Sigma_u)$

The first positive system of  $N_2$  is the main component of the Lewis-Rayleigh afterglow and results from the transition  $N_2(B^3\Pi_g) \rightarrow N_2(A^3\Sigma_u)$  with emission in the region 500-2500nm. The dominant energy carriers are  $N(^4S)$  atoms and excited molecular  $N_2$  species.

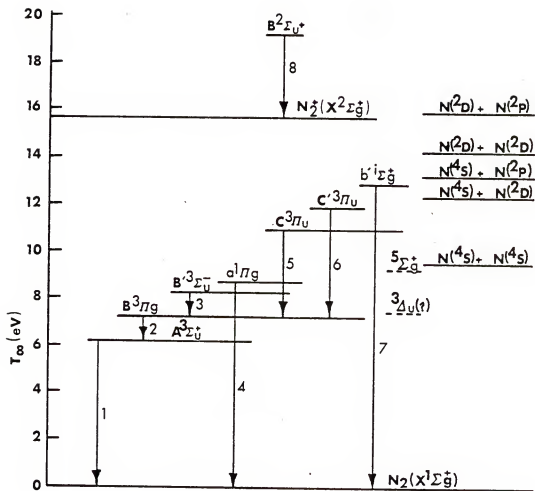


Figure 2-1 States and transitions of  $N_2$  and  $N_2^+$  observed in various modifications of active nitrogen.

Table 2-1 Active Nitrogen Systems\*

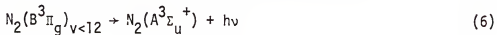
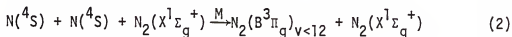
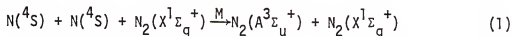
Nitrogen System	Transition	Wave length (nm)
First Positive System	$B^3\Pi_g \rightarrow A^3\Sigma_u^+$	500 - 2500
The "Y" Bands	$B^3\Sigma_u^- \rightarrow B^3\Pi_g$	600 - 1080
Vegard-Kaplan Systems	$A^3\Sigma_u^+ \rightarrow X^1\Sigma_g^+$	210 - 500
Lyman-Birge-Hopfield System	$a^1\Pi_g \rightarrow X^1\Sigma_g^+$	120 - 260
Second Positive System	$C^3\Pi_u \rightarrow B^3\Pi_g$	280 - 545
Goldstein-Kaplan System	$C^3\Pi_u \rightarrow B^3\Pi_g$	285 - 510
Birge-Hopfield System	$b^1\Pi_u \rightarrow X^1\Sigma_g^+$	93 - 165
	$b^1\Sigma_u^+ \rightarrow X^1\Sigma_g^+$	93 - 165
First Negative System of $N_2^+$	$B^2\Sigma_u^+ \rightarrow X^2\Sigma_g^+$	290 - 590

\*Ref. 55

Table 2-2 Lifetimes and Energies of Principle Species  
in Active Nitrogen

Species	Energy (eV)	Lifetime(s)	Reference
$N(^4S)$	4.76		77
$N(^2D)$	2.38	$9.4 \times 10^4$	78,79
$N(^2P)$	3.58	12	78,79
$N_2(A^3\Sigma_u^+)$	6.2 - 6.4	0.9 - 1.36 ( $v=0$ ) 2.5 - 2.7 ( $v=-1, +1$ )	81-83
$N_2(B^3\Pi_g)$	7.35	$4.4 - 9.1 \times 10^{-6}$ ( $v < 9$ ) $4 \times 10^{-6}$ ( $v=10, 11, 12$ )	83,84 84,85
$N_2(^3\Delta_u)$	7.5	-	83
$N_2(B^3\Sigma_u^-)$	8.16	-	83
$N_2(a^1\Sigma_u^-)$	8.40	$4 \times 10^{-2}$	74,83
$N_2(a^1\Pi_g)$	8.55	$1.4 - 1.5 \times 10^{-4}$ $1.1 \times 10^{-3}$ (electric quadrupole) $1.7 \times 10^{-4}$ (magnetic quadrupole)	83,86 74 74
$N_2(w^1\Delta_u)$	8.89	$4 \times 10^{-2}$	83
$N_2(^5\Sigma_g^+)$	9.66	$\sim 0.02$	87
$N_2(C^3\Pi_u)$	11.0 - 11.7	$4.5 \times 10^{-8}$	80,84
$N_2(C^3\Pi_u)$	12.10	-	88
$N_2(b^1\Pi_u)$	12.85	-	89
$N_2(b^1\Sigma_u^+)$	12.85	-	89
$N_2(B^2\Sigma_u^+)$	18.75	-	88

In general, it is agreed that this yellow afterglow is associated with the recombination of ground state ( $^4S$ ) nitrogen atoms (90,91). Approximately 70% of all nitrogen atom recombinations result from a collision between two nitrogen atoms, N, and a third body, M (92,93). The experimental results can be explained by the following mechanism (90,92-94):



Note, that  $N_2(A)_{\text{vhigh}}$  is a vibrationally excited molecule that can undergo a series of vibrational or electronic transfer reactions, and that  $N_2(^5\Sigma_g^+)$  is a very shallow, collisionally induced state (90,91, 94-97). Additionally, note that atomic recombination populates mainly the  $v^1 = 11$  and 12 vibrational levels of the  $B^3\Pi_g$  state. The reaction rates for reactions (1) and (2) for M equal to another nitrogen atom, nitrogen molecule or trace gas impurity are the following:

$$k_1 = 1.4 \times 10^{15} \text{ cm}^6 \text{ mol}^{-2} \text{ s}^{-1} \quad (91,98)$$

$$k_2 = 6 \times 10^{14} \text{ cm}^6 \text{ mol}^{-2} \text{ s}^{-1} \quad (95,98)$$

The reaction rates can be increased substantially for M equal to a  $\text{H}_2\text{O}$  or  $\text{HCl}$  molecule in the above reactions (55,92,99,100).

The transition given in equation 6 results in the first positive (1P) emission. Interestingly, the emission can account for a maximum of only 3.6eV (~84 kcal) which is a fraction of the total energy (9.76eV or 225 kcal) available from the recombination of ground state atoms (55,98). The fact that the energy of the afterglow is less than 9.76eV lends credence to the argument that ground state atom recombination is the main source of the glow. However, chemical studies (e.g., reactions with ammonia) suggest that active nitrogen contains energetic species other than atoms (83).

Jonathan and Petty (95) found that the Lewis-Rayleigh afterglow at low pressure was related to the N atom population by

$$I = I_0 [N]^2 \quad (7)$$

where  $I$  is the afterglow emission intensity and  $I_0$  is a proportionality constant. The precise dependence of  $I$  on  $[N]$  was reported by Brennen (98) and Shane (101). They performed pressure jump experiments in static samples of decaying active nitrogen. They found that

$$I = \left( \frac{K[M]}{k\tau_B[M] + 1} \right) [N]^2 \quad (8)$$

where

$I$  = intensity of emission, intensity units

$K$  = constant determined by NO titration, intensity units  $(\text{mole m}^{-3})^{-3}$

$[M]$  = third body concentration,  $\text{mole m}^{-3}$

$k$  = rate constant for the reaction  $\text{N}_2(\text{B}^3\Pi_g) + \text{N}_2 \rightarrow \text{quench}$ ,

$$6.2 \times 10^{-17} \text{ m}^3 \text{ mol}^{-1} \text{ s}^{-1}$$

$\tau_B$  = lifetime of contributing levels of  $\text{N}_2(\text{B}^3\Pi_g)$  ( $v' = 10, 11, 12$ ),

$$4 \times 10^{-6} \text{ s}$$

This relates I to N at any pressure. An EPR study by Brennen (94) showed that [N] is not dependent on pressure over a 600-fold variation of total pressure.

Berkowitz et al. (90) examined the Lewis-Rayleigh afterglow by simultaneous observation of the optical intensity of the afterglow and its mass spectrum and correlated the magnitude of some of the mass peaks with the afterglow intensity. They found, in agreement with Brennen, that the afterglow intensity was proportional to the square of the ground state nitrogen atom concentration under numerous conditions. However, they determined that the afterglow intensity was linearly dependent upon the total pressure of nitrogen molecules. In addition, they noted that the addition of nitric oxide to the nitrogen afterglow results primarily in the production of nitrous oxide. The importance of this will become clearer in Chapter 5.

Recent clarifications of the excitation mechanisms in the Lewis-Rayleigh afterglow have been made by Hays and Oskam (102). They utilized a pulsed discharge produced by an rf transmitter to generate active nitrogen at  $10^{-9}$  torr. The resultant chemiluminescence was chopped by a chopper wheel equipped with an extended blade which served to block light transmission during the active discharge. Discharge pulse lengths of  $10\mu\text{s}$  to 2ms were used. Hays and Oskan discovered that the spectral intensity distribution of the first positive (1P) band emission is different during the early afterglow period from that later in the afterglow period, e.g., later than 4ms. They found that during the early afterglow, the 1P and second

positive (2P) band emission intensity have about the same time dependency and dependence on discharge pulse length. However, the initial intensity of the 1P system increases with pulse length, while the 2P intensity decreases. Since the 1P emission exhibits a close relationship with the 2P emission, it is probable that the  $B^3\Pi_g$  level is populated either directly or cascading from the C and C' states or by a mechanism similar to the population of these levels. This latter explanation implies that the  $A^2\Sigma_u^+$  state is involved in populating the  $B^3\Pi_g$  state. Late in the afterglow period, the 1P emission exhibits properties consistent with those of the Lewis-Rayleigh afterglow, i.e., population of the B state by recombination of N atoms. Therefore, the B state is being populated by more than one mechanism.

Note, however, that the remaining 30% of the total nitrogen atom recombinations in the presence of a third body (M) directly populate the ground state  $N_2(X^1\Sigma_g^+)$ :



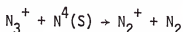
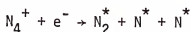
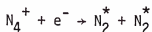
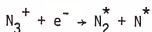
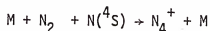
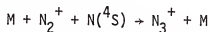
The lower vibrational levels of  $N_2(X)$  have a Boltzmannian distribution (89).

There are also numerous vibrationally excited ground state nitrogen molecules (103,104). Their collisional deactivation and vibrational relaxation rates have been reported to be small (105). They can be removed from flowing active nitrogen by inserting a glass wool plug downstream from the discharge (106-108).



### The Pink Afterglow

The "pink" afterglow is a short-lived, highly energetic afterglow that was first reported by Kaplan in 1932 (109) as a strong flash at the beginning of the afterglow. It is composed of  $N_2$  1P emission ( $B^3\Pi_g \rightarrow A^3\Sigma_u^+$ ) and  $N_2^+$  emission ( $B^2\Sigma_u^+ \rightarrow X^2\Sigma_g^+$ ) and has a weak contribution from  $N_2$ , 2P emission ( $C^3\Pi_u \rightarrow B^3\Pi_g$ ). The "pink" afterglow is observed for 20ms after a pulsed discharge through high purity nitrogen and contains many high energy species that exhibit excitation energies in excess of 20eV (110). The phenomenon of the "pink" afterglow is not understood, and numerous theories have been reported (111-113). Young studied the quenching of the "pink" afterglow by an ac electric field and by the addition of mercury atoms, and observed its vacuum UV spectrum (114). He reported that a large fraction of the stored energy in the "pink" afterglow appeared to exist as ground state atoms rather than as metastable atomic states, ionized states, or trapped resonance radiation. He suggested that the "pink" afterglow might be a result of the following mechanism:



The "Y" Bands  $N_2(B^3\Sigma_u^-) \rightarrow N_2(B^3\Pi_g)$

The "Y" bands, also called the infrared afterglow system, were discovered by Carroll and Rubaclava in a transformer discharge through very pure nitrogen (115). They consist of emission of triplet transitions of nitrogen in the infrared between 693 and 1043nm (116). The "Y" state is populated during a collision-induced radiationless transition from the  $^5\Sigma_g^+$  of nitrogen. This reaction competes with the transition that directly populates the high ( $v \sim 11$ ) vibrational levels of the  $B^3\Pi_g$  state. The dependence of the afterglow emission in the "Y" system is similar to the first positive system (117). Decreasing the temperature favors emission from the highest vibrational level.

The Vegard-Kaplan System  $N_2(A^3\Sigma_u^+) \rightarrow N_2(X^1\Sigma_g^+)$

The Vegard-Kaplan is an "intercombination" system resulting in emission between 210-500nm. It is forbidden in the sense that it can occur only by violating the approximate spin selection rule  $\Delta S = 0$  (82,118). Ordinarily, it is not observed in either discharge or afterglow regions; however, there is usually a small steady concentration of A-state molecules in most discharge systems (81,119,120). Although the forbidden nature of this system makes measurements and analysis difficult, this system is of considerable interest because its upper state is populated continually by the first positive system and because it is involved in an energy pooling reaction which produces  $N_2(C^3\Pi_u)$  molecules.

The Vegard-Kaplan system was first detected by Vegard in the luminescence of solid nitrogen (121). Kaplan later detected emission of 14 bands in the system in a special discharge tube consisting of

a short piece of 1mm. capillary and a 500ml. bulb (122). Later Hamada (123) studied the glow from short-lived metastable nitrogen produced by a discharge through nitrogen immersed in liquid air at pressures of a few tenths of a torr to a few torr. He reported emission from Vegard-Kaplan bands with nearly equal intensity from  $v' = 0, 1$  and  $2$ . He also found that the intensity of the bands increased with pressure. Hamada believed that this metastable nitrogen had a fairly high concentration of metastable  $N_2(A^3\Sigma_u^+)$  molecules. It is interesting to note that some of the Vegard-Kaplan bands occur in the aurora and the night sky (124).

The Lyman-Birge-Hopfield System of  $N_2$   $N_2(a^1\Pi_g) \rightarrow N_2(x^1\Sigma_g^+)$

The Lyman-Birge-Hopfield is a singlet band system that occurs primarily in the vacuum ultra violet in the region 120-260 nm. The transition is  $a^1\Pi_g \rightarrow x^1\Sigma_g^+$ . This system, then, is  $(g \rightarrow g)$ , which is forbidden as an electric dipole transition but allowed as a magnetic dipole and quadrupole transition. Consequently, this system exhibits S and O branches (electric quadrupole lines) in addition to P, Q, R branches (approximately 85% contribution from magnetic dipole and 15% from electric dipole transitions) (125,126). The  $a^1\Pi_g$  state dissociates into two  $^2D$  nitrogen atoms (127,128).

The emission of this system was first discovered by Lyman in 1911 in a high-voltage transformer discharge through pure nitrogen at low pressure (129). In 1928, Birge and Hopfield detected numerous bands of this system, in both emission and absorption, and reported a detailed examination of their vibrational structures (130).

Tanaka and coworkers were the first to report emission of the Lyman-Birge-Hopfield bands from active nitrogen (131,132). They saw very weak emission from low vibrational levels of the  $a^1\Pi_g$  in the vacuum UV region of the Lewis-Rayleigh afterglow in pure nitrogen at pressures below 12 torr.

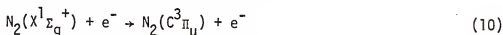
The Second Positive System of  $N_2$   $N_2(C^3\Pi_u) \rightarrow N_2(B^3\Pi_g)$

The second positive system, the system studied in this research effort, is emission in the wavelength range 280-545 nm. It is the result of a fully allowed transition,  $C^3\Pi_u \rightarrow B^3\Pi_g$ . The zero vibrational level of the upper state lies at 11.05eV (127,133); thus, this system contains considerably more energy than is available from  $N(^4S)$  atom recombination (9.7eV). Emission from the second positive system is not usually detected in the Lewis-Rayleigh afterglow. Thirty emission lines have been identified in the range 300-400 nm with the maximum intensity occurring at 337 nm. It is interesting to note that UV coherent light (laser action of about  $20 \times 10^{-9}$  s pulse width) that is generated at room temperature in a pulsed, high voltage (100-150keV) nitrogen discharge is attributed to emission of the second positive system due to an inversion in the triplet state of nitrogen (134,135).

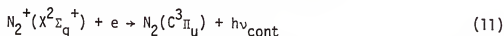
Lindau (136), and Mecke and Lindau (137) and Hulthen and Johansson (138) published the first systematic studies of this system in 1954. These studies showed that there was a sharp cutoff of the rotational levels in the fourth vibrational level. Later, Kaplan was unable to detect any bands with  $v' > 4$  (139). Herzberg attributed these observations to a predissociation in the  $C^3\Pi_u$  state at  $v' > 4$  (140). The  $C^3\Pi_u$  state dissociates into one  $sp^4$   $^4P$  and one  $^4S$  nitrogen atom (127).

Büttenbender and Herzberg found the limit of the occurrence of this predissociation to be about 12.14eV (141).

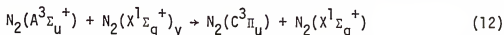
The second positive system of  $N_2$  is an emission from the earth's upper atmosphere, i.e., the "airglow" (142,143) or the "light of the night sky" (144) and in both auroras (145,146). It has been suggested that in the auroral regions, the  $N_2(C^3\Pi_u)$  state is excited through electronic excitation of the ground state (142)



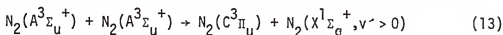
or through radiative recombination of an ionized nitrogen molecule in the ground state and an electron (142,147,148):



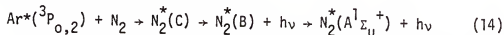
Research has shown that the  $C^3\Pi_u$  level could be populated from the  $X^1\Sigma_g^+$  ground state by photon absorption in the region 107.5 to 165.0 nm (149,150,151) and electronic excitation (152-156). The theoretically expected vibrational (intensity) distribution for the  $C^3\Pi_u$  state for all experimentally observed bands of the second positive system produced in a discharge has been calculated (147) and found to agree with experimental data (157). It is also possible that the  $C^3\Pi_u$  state produced in a dielectric discharge could be due to the reaction of an  $A^3\Sigma_u^+$  state molecule with a vibrationally excited state nitrogen molecule ( $v > 20$ ) with an excitation energy greater than 5eV (95):



Currently, most researchers agree that the  $C^3\Pi_u$  state is formed via a process called metastable energy pooling (80,102,158-160):



This theory was confirmed by an experiment performed by Stedman and Setser in 1969 (80). They produced  $N_2(A^1\Sigma_u^+)$  in the absence of other species via the following process:



They observed strong Vegard-Kaplan and weak second positive emission. As predicted by equation (10), a plot of the second positive emission intensity versus the square of the Vegard-Kaplan emission of intensity had a slope equal to 1. The rate law involved is as follows:

$$\frac{d[N_2(C)]}{dt} = k_{10}[N_2(A)]^2 \quad (15)$$

$k_{10}(\text{cm}^3 \text{ mole}^{-1} \text{ s}^{-1})$  was calculated from the equation (160):

$$\frac{I[N_2(C)]}{[I[N_2(A)]]^2} = k_{10}\tau_A \quad (16)$$

where  $I$  is the intensity of the emission indicated (in intensity units) and  $\tau_A$  is the lifetime of the  $N_2(A)$  state(s). Using Shemansky's (82) value for  $\tau_A$  (2.0s),  $k_{10}$  was calculated to be  $1.25 \times 10^{13} \text{ cm}^3 \text{ mole}^{-1} \text{ s}^{-1}$  (80). The energies and vibrational states involved in equation (10) are listed in Table 2-3 (80).

Further evidence was discovered by Hays and Oskam 1973 (102). They noticed that the decay rate of emission intensity for the second positive system increased with increasing discharge pulse length in the early afterglow period. This result would be expected of the  $A^3\Sigma_u^+$  pools to produce the  $C^3\Pi_g$  state because the increase in discharge pulse length increases the number density of nitrogen atoms which effectively quench nitrogen  $A^3\Sigma_u^+$  state molecules.

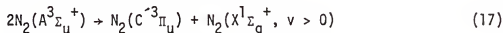
Table 2-3 Species Involved in Metastable -  
Metastable Energy Pooling

Metastable Species	Vibrational State	Excitation Energy (eV)
$N_2(A)$	$v' = 0$	6.2*
	$v' = 1$	6.4*
$N_2(C)$	$v' = 0$	11.0
	$v' = 1$	11.3
	$v' = 2$	11.5
	$v' = 3$	11.7

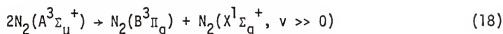
\*These are present in equal populations

The  $C^3\Pi_u$  state is not collisionally deactivated at 1 torr (102). The only loss of the  $C^3\Pi_u$  state is through radiative transitions to the  $N_2(B)$  state with a radiative lifetime on the order of  $10^{-8}$ s (161).

The energy pooling of the metastable  $A^3\Sigma_u^+$  states also populates the  $C^3\Pi_u$  and the  $B^3\Pi_g$  states (102,159):



$$k_5 \approx 0.25 \times 10^{-10} \text{ cm}^3 \text{ s}^{-1} \text{ molecule}^{-1}$$



$$k_{15} \approx 1.5 \times 10^{-9} \text{ cm}^3 \text{ s}^{-1} \text{ molecule}^{-1}$$

These energy pooling reactions populate the C,  $C'$  and B states with relative cross sections of 1, 0.1 and 4.4 respectively.

Because  $A^3\Sigma_u^+$  state molecules and the energy stored in them play such an important role in the properties of the second positive system, it is necessary to examine the characteristics of these molecules including lifetime measurements and mechanisms for production and deactivation.

Phillips (162) conducted an experiment to determine the lifetime of the  $A^3\Sigma_u^+$  state by measuring the decay of the blue emission from an active nitrogen-iodine flame at iodine pressures down to  $1.4 \times 10^{-4}$  torr. The decay rate constant in the absence of iodine was found to be  $0.89 \pm 0.41 \text{ s}^{-1}$  which corresponds to a mean lifetime of 1.1s for the  $A^3\Sigma_u^+$  state of nitrogen. Shemansky (81) reported the lifetime for  $A^3\Sigma_u^+$  to be 1.27s ( $v = 0$ ) and 2.5s ( $v = +1, -1$ ). He also published another set of lifetimes with Carleton at the same



time. These lifetimes are 1.36s ( $v = 0$ ) and 2.7s ( $v = +1, -1$ ) (82). Most researchers use a lifetime of about 2s in their calculations.

There are no current theories to explain how energy levels of nitrogen molecules, many eV below those formed by atom association, are populated at low pressures (97), even though more than half of the observed emissions from nitrogen occur from such levels. Berkowitz, Chupka, and Kistiakowsky proposed an early theory which many researchers favored because its initial step involved the formation of  $N_2(^5\Sigma)$  by a three body association (163). A later theory by Thrush and Campbell (69,164-165) rejected this premise because this initial step would be too slow to account for the subsequent rate of population of the  $B^3\Pi$ , as required from studies of the emission intensity of the first positive bands under conditions of rapid collisional removal of this level.

The theory by Thrush and Campbell (69,164-165) makes the assumption that  $N_2(B^3\Pi_u)$  is quenched to  $N_2(A^3\Sigma_u^+)$  and that the  $N_2(B^3\Pi_u)$  is populated via collisions of the  $N_2(A^3\Sigma_u^+)$  molecules. A new theory of active nitrogen suggested by Young in 1973 (97) rejects the Thrush and Campbell theory because of this assumption. If the  $N_2(B^3\Pi_u)$  and  $N_2(A^3\Sigma_u^+)$  populations were so closely related as Thrush and Campbell suggest, then once an equilibrium was established, any quenching of one of these states would have to be observed as a quenching of both. Unfortunately, no quenching mechanism has been proposed that could account for such efficient energy degradation. Young concluded that the quenching of the  $N_2(B^3\Pi)_v$  state corresponds to a rapid rotational relaxation and electronic state interchange

that appears as fast vibrational relaxation down a ladder formed of both A and B vibrational levels.

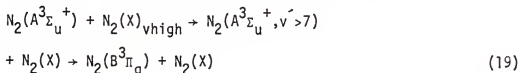
The  $A^3\Sigma_u^+$  state can also be populated by inelastic collisions with threshold energy, equal to 6.7eV. The cross section for this reaction is approximately  $0.6 \times 10^{-16} \text{ cm}^2$  (153).

Mechanisms by which the  $A^3\Sigma_u^+$  state population is decreased are crucial to this work. The three principal ways that  $A^3\Sigma_u^+$  state molecules are quenched are through population of the nitrogen B state and collisions with nitrogen atoms and the walls of the container. Nitrogen  $A^3\Sigma_u^+$  molecules are not appreciably quenched by molecular nitrogen (92):



$$k_{16} = 6 \times 10^6 \text{ cm}^3 \text{mol}^{-1} \text{s}^{-1}$$

The population of the  $B^3\Pi_g$  state reduces the  $A^3\Sigma_u^+$  state via (102):



Collision of  $A^3\Sigma_u^+$  molecules with nitrogen atoms in the central volume of the afterglow is a major and rapid source of quenching (166):



$$k_{18} = 3 \times 10^{13} \text{ cm}^3 \text{mol}^{-1} \text{s}^{-1}$$

Note, that the nitrogen atoms are not removed in equation (18) and that they gain transitional energy. Young and St. John (167) found that there was a linear relationship between the nitrogen atom concentration and the intensity of the Vegard-Kaplan emission. They determined that the slope of the curve plotting nitrogen atom concentration versus the

the Vegard-Kaplan intensity was approximately 1000. This means that a single nitrogen atom can quench numerous metastable molecules during its lifetime.

Near the walls of the container, collisional deactivation of  $A^3\Sigma_u^+$  state molecules is the limiting factor (88,92,93,168):



$$k_{19} \approx 120 \text{ s}^{-1}$$

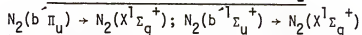
This was especially evident in the study done by Campbell and Thrush (169). They injected hydrocarbons into a nitrogen plasma. These hydrocarbons reacted to produce cyanogen and the cyanogen was excited by the  $A^3\Sigma_u^+$  state molecules. The resultant emission was seen to stop noticeably short of the walls, proving that collisional deactivation of the  $A^3\Sigma_u^+$  state on the walls was so effective that no cyanogen emission could be produced here.

There are numerous methods of producing a nitrogen plasma that emits a strong second positive band system. As this paper discussed, these methods all rely on the ability to generate large populations of metastable nitrogen molecules. Second positive emission has been produced by bombarding nitrogen with soft X-rays (170) between pressures of 1 and 760 torr, and with ions (protons, deuterons,  $H_2^+$ ) of energies around 5keV (171) at pressures of 0.0001 and 1 torr. The method of mixing nitrogen with metastable argon was detailed in equation (11). Shemansky produced a second positive system through electron impact by bombarding flowing nitrogen with 10eV electrons at a pressure of 0.010 torr (168). Other researchers have used dielectric discharges through nitrogen (119,172). Even controlled thermal decomposition of silver azide has been employed (173).

The Goldstein-Kaplan System of  $N_2$   $N_2(C^3\Pi_u) \rightarrow N_2(B^3\Pi_g)$

The Goldstein-Kaplan system results from the  $C^3\Pi_u \rightarrow B^3\Pi_g$  transition and results in emission in the 285-510 nm region. It was first discovered by Goldstein in 1905 from an induction-coil discharge in nitrogen at liquid air temperature (174) and later studied by Kaplan (175, 176) and Hamada (177). These bands appear to be emitted from the aurora (176,177) and in the "light of the night sky" (175,177).

The Birge-Hopfield Systems of  $N_2$



The Birge-Hopfield systems are singlet systems from the transitions  $b^1\Pi_u \rightarrow X^1\Sigma_g^+$  and  $b^1\Sigma_u^+ \rightarrow X^1\Sigma_h^+$ . Their emission falls in the region 93-165 nm. They were first discovered by Birge and Hopfield in the emission of an ordinary discharge through pure nitrogen at low pressure (130).

The system  $b^1\Sigma_u^+ \rightarrow X^1\Sigma_g^+$  is very prominent in the vacuum UV spectrum of nitrogen and has been detected during observations of the "pink" afterglow of nitrogen (114). This radiation originated from the  $b^1\Sigma_u^+$  state (12.94eV) and extended to the cutoff of the lithium fluoride observation window.

The First Negative System of  $N_2^+$   $N_2^+(B^2\Sigma_u^+) \rightarrow N_2^+(X^2\Sigma_g^+)$

This system involves a transition of the  $B^2\Sigma_u^+$  state of nitrogen to the ground state, and emission is in the region 290-590 nm. It is the main system of  $N_2^+$  and is observed in discharge tubes at very low pressure or in the presence of excess helium at moderate pressure (124).

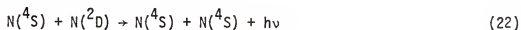
The first negative bands of  $N_2^+$  are important parts of emission from the earth's upper atmosphere. These bands have been identified in the spectrum of both auroras and the "airglow" (146). During the

"Great Aurora of 1958," the (0,0) and (0,1) bands were observed and the rotational temperatures involved were measured (145). Because studies of emission in the 4652 to 4709 Å region have indicated the presence of high vibrational excitation ( $v' = 2,1$ ) in the  $B^2\Sigma_u^+$  state of  $N_2^+$  (178), it has been suggested that excitation of the first negative bands is through absorption of sunlight by  $N_2^+(X^2\Sigma_g^+)$  (142,179).

Emission from Atomic Nitrogen  $N(^2D) \rightarrow N(^4S)$ ;  $N(^2P) \rightarrow N(^4S)$

Light emission due to the transitions ( $^2D \rightarrow ^4S$ ) and ( $^2P \rightarrow ^4S$ ) are observed at 5200 Å and 3466 Å, respectively, even though they are forbidden by electric dipole selection rules. However, since the  $^2D$  state [2.38 eV above  $N(^4S)$ ] (79) and the  $^2P$  state [3.57 above  $N(^4S)$ ] (79) have extremely long theoretical radiative lifetimes of approximately 26 hours (180) and 12s (78), respectively toward these transitions, these emissions are seen only under special conditions. Emission from the  $3s\ ^2P$  state of atomic nitrogen (10.6eV) to the  $2p^3\ ^4S$  ground state of the nitrogen atom is forbidden. However, radiation is allowed from the  $3s\ ^2P$  state to the metastable  $2p^3\ ^2D$  and  $2p^3\ ^2P$ , resulting in emission at 1495 Å and 1745 Å, respectively (181). These are  $N_I$  lines.

There is a short-duration afterglow produced by metastable nitrogen atoms that are excited in the positive column of a dc discharge through extremely pure nitrogen mixed with xenon (182). The mechanism producing the emission is suggested to be the result of a two-body atom recombination,



### Effect of Additive Gases

The effect of adding argon or helium to active nitrogen has been studied minimally. Argon is known to quench strongly the  $N_2(B^3\Pi_g, v>6)$  level (97) which enhances the Lewis-Rayleigh afterglow (84,99,183). Helium also enhances first positive emission (99).

The  $N_2(A^3\Sigma_u^+)$  state has much smaller quenching rate coefficients by Ar and He than  $N_2(B^3\Pi_u)$ . The efficiency of collisional deactivation on the walls for metastable nitrogen molecules is  $4.75 \times 10^{-4}$ . In comparison, collision efficiencies for gas-phase deactivation by Ar and  $N_2$  are  $1.5 \times 10^{-6}$  and  $3.3 \times 10^{-8}$  respectively (184,185).

### Analytical Studies with Active Nitrogen

The most studied analytical application of active nitrogen has been the detection of metals. Recent results of active nitrogen-induced chemiluminescence of metals are discussed below and listed in Table 2-4. Lewis (61-63) was the first to observe metallic lines corresponding to electrode materials in an active nitrogen afterglow. He also observed mercury lines due to the diffusion of mercury vapor into a nitrogen afterglow from the pumping system. In 1954, 1955 and 1960, Kenty (186-188) conducted a series of experiments examining metal atomic emission in an atmosphere of 300 torr Ar and 10 torr  $N_2$ . He passed a condensed discharge through gaps made from the metal of interest and obtained the metal arc spectra. Later in 1966, Brennen and Kistiakowsky (189) studied the active nitrogen-induced chemiluminescence of metal carbonyls. Active nitrogen was produced by a microwave discharge at low-pressure (1-5 torr) in a steady-flow apparatus. They discovered that  $Ni(CO)_4$ ,  $Fe(CO)_5$ ,  $Cr(CO)_6$ ,  $W(CO)_6$ ,  $Mo_2(CO)_{10}$  and  $Co(NO)(CO)_3$  reacted very rapidly to form metal atoms and produced

Table 2-4 Detection of Metals by Active Nitrogen

Metal	Date	Emission	Other Information <sup>†</sup>	Reference
Ag	1954	"Brush" flame	Produced by passing a condensed spark across Ag gaps in (300 torr Ar + 10 torr N <sub>2</sub> ).	187
Ag	1982	328.1nm	Microwave induced N <sub>2</sub> <sup>*</sup> at low pressure. LOD = 2 pg. LDR = 10 <sup>4</sup> - 10 <sup>5</sup> .	190
Al	1954	"Brush" flame	Produced by passing a condensed spark across Al gaps in (300 torr Ar + 10 torr N <sub>2</sub> ).	187
Al	1969	396.2nm	Microwave induced N <sub>2</sub> <sup>*</sup> at low pressure.	191
Au	1954	"Brush" flame	Produced by passing a condensed spark across Au gaps in (300 torr Ar + 10 torr N <sub>2</sub> ).	187
As	1980	193.7nm	N <sub>2</sub> <sup>*</sup> excited in a electrodeless ozonizer discharge at 1 atm pressure. LOD = 0.2 ng. LDR = 10 <sup>3</sup> .	45
Ba	1969	Resonance lines of Ba <sup>+</sup> at 493.4nm and 455.4nm	Ba vapor added to N <sub>2</sub> <sup>*</sup> afterglow produced by a weak discharge through Xe containing a trace of N <sub>2</sub> .	192,193
Be	1954	Arc lines emitted in a "brush" flame.	Produced by passing a condensed spark across Be gaps in (300 torr Ar + 10 torr N <sub>2</sub> ).	187

Table 2-4 - Continued

Metal	Date	Emission	Other Information	Reference
Bi	1977	306.8nm	Microwave induced $N_2^*$ at low pressure. $1.5 \times 10^4 \text{ cm}^{-3}$ was detected.	194
Bi	1980	306.8nm	$N_2^*$ excited in an electrodeless ozonizer discharge at 1 atm pressure. LOD < 0.1 ng. LDR = $10^2$ .	45
Bi	1982	306.8nm	Microwave induced $N_2^*$ at low pressure. LOD = 300 pg. LDR = $10^4 - 10^5$ .	190
Ca	1955	"Fountain" flame	Produced by low-current discharge through inert gas with trace of $N_2$ .	186,188
Ca	1969	393.4; 422.7nm	Impurity in $N_2$ .	192
Cd	1955 1960	"Fountain" flame	Produced by low-current discharge through inert gases containing a trace of $N_2$ .	186,188
Cd	1973	321.6nm	Microwave induced $N_2^*$ . Pressure dependent with $E_{\max}$ at 10 torr.	195
Cd	1982	326.1nm	Microwave induced $N_2^*$ at low pressure. LOD = 30 pg. LDR = $10^4 - 10^5$ .	190
Co	1954	Co arc lines emitted from brush flame	Produced by passing a condensed spark across Co gaps in (300 torr Ar + 10 torr $N_2$ ).	187



Table 2-4 - Continued

Metal	Date	Emission	Other Information	Reference
Co	1966	345.4nm	Microwave degradation and excitation of $\text{Co(NO)(CO)}_3$ .	189
Cr	1954	Cr arc lines emitted from "brush" flame	Produced by passing a condensed spark across Cr gaps in (300 torr Ar + 10 torr $\text{N}_2$ ).	187
Cs	1977	455.5nm	Cs impurity in a laser.	194
Cu	1954	Cu lines emitted from "brush" flame	Produced by passing a condensed spark across Cu gaps in (300 torr Ar + 10 torr $\text{N}_2$ ).	187
Cu	1982	324.7nm	Microwave induced $\text{N}_2^*$ at low pressure. LOD = 20 pg.; LDR = $10^4$ - $10^5$ .	190
Cu	1963	324.8nm	Microwave degradation and excitation of Cu halides.	87
Fe	1954	Fe arc lines emitted from violet "brush"	Produced by passing a condensed spark across Fe gaps in (300 torr Ar + 10 torr $\text{N}_2$ ).	187
Fe	1966	372.0nm	Microwave degradation and excitation of $\text{Fe(CO)}_5$ .	189
Ga	1955 1960	"Fountain" flame	Produced by low-current discharge through inert gases containing traces of $\text{N}_2$ .	186,188
Ge	1980	265.1nm	$\text{N}_2^*$ generated in electrodeless ozonizer discharge at 1 atm LOD = 20 ng. LDR = $10^2$ .	45

Table 2-4 - Continued

Metal	Date	Emission	Other Information	Reference
Hg	1967	253.7nm	Microwave induced $N_2^*$ . $E_{max}$ at 10 torr. Relative line intensity was pressure dependent.	195
Hg	1972	253.7nm	Microwave induced $N_2^*$ . Less than $10^9$ atoms/cm <sup>3</sup> were detected.	92
Hg	1981	253.7nm	$N_2^*$ generated by dielectric discharge at low pressure. LOD = $10^7$ atoms/cm <sup>3</sup> .	196
Hg	1980	253.7nm	$N_2^*$ generated in electrodeless ozonizer discharge at 1 atm. LOD < 0.02ng. LDR = $10^3$ .	45
In	1955	"Fountain" flame	Produced by a low-current discharge through inert gases containing a trace of $N_2$ .	186,188
Ir	1954	"Brush" flame	Produced by passing a condensed spark across Ir gaps in (300 torr Ar + 10 torr $N_2$ ).	187
K	1973	404.4nm	Microwave induced $N_2^*$ at low pressure. $E_{max}$ at 0.7 torr.	195
Li	1955 1960	"Fountain" flame	Excited by a long-lived excited nitrogen species.	186,188
Li	1973	670.8nm	Microwave induced $N_2^*$ at low pressure. $E_{max}$ at 0.7 torr.	195

Table 2-4 - Continued

Metal	Date	Emission	Other Information	Reference
Mg	1937	Lines in 284.7-518.4nm region.	Mg wire cathode	198
Mg	1955	"Fountain" flame	$N_2^*$ produced by a low-current discharge through inert gases containing a trace of $N_2$ .	186
Mg	1982	383.8nm	Microwave induced $N_2^*$ at low pressure. LOD = 80 pg. LDR = $10^4$ - $10^5$ .	190
Mn	1966	257.6nm	Microwave degradation and excitation of $Mn_2(CO)_{10}$ .	189
Mo	1954 1955	550.6nm "blue" flame	Produced by passing a condensed spark across Mo electrodes in Ar containing a trace of $N_2$ .	
Na	1955 1960	"Fountain" flame	$N_2^*$ produced by a low-current discharge through inert gases containing a trace of $N_2$ .	186,188
Na	1958	D-line emission	Detected in daytime in upper atmosphere over 90-110 km levels when Na was ejected from a rocket.	198
Na	1973	589.0nm, 589.6nm 330.2nm	Microwave induced $N_2$ . $E_{max}$ at 0.7 torr.	195
Nb	1954 1955	Yellow "brush" flame emitted Nb lines	Produced by passing a condensed spark across Nb (columbium) electrodes in Ar containing a trace of $N_2$ .	186,187

Table 2-4 - Continued

Metal	Date	Emission	Other Information	Reference
Ni	1954	Ni arc lines emitted from "brush" flame	Produced by passing a condensed spark across Ni gaps in (300 torr Ar + 10 torr N <sub>2</sub> ).	187
Ni	1966	341.5nm	Microwave degradation and excitation of Ni(CO) <sub>4</sub> .	189
Pb	1963	368.3nm, 405.8nm	Microwave degradation and excitation of Pb halides.	89
Pb	1980	368.3nm	Microwave induced N <sub>2</sub> <sup>*</sup> at low pressure. LOD = 0.2 ng.	199
Pb	1980	283.3nm	Microwave generated in electrodeless ozonizer discharge at 1 atm. LOD = 5 ng. LDR = 10 <sup>3</sup> .	45
Pb	1982	368.3nm	Microwave induced N <sub>2</sub> at low pressure. LOD = 40 pg. LDR = 10 <sup>4</sup> - 10 <sup>5</sup> .	190
Pd	1954 1955	Green "brush" flame	Produced by passing a condensed spark across Pd gaps in (300 torr Ar + 10 torr N <sub>2</sub> ).	186,187
Pt	1954	"Brush" flame	Produced by passing a condensed spark across Pt gaps in (300 torr Ar + 10 torr N <sub>2</sub> ).	187
Re	1954	"Brush" flame	Produced by passing a condensed spark across Re gaps in (300 torr Ar + 10 torr N <sub>2</sub> ).	187

Table 2-4 - Continued

Metal	Date	Emission	Other Information	Reference
Rh	1954	"Brush" flame	Produced by passing a condensed spark across Rh gaps in (300 torr Ar + 10 torr N <sub>2</sub> ).	187
Sb	1952	206.8nm	Excitation by active nitrogen formed in the thermal decomposition of silver azide.	173
Sb	1980	206.8nm	N <sub>2</sub> <sup>*</sup> generated in electrodeless ozonizer discharge at 1 atm. LOD = 1 ng. LDR = 10 <sup>3</sup> .	173
Se	1980	196.0nm	N <sub>2</sub> <sup>*</sup> generated in electrodeless ozonizer discharge at 1 atm. LOD = 5 ng. LDR = 10 <sup>3</sup> .	45
Sn	1980	326.2nm	N <sub>2</sub> <sup>*</sup> generated in electrodeless ozonizer discharge at 1 atm. LOD = 20 ng. LDR = 10 <sup>2</sup> .	45
Sr	1955 1960	"Fountain" flame	Produced by low-current discharge through inert gases containing a trace of N <sub>2</sub> .	186,188
Ta	1954	Blue flame emission at 521.3nm	Produced by passing a condensed discharge spark across Ta gaps in (300 torr Ar + 10 torr N <sub>2</sub> ).	184,188
Te	1980	214.3nm	N <sub>2</sub> <sup>*</sup> generated in electrodeless ozonizer discharge at 1 atm. LOD = 50 ng. LDR = 10 <sup>2</sup> .	45

Table 2-4 - Continued

Metal	Date	Emission	Other Information	Reference
Th	1954	535.1nm	Produced by passing a condensed spark across Th gap in (300 torr Ar + 10 torr N <sub>2</sub> ).	187
Ti	1954	Ti, arc lines from "brush" flame	Produced by passing a condensed spark across Ti gaps in (300 torr Ar + 10 torr N <sub>2</sub> ).	187
Tl	1963	258.0-535.0nm	Correlated N <sub>2</sub> excited states with Tl transitions.	87
Tl	1963	535.0nm	The efficiency of excitation of Tl atoms by active nitrogen was very low.	200
Tl	1982	351.9nm	Microwave induced N <sub>2</sub> <sup>*</sup> at low pressure. LOD = 5 pg. LDR = 10 <sup>4</sup> - 10 <sup>5</sup> .	190
U	1954	"Brush" flame	Produced by passing a condensed spark across U gaps in (300 torr Ar + 10 torr N <sub>2</sub> ).	187
V	1954 1955	Brilliant red brush flame	Produced by passing a condensed spark between V electrodes in Ar containing a trace of N <sub>2</sub> .	187,188
W	1954	Blue "brush" flame	Produced by passing a condensed discharge spark across W gaps in (300 torr Ar + 10 torr N <sub>2</sub> ).	187
W	1966	430.2nm	Microwave degradation and excitation of W(CO) <sub>6</sub> .	189

Table 2-4 - Continued

Metal	Date	Emission	Other Information	Reference
Zr	1954	Zr arc lines produced from "brush" flame	Produced by passing a condensed spark across Zr gaps in (300 torr Ar + 10 torr N <sub>2</sub> ).	187
Zn	1955 1960	Zn line emission in "Fountain" flame	Produced by low-current discharge through inert gases containing trace of N <sub>2</sub> .	186,188
Zn	1973	308nm, 481nm, 472nm and 468nm	Microwave induced N <sub>2</sub> <sup>*</sup> at low pressure. E <sub>max</sub> at 10 torr.	195
Zn	1981	468nm	N <sub>2</sub> <sup>*</sup> generated by dielectric discharge at low pressure. LOD = 10 <sup>8</sup> atoms cm <sup>-3</sup> ; LDR = 10 <sup>7</sup> .	196

†LOD refers to the limit of detection. LDR refers to the linear dynamic range.

intense flames due to neutral metal atomic emission spectra. The reaction mechanism was concluded to be a stepwise degradation:  $\text{Me}(\text{CO})_n + \text{N} \rightarrow \text{Me}(\text{CO})_{n-1} + \text{NCO}$ . The metal atoms were probably excited by collision with  $\text{N}_2(\text{A}^3\Sigma_u^+)$  molecules.

The analytical potential of active nitrogen-induced chemiluminescence was clearly indicated in an active nitrogen study conducted by Meyer et al. in 1972 (92). Meyer observed Hg at the 253.7nm line at concentrations of  $<10^9$  atoms  $\text{cm}^{-3}$ . Meyer produced active nitrogen with a microwave discharge and observed the Lewis-Rayleigh afterglow with an E.M.I. 9558Q photomultiplier tube.

Capelle and Sutton (194) introduced Bi vapor produced in a resistively heated crucible into a Lewis-Rayleigh afterglow. Argon flow ( $10^{21}$  molec  $\text{s}^{-1}$ ) was used to sweep the Bi vapor into a quartz tube viewing region. The active nitrogen was generated by a microwave discharge at a flow rate of  $2 \times 10^{20}$  molec  $\text{s}^{-1}$ . Bi concentrations as low as  $1.5 \times 10^4$   $\text{cm}^{-3}$  were measured.

In 1978, Capelle and Sutton (201) named this technique MTES, for metastable transfer emission spectroscopy and presented further uses for this low pressure, microwave discharge generated, active nitrogen system. They introduced gas phase samples via a stainless steel capillary into a flow tube where the sample was mixed with an active nitrogen-argon mixture at 1-5 torr. Germane ( $\text{GeH}_4$ ) concentrations as low as  $7 \times 10^7$  molecules  $\text{cm}^{-3}$  (corresponding to 1 ppb in gas) were detected.

The applications of MTES for the determination of lead in water were demonstrated by Melzer, Jordan and Sutton (199). The apparatus was improved over the one employed for the detection of Bi (194)



and the crucible was replaced by a small tantalum boat. A limit of detection of 0.2 ng Pb was achieved.

The first analytical study of inorganic species with a nitrogen afterglow produced at atmospheric pressure was published by D'Silva, Rice and Fassel in 1980 (45). The active nitrogen was generated in an electrodeless ozonizer discharge operated at 20kV and 1800Hz. The hydrides of As, Bi, Ge, Pb, Sb, Se, Sn and Te were produced and mixed with the afterglow in the observation region. Limits of detection for these elements (listed in Table 2-4) were compared with other spectrometric techniques employing hydride generation. The results were of the same order of magnitude as atomic absorption spectroscopy.

Another active nitrogen approach for the measurement of metals at low pressure was introduced by Dodge and Allen (196). This technique was called METAL (for metastable energy transfer for atomic luminescence) and differed from the system put forth by Sutton and coworkers (194,199,201) in terms of the method of active nitrogen generation and the nitrogen emission system. The apparatus of Sutton and coworkers (194,199,201) utilized a microwave discharge for the production of active nitrogen. The nitrogen emission was the straw yellow Lewis-Rayleigh afterglow (194). A microwave discharge produces nitrogen plasmas with a high concentration of nitrogen atoms and hence the concentration of  $N_2(A^3\Sigma_u^+)$  is on the order of  $5 \times 10^9$  molecules  $cm^{-3}$  (99). The concentration of  $N_2(A^3\Sigma_u^+)$  is crucial since it is the principal energy carrier (190,196). Dodge and Allen (196,202) generated active nitrogen via a dielectric discharge. The nitrogen emission observed was the second positive system of nitrogen. The concentration of  $N_2(A^3\Sigma_u^+)$  was reported to be on the order of  $10^{17}$  metastable  $cm^{-3}$ .

Detection limits of  $10^8$  atoms  $\text{cm}^{-3}$  and  $10^7$  atoms  $\text{cm}^{-3}$  were obtained for Hg and Zn, respectively. The linear dynamic range for Zn was reported to be 7 orders of magnitude.

More recently, Na and Niemczyk (190) measured a series of metals by MTES. Aqueous solutions of trace metals were dried and atomized in a tantalum boat. The metal vapor was mixed with microwave discharge generated active nitrogen in a flow cell. The limits of detection were obtained for Ag, Bi, Cd, Cu, Mg, Pb and Tl and ranged from 2-300 pg. The measurements were performed at 1-2.4 torr. The effect of various interferences in electrothermal atomization metastable emission spectrometry have also been examined (203). The anion effect on the analyte signal is an important parameter since in furnace atomic absorption spectroscopy (AAS), the magnitude of the analyte signal intensity depends strongly on sample composition (203). For example, cadmium and lead nitrates give higher sensitivities than their chloride counterparts (204,205), while copper nitrate has been found to give the same or lower sensitivity than copper chloride (206). Na and Niemczyk have shown that the anion effect of  $\text{SO}_4^{2-}$ ,  $\text{NO}_3^-$ , and  $\text{Cl}^-$  on Cu, Cd and Pb signal intensities detected by MTES is minimal (203). Na and Niemczyk have also investigated the matrix effects of  $\text{NH}_4\text{Cl}$ ,  $\text{NH}_4\text{NO}_3$ ,  $\text{NaCl}$ ,  $\text{NaNO}_3$ ,  $\text{MgCl}_2$  and  $\text{Mg}(\text{NO}_3)_2$  on the analyte signals of Cd, Cu and Pb chlorides and nitrates. In general, there were no matrix effects detected except for negative interferences at high concentrations of matrix materials.

Active nitrogen-induced chemiluminescence of molecules, especially hydrocarbons, is a relatively new research topic. Recent work in this area is discussed below and the results are tabulated in Table 2-5.

Table 2-5 Detection of Several Compounds with Active Nitrogen

Compound	Date	Emission	Other Information <sup>†</sup>	Reference
Al(CH <sub>3</sub> ) <sub>3</sub>	1979	Al line.	MTES system.	207
AsH <sub>3</sub>	1978	As line.	MTES system.	207
Bi(CH <sub>3</sub> ) <sub>3</sub>	1978	Bi line.	MTES system. Detected 10 <sup>7</sup> - 10 <sup>10</sup> molec cm <sup>-3</sup> .	207 -
Bi(CH <sub>3</sub> ) <sub>3</sub>	1979	Bi line.	MTES system.	201
CH <sub>4</sub>	1979	CN emission	MTES system. LOD = 4 ng. HCl added.	208
CH <sub>2</sub> CHCl	1979	CN emission	MTES system. LOD = 100 pg.	208
GeH <sub>4</sub>	1978	Ge line.	MTES system. LOD = 0.1 ppb.	207
GeH <sub>4</sub>	1978	Ge line.	MTES system. LOD = 7 x 10 <sup>7</sup> molec cm <sup>-3</sup> .	201
Ge(C <sub>2</sub> H <sub>5</sub> ) <sub>4</sub>	1978	Ge line.	MTES system.	207
Hexadecane	1982	383.3nm	APAN system. LOD = 0.8 ng.	209
Hg(CH <sub>3</sub> ) <sub>2</sub>	1981	Hg line.	APAN system. LOD = 0.002 ng.	209
Hg(CH <sub>3</sub> ) <sub>3</sub>	1982	Hg line.	APAN system. LOD = 2 pg.	210
Hg(C <sub>2</sub> H <sub>5</sub> ) <sub>2</sub>	1982	Hg line.	APAN system. LOD = 5 pg.	210
Hg(C <sub>3</sub> H <sub>7</sub> ) <sub>2</sub>	1982	Hg line.	APAN system. LOD = 10 pg.	210
Hg(C <sub>4</sub> H <sub>9</sub> ) <sub>2</sub>	1982	Hg line.	APAN system. LOD = 20 pg.	210
Hg(C <sub>6</sub> H <sub>13</sub> ) <sub>2</sub>	1982	Hg line.	APAN system. LOD = 30 pg.	210
Hg(C <sub>6</sub> H <sub>5</sub> ) <sub>2</sub>	1982	Hg line.	APAN system. LOD = 50 pg.	210

Table 2-5 - Continued

Compound	Date	Emission	Other Information	Reference
$\text{Hg}(\text{CH}_3)\text{Cl}$	1982	Hg Line.	APAN system. LOD = 50 pg.	210
Naphthalene	1982	383.3nm	APAN system. LOD = 2 ng.	207
$\text{Pb}(\text{C}_4\text{H}_9)_4$	1981	Pb line.	MTES system. LOD = 100 pg.	208
$\text{PH}_3$	1978	P line.	MTES system.	207
$\text{SiH}_4$	1978	Si line.	MTES system.	207
$\text{Sn}(\text{C}_5\text{H}_{11})_4$	1981	Sn line.	APAN system. LOD = 2 ng.	209

† MTES stands for metastable transfer emission spectroscopy. The active nitrogen is microwave induced at low pressure.  
 APAN stands for atmospheric pressure active nitrogen. The active nitrogen is microwave induced at 1 atm.

Two research groups, Sutton and coworkers (208,211) and Rice and coworkers (45,209,210) have examined the application of an active nitrogen-induced chemiluminescence gas chromatographic detector. The system of Sutton et al. (208) utilized a microwave induced nitrogen plasma operated at 8 - 30 torr. A 0.05 mm i.d. stainless steel capillary tube was used to couple the gas chromatographs (operated at 1 atm) to the active nitrogen detector. When small hydrocarbons (6 carbons or less) are mixed with active nitrogen, CN is produced and emission from the  $\text{CN}(\text{B}^2_\Sigma^+ \rightarrow \text{X}^2_\Sigma^+)$  transition can be detected. By monitoring the CN chemiluminescence at 1 wavelength as the eluent from a gas chromatograph was mixed with the active nitrogen, a chromatogram was obtained. To reduce the limits of detection, a 1% mixture of HCl in nitrogen was added to the nitrogen afterglow. The addition of HCl is known to increase the degradation of hydrocarbons in active nitrogen and hence increase the production of CN (212). Limits of detection of 100 pg for vinyl chloride and 4 ng for  $\text{CH}_4$  were obtained. To make the detector specific for oxygen-containing compounds (as well as air leaks), either the  $\text{NO}(\text{A}^2_\Sigma^+ \rightarrow \text{X}^2_\Pi)$  bands or  $\text{OH}(\text{A}^2_\Sigma^+ \rightarrow \text{X}^2_\Pi)$  transition could be monitored. This specificity was demonstrated (211) but no limits of detection were obtained.

Rice et al. (210) have applied an atmospheric pressure active nitrogen afterglow (APAN) as a detector for gas chromatography. A glass capillary transfer line was used to couple the gas chromatographic column with the APAN system previously described (45). Selective trace level detection of organo-Hg, Pb, and Sn species was achieved by monitoring the metal line emissions. Hexadecane and naphthalene were detected by observing the CN emission at 388.3 nm. Methods for

determining methylmercury in fish, water, urine, and sediments, and diorganomercury compounds in water have been reported (209) using the GC-APAN system.

## CHAPTER III INSTRUMENT DESIGN

### Introduction

Active nitrogen is an especially promising excitation source since the energy involved (6.2eV) is not enough to dissociate or ionize most molecules or ionize atomic species. Because the major metastable constituent,  $N_2(A^3\Sigma_u^+)$ , has a radiative lifetime of  $\sim 2$ s (82) the active nitrogen source can be isolated from the reaction chamber. The physical separation of the reaction chamber and detection system away from the active nitrogen source prevents the intense emission of species in the discharge region from masking the analyte signal. In addition, since it takes several milliseconds for the nitrogen metastables to pass from the dielectric discharge generator to the reaction chamber, virtually all excited species except  $N_2(A^3\Sigma_u^+)$  have radiatively decayed before reaching the reaction chamber. Both of these factors help to eliminate stray light and undesired nitrogen metastable emission, resulting in a low background excitation source.

The instrumental design described in this Chapter has been optimized to produce a maximal concentration of nitrogen  $A^3\Sigma_u^+$  state molecules and minimal limits of detection (LOD).

Much time and effort were spent to maximize the  $N_2(A^3\Sigma_u^+)$  concentration. First, the discharge generator was optimized through a series of improved models. Secondly, large diameter tubing treated with phosphoric acid (189,213) was used to reduce wall-induced deactivations. Third, since the discharge generator utilized produced nitrogen  $A^3\Sigma_u^+$

molecules by metastable energy pooling, very few nitrogen atoms were formed. This was extremely important since nitrogen atoms are effective quenching agents. Because of these efforts, the nitrogen metastable concentration produced was  $> 10^{17}$  molecules  $\text{cm}^{-3}$ .

Many of the experimental methods used to lower the limits of detection were specific to the type of analysis. These are discussed in detail in Chapter 4. Some of the experimental parameters optimized were general to all measurements. These include: alignment of the system; nitrogen flow rate; wall treatment; diameter and length of the discharge tube, light traps, and reaction cell; and, reaction cell design.

The single most important design parameter was proper alignment of the system to obtain maximum optical system efficiency. Procedures for optimally aligning the system for either a photomultiplier tube or a silicon intensified target detection were developed. A slow flow rate of  $10 \text{ mL min}^{-1}$  of nitrogen was used in all measurements. The slow flow rate increased the reaction time and hence the probability of metastable energy transfer to the analyte provided the reaction time was less than the metastable  $\text{N}_2$  lifetime and the metastable  $\text{N}_2$  concentration was much greater than the analyte concentration.

#### Active Nitrogen Generator

Active nitrogen was generated in the Berthelot type of dielectric discharge generator illustrated in Figure 3-1. The discharge generator consisted of two concentric glass NMR tubes with an annular space of 3 mm. The outer glass wall was a 12 mm NMR tube (Wilmad Glass Co, Inc., Buena, N.J., 08310), 15.5 mm long, with wall thickness  $0.0500 \pm 0.0015$  in. The inner tube was a standard 6 mm NMR tube (Wilmad Glass Co, Inc.,



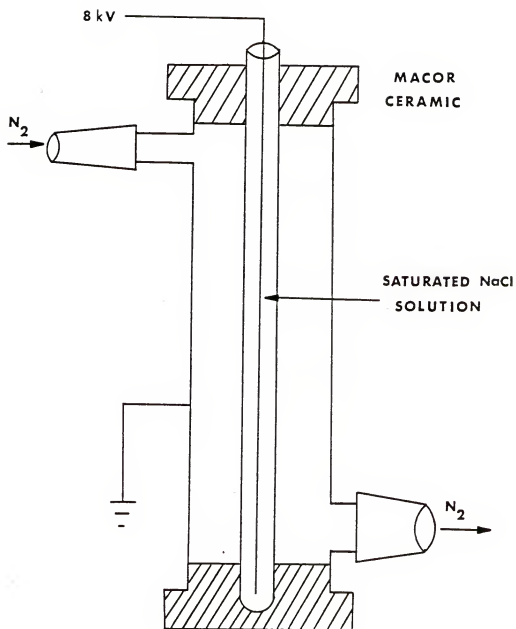


Figure 3-1 Dielectric discharge active nitrogen source (not drawn to scale).

Buena, NJ, 08310), 16.5 mm long. The glass tubes were held in place and electrically isolated by two ceramic spacers made from MACOR machinable ceramic. The ceramic spacers were epoxied to both the inner and outer tubes to form a vacuum tight seal. Nitrogen was introduced to the annular region between these tubes by a 2 in long section of 1/4 in tubing with a female 10/30 ground glass joint and exited via 3/8 in tubing that had a male 14/20 ground glass joint. The distance the nitrogen traveled through the discharge tube was approximately 18 mm.

To generate the metastable nitrogen plasma, a 20 gauge solid copper wire was inserted in the electrolytic solution which filled the inner NMR tube. A 7500 V, 60 Hz, alternating current discharge was applied via this copper wire and the coaxial glass tubes acted as electrodes surrounding the flowing nitrogen.

The construction of this dielectric discharge generator was completely glass that had been soaked overnight in phosphoric acid to eliminate metal excitation lines associated with metal electrode discharges (196) and metals absorbed on the surfaces of the glass tubing (189,213). The glass construction also minimized collisional deactivation of the metastable nitrogen due to metallic surfaces (189,213). The inner glass electrode was filled with NaCl solution and glass of uniform thickness was utilized to spread the discharge evenly throughout the length of the tube. It was also necessary to have the outer tube grounded as evenly as possible so that the high voltage did not preferentially discharge to one spot on the outer tubes. To achieve this, the outer glass tube was painted with  $\text{H}_3\text{AuO}_4$  (Rynne China, Co., Hazel Park, MI, 48030) and dried overnight at 600° C. This procedure coated the outside surface of the discharge tube with a thin layer of gold.

Then discharge tube was wrapped in aluminum foil and 1/4 in ground braid was placed along the axis of the tube. The tube was wrapped tightly with electrical tape. The braid was electrically connected to the laboratory ground by a 1 in ground braid. To further reduce the possibility of electrical shock and to shield the other equipment from the high voltage, the entire discharge generator and high voltage lines were surrounded with 1 in thick pipe insulation and 1/16 in thick copper foil. The copper foil was also grounded.

The high voltage power supply and associated circuitry are illustrated in Fig. 3-2. The high voltage power supply consisted of a 15 kV neon sign transformer. The transformer and one terminal of the high voltage secondary were grounded. The voltage applied to the discharge could be varied from 0 - 9 kV A.C. by varying the primary voltage from 0 - 140V A.C. via a variac.

The discharge voltage was sampled by a 1000:1 voltage divider so that a 1V reading corresponded to a discharge voltage of 1 kV. The current flow through the discharge was found by determining the potential across a 1 k $\Omega$  precision resistor that was in series with the ground return from the outer electrode to the transformer. From Ohm's law, a reading of 1V corresponded to a current flow of 1mA. All voltage and current measurements were made by a Fluke (John Fluke Mfg. Co., Inc., Seattle, WA, 98111) digital voltmeter.

#### Light Trap

The light trap served to isolate the discharge region from the reaction chamber as illustrated in Fig. 3-3. Active nitrogen flowed from the discharge generator through tube A and exited into the reaction chamber via tube C. The light trap was constructed from two glass tubes

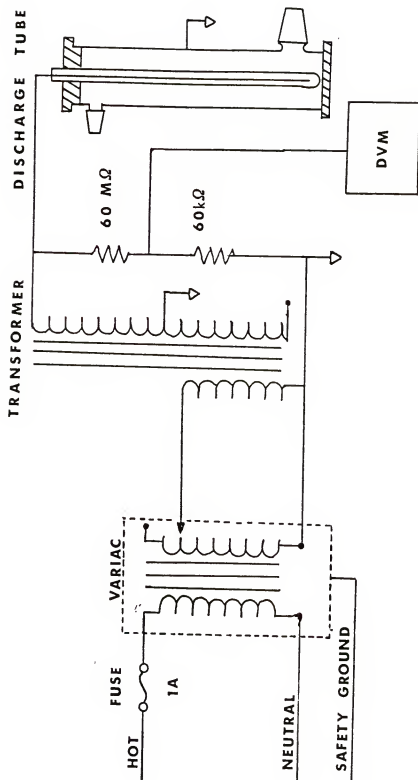


Figure 3-2 Circuit diagram of the power supply for the dielectric discharge.

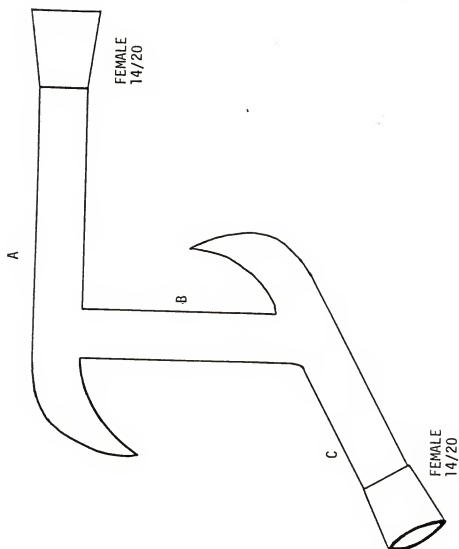


Figure 3-3 Light trap.

(A,C) 3 in long and 1/2 in in diameter that were sealed at one end in a Wood's horn configuration and had a female 14/20 standard taper ground glass joint at the opposite end. These two tubes were joined by a 2 in long section of 1/2 in tubing (B), that had been sealed to the longer tubes 1 in from the Wood's horns. Tubes A and B lay in the same plane and tube C was normal to the surface of this plane. The Wood's horns were painted flat black to reduce reflections.

The light trap was constructed with two Wood's horns at right angle bends to prevent light from the discharge from reflecting around the bends of the tubing and entering the reaction cell. During measurements, the light trap was wrapped in black felt to reduce further stray light. The trap was treated overnight with phosphoric acid and made of relatively large inside diameter tubing to reduce collisional deactivation of the nitrogen metastable on the walls.

#### Reaction Chamber

The metastable nitrogen was mixed with the analyte species in the reaction chamber illustrated in Figure 3-4. The reaction chamber was fabricated of 3/8 in outside diameter tubing 6 in long and had a quartz window epoxied at one end. The opposite end had a 14/20 male ground glass joint to which the light trap was attached. One inch from this joint and at right angles were two male ground glass joints used for sample introduction. When not in use, these joints were capped. Methods of sample introduction are discussed in Chapter 4. The reaction cell was connected to the vacuum system by a 1 in length of 3/8 in glass tubing sealed to the reaction tube 1/4 in from the quartz window. Polyethylene tubing, 3/8 in in diameter was used to connect the reaction chamber exit to the trap entrance and the trap exit to the vacuum

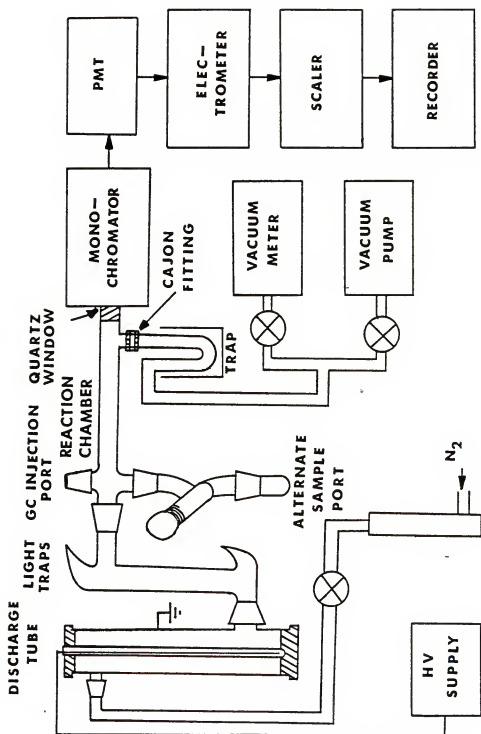


Figure 3-4 Block diagram of active nitrogen experimental apparatus with conventional sample introduction and single channel detection.

system, Ultratorr Cajon fittings were used for the glass to polyethylene connections.

This reaction chamber design was chosen over many other models because it resulted in the best signal to noise ratio. Other reaction cell designs tested included a cell made of square quartz tubing that was placed in front of the monochromator entrance slits so that the long axis was parallel to the slit height, and reaction cells similar to the one chosen but of varying lengths, 4-12 in and inside diameters 1/4, 3/8 and 1/2 in.

#### Vacuum System

The active nitrogen apparatus was kept at 1-2 torr by a Vactorr 150 vacuum pump (GCA Precision Scientific, Chicago, IL, 60647). The pressure in the cell was constantly monitored by a Baratron 321A pressure gauge (MKS Instruments, Inc., Burlington, MA, 01803). A 1V signal from the Baratron gauge corresponded to a 1 torr pressure in the reaction chamber. The vacuum system, consisting of vacuum pump and pressure gauge was made of 3/8 in polyethylene tubing connected by Swagelok fittings. Cajon fittings were used for glass to polyethylene connections.

#### Emission Detection

Spectroscopic data can be collected by two methods. In the single channel method, the intensity of each spectral element M, is determined one at a time as in the scanning monochromator PMT system discussed in the following section. In the multichannel method, several M spectral elements are determined simultaneously. This reduces the



the observation time by M for a measurement taken by a detector that is limited by random (shot) noise. For other sources of noise the observation time is reduced by a factor less than M (214).

#### Single Channel Detection

In the single channel detection system, the luminescence of the analyte in the reaction chamber was focused on the entrance slit of a 350 mm, f/6.8 scanning monochromator (GCA/McPherson Instrument, Co., EU/E - 700, Acton, MA, 01720). The monochromator was equipped with a scan drive (GCA/McPherson Instrument, Co., Model 700-5, Acton, MA, 01720) so that luminescence spectra (intensity versus wavelength) could be recorded.

The light intensity was detected by either a Hamamatsu 1P28A or R166 Photomultiplier tube (PMT) depending on the wavelength of interest. The R166 solar blind PMT has a Cs-Te window and was used in the wavelength region 160-320 nm. The 1P28A was used for wavelengths above 320 nm although it can be used down to 200 nm. The output signal from the PMT was current (or charge flow). The magnitude of the current (or rate of charge flow) is directly proportional to the rate at which photons struck the photocathode and independent of the observation time (215). The PMT was operated with 750V applied across the dynode string by a high voltage DC supply (Model 412A, John Fluke Mfg. Co., Inc., Seattle, WA, 98111).

The current output from the PMT was amplified and converted to a voltage by a home-built O'Haver electrometer (216). The signal was then sent to a scaler (also home-built) which amplified the voltage by a factor of 100 and inverted it. The spectra was recorded by a Sargent-Welch Recorder (Model SRG, Sargent Welch Scientific, Skokie, IL, 60076).

### Multichannel Detection

Types of multichannel detection fall into two general categories. First, there are multiplex spectrometric systems based on Hadamard and Fourier transforms. Hadamard and Fourier based systems have been applied successfully in the infrared (IR) region where light detection is detector noise limited. The multichannel approach is better for ultraviolet-visible (UV-VIS), X-ray, electron or any other type of spectroscopy where the noise is statistical and dependent on the signal (214).

Image devices are types of multichannel detection that are becoming more popular in atomic and molecular spectroscopy (214,217-218). They have been used in molecular absorption (219-222) and molecular fluorescence (223-224).

This research is the first to apply image detection to an active nitrogen chemiluminescence system. The emission of the analyte species was focused on the entrance slit of a grating monochromator (Bausch and Lomb Inc., Rochester, NY, 14601, Cat. No. 33-86-07) with 1200 grooves/mm. The image device used was a silicon intensified target (SIT) image vidicon (Model 1205, Princeton Applied Research, Princeton, NJ, 08540) that was equipped with an optical multichannel analyzer (OMA) (Model 1205A, Princeton Applied Research, Princeton, NJ, 08540). The signal was displayed on a Tektronix 60MHz Oscilloscope (Model 2213, Beaverton, OR, 97077) and was recorded on a Sargent-Welch strip chart recorder (Model SRG, Sargent Welch Scientific, Skokie, IL, 60076).

In contrast to a PMT, the SIT is an integrating detector, since its output signal is determined by the total accumulated charge. The SIT can integrate up to 10 scans on the target. Thus, the SIT output

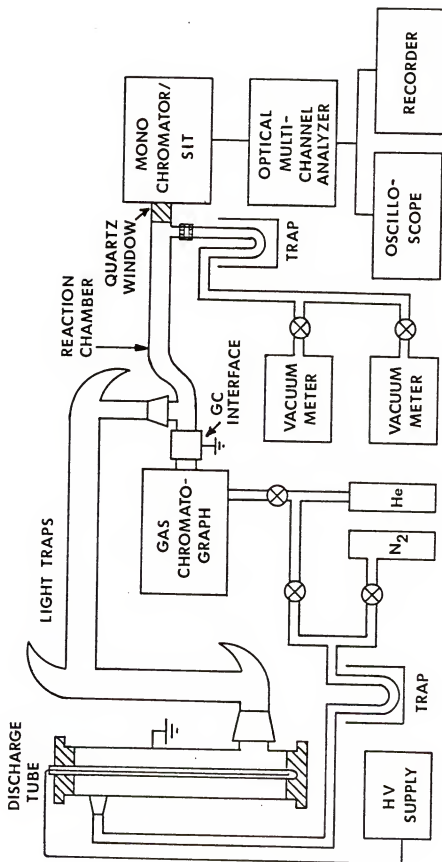


Figure 3-5 Black diagram of active nitrogen experimental apparatus with gas chromatographic sample introduction and multichannel detection.

signal is dependent upon the rate at which photons strike the detector and the observation time (215). Integration can also be achieved through the OMA. In this case, detection is semi-rate dependent.

With both the PMT and the SIT, spectra consist of plots of intensity versus wavelength. However, the wavelength axis of the PMT spectrum is also a time axis since as the spectrometer scans wavelength, the intensity of each spectral interval is detected one at a time sequentially. The wavelength axis of the SIT is not a time axis since the information in all M spectral elements is determined simultaneously (215).

The SIT is a type of electron beam imager consisting of a 16 mm diameter silicon target made up of a 1000 x 1000 array of islands of p-type silicon deposited on a n-type single crystal silicon wafer. A diode is formed by each of these islands. Each cathode is addressed by the scanning electron beam and all the anodes are connected to a common ground.

When the SIT is operated, the target is continuously scanned, sequentially reverse-biasing each diode. Since the diodes are reverse-biased, the majority carriers are drawn away from the junction, extending the depletion region. The movement of charge results in the diode capacitance.

When the light hits the photocathode, the photons produce photoelectrons that are focused by an electrostatic lens and accelerated at 6-9kV into the silicon target. These electrons penetrate into the depletion region where they produce approximately 1000-2000 electron hole pairs thus amplifying the signal. The electrons and holes move to opposite ends of the diode neutralizing the excess charge. When

the scanning electron beam hits the target, current flows in order to recharge the diode capacitance. The amount of charge that flows through an amplifier connected to the silicon substrate is proportional to the number of photoelectrons that hit the particular diode between readout times. The overall amplification is less than 1000-2000 because of the reduced efficiency of electron-hole pairs produced per photon reaching the photocathode. A net gain of  $\sim 200$  is average for visible light. The SIT has an accumulated linear dynamic range of at least  $10^4:1$  (225).

SIT's and photographic plates are similar since both are energy rather than power detectors. (The PMT is a power detector.) Both the SIT and photographic plate have storage capabilities. An SIT can store an image for up to 100ms at room temperature and up to several hours at dry ice temperature. Because the SIT responds to energy, it also can respond to very fast signals (e.g., single flash phenomena) provided the signal contains  $6.4 \times 10^{-18} \text{ J}$  (225). With a gated intensifier detector, the focus grid of the intensifier can be turned on and off like an electronic shutter. As in a camera, the shutter speed will determine the time resolution rather than the development time.

The SIT is an improvement over the photographic plate since the SIT responds linearly to light intensity rather than logarithmically. It is also more efficient. There is an 80% chance that a visible light photon will cause electron-hole production on the target (225). The probability for the light sensitive reaction in a photographic emulsion is much smaller. The SIT is faster and more convenient than film

because the scanning process develops the image and recharges the surface, readying it for a new exposure. The information read electronically is ready for immediate interpretation.

The signal from the SIT is processed by the OMA. The OMA records the data into one of two 500-word, 21-bit memories (memory "A" or "B"). Each channel has a dynamic range of 750 to 1 and can store up to 100,000 counts. The SIT/OMA system can be used as a real-time mode or an integration mode. In the integration mode, the signal can be accumulated for a specified time. This is determined by the number of presets (0-9999) which is the number of scans over which the signal will be integrated. The length of each scan is 32.8 ms. The integrated data can be stored in "A" or "B", and memory "B" can be subtracted from "A" and displayed via the "A-B" mode. By recording the analyte signal in "A" and the luminescence background from the blank in "B," background correction can be achieved by employing the "A-B" mode.

## CHAPTER IV METHODS OF ANALYSIS

### Diagnostic Methods

#### Discharge Emission

To obtain the discharge spectrum, it was necessary to extend the discharge region into the reaction cell where it could be detected by the PMT. This was accomplished by grounding the Cajon connector at the reaction cell - vacuum line junction indicated in Figure 3-4. Moving the ground to this junction effectively made the light trap and reaction cell all part of the discharge region. The spectrum was recorded using the single channel-PMT detection system. The PMT was operated at 750V, the monochromator had 20 $\mu$ m slits, and the amplification was  $10^7$  VA<sup>-1</sup>. The discharge was operated at 7kV, and the system pressure was 0.5 torr.

#### Afterglow Emission

All afterglow experiments were accomplished with the system in Figure 3-4, with one improvement. In order to obtain optimal alignment, a "box" was designed to hold the reaction chamber exactly perpendicular to the monochromator. This "box", machined out of bakelite, was designed so that its six faces could be placed together around the reaction chamber to be held in place by finger screws. The reaction cell and sample introduction systems extended through holes in the "box" and were held in place by rubber O-rings. The box was screwed on to the face of the monochromator, aligning the reaction cell with the entrance slits.

The nitrogen afterglow spectrum was detected by the single channel-PMT system. The PMT was operated at 750V, the monochromator had 50 $\mu$ m

slits, and the signal amplification was  $10^8 \text{ VA}^{-1}$ . The discharge was operated at 7kV, and the system pressure was 0.5 torr.

The experimental set-up was changed to determine how the nitrogen intensity at 337.1 nm,  $\text{N}_2(\text{C}^3\Pi_u, v=0 \rightarrow \text{B}^3\Pi_g, v=0)$ , changed with time (or distance from the discharge). The light trap was removed and a 200 cm length of polyethylene tubing was substituted. The intensity of the 337.1 line emission was determined and a 10 cm length of the polyethylene tubing was cut off. By alternately taking measurements (at 0.5 torr) and cutting off lengths of tubing, the desired plot was obtained.

#### Temperature Determination

The electronic temperature is an extremely important plasma diagnostical parameter. The temperature method employed was developed by Ornstein and coworkers (226,227). Assuming that the plasma in question is in thermal equilibrium, the intensities of any two lines in the emission spectrum of an element introduced into the system can be related by the following (228):

$$\frac{I}{I'} = \frac{A' \cdot g' \cdot \nu' \cdot \exp(-E'/kT)}{A \cdot g \cdot \nu \cdot \exp(-E/kT)} \quad (4-1)$$

where  $A, A'$  = transition probabilities for the lines ( $\text{s}^{-1}$ )

$g, g'$  = statistical weight of the states (no units)

$\nu, \nu'$  = frequencies of the lines ( $\text{s}^{-1}$ )

$E, E'$  = excitation energies (J)

$k$  = Boltzman constant ( $\text{JK}^{-1}$ )

$T$  = absolute temperature (K)

$I$  = intensity ( $\text{W sr}^{-1}$ )



Thus, the absolute temperature can be determined when the intensities, statistical weights and energy levels of two lines are known. These equations can be applied to atomic and molecular spectra. When the temperature is calculated from the relative populations of two electronically excited states of an atomic (or molecular) thermometric seed, the result is an "electronic temperature." When the temperature is determined from the relative intensities of two rotational lines within the same vibrational electronic band system of a molecular species introduced into the plasma, the result is a "rotational" temperature since it represents a ratio of the populations of the rotational levels. Similarly, a "vibrational" temperature is calculated for a molecular thermometric seed when the intensities of two vibrational bands within a single electronic transition are utilized.

In this experiment, iron was chosen for measurement of the electronic temperature of the nitrogen afterglow. When choosing the proper thermometric seed, it must be noted that the two-line method is not normally used with resonance lines due to the possibility of self-absorption. Iron was chosen because it has a series of non-resonance lines at wavelengths relatively free from the nitrogen background, and because the transition probabilities of the lines used are well-known.

Iron was introduced continuously into the plasma in the form of iron carbonyl ( $\text{Fe}(\text{CO})_5$ ) via the alternate sample port illustrated in Figure 3-4. The sample container is a small, 2 in test tube with a 14/20 female ground glass joint. The sample is introduced without any increase in pressure via a Corning Rotaflo (Corning Limited Laboratory Division, Stone Staffordshire, England). The Rotaflo has a PTFE valve stem that

fits into a tempered glass seat when the valve is shut. Unscrewing this valve lifts the stem allowing the sample to pass through into the reaction chamber. A "gland" seal along the upper circumference of the valve stem minimizes air leakage into the system.

The temperature of the afterglow was obtained at several different nitrogen flow rates and discharge voltages. Three line pairs were used for each experimental condition.

#### Nitrogen Atom Detection

The concentration of nitrogen atoms is a crucial parameter in a second positive nitrogen system because the major energy carrier  $N_2(A^3\Sigma_u^+)$  is effectively quenched by nitrogen atoms by the equation (2-18) repeated below:

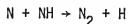


$$k_{18} = 3 \times 10^{13} \text{ cm}^3 \text{ mol}^{-1} \text{ s}^{-1}$$

Since nitrogen atoms are not consumed by this reaction, one nitrogen atom can quench numerous metastables.

In early studies (229-231), the nitrogen atom concentration was determined via reactions between active nitrogen and various small hydrocarbons (231-233). Herron (83,234) studied the reaction of nitrogen atoms with ethylene using a mass spectrometer to follow the partial pressures of reactants and products. The reactions were as follows:





A more popular method is the titration of nitrogen atoms with nitric oxide (233,235,236). This titration also has been used to study the kinetics of recombination of nitrogen atoms (234,238). The reactions involved in this titration are as follows (184,235):



$$k = 2.2 \times 10^{-11} \text{ cm}^3 \text{ molec}^{-1} \text{ s}^{-1}$$



$$k = 5 \times 10^{-33} \text{ cm}^6 \text{ molec}^{-2} \text{ s}^{-1}$$



$$k = 6 \times 10^{-32} \text{ cm}^6 \text{ molec}^{-2} \text{ s}^{-1}$$



$$k = 3 \times 10^{-17} \text{ cm}^3 \text{ molec}^{-1} \text{ s}^{-1}$$

Note that reaction (4-8) is much more rapid than reactions (4-9) through (4-11). Reaction (4-8) has been shown to be stoichiometric and mass spectrometric experiments with  $^{15}\text{NO}$  show the absence of any other species capable of decomposing nitric oxide (96,236). When NO is added downstream from the discharge, the Lewis-Rayleigh afterglow is weakened. There is a pronounced change in the emission spectrum of the afterglow and the afterglow color changes from orange yellow through pink and purplish blue. The pink and blue states are due to the production of  $\text{NO}^*$  and subsequent emission of the NO -  $\beta$  - and NO -  $\gamma$  - bands systems (Eq. 4-9) (239). Reactions (4-8) and (4-9) occur as long as there is

an excess of N over NO. When the afterglow turns blue, there is little N but much O produced (236). When more NO is added, the supply of N is exhausted. The  $\text{NO}^*$  bands disappear and the afterglow is extinguished. The addition of excess NO results in the production of the greenish-yellow  $\text{NO} + \text{O}$  continuum via reaction (4-11). The emission is fairly intense since there are high concentrations of atomic oxygen and nitric oxide (233,235,236).

To perform this experiment, a 30 in glass tube 1/2 in in diameter was fabricated with a male 14/20 ground glass joint at one end to attach to the light trap and a 2 in section of 3/8 in diameter tubing to connect to the vacuum system. The NO was delivered from a tank and metered into the afterglow via a 1/4 in diameter tube sealed 1 in from the ground glass joint. NO was introduced at increasing flow rates to a steady flow of 20mL/min of active nitrogen and the color noted.

#### Metastable Concentration

The nitrogen metastable ( $\text{A}^3\Sigma_u^+$ ) concentration was estimated by two methods. First, the 337.1 nm band of nitrogen was monitored by PMT detection with 25 $\mu\text{m}$  slits. Successive volumes of pure toluene were introduced from 0.05 $\mu\text{l}$  to 0.5 $\mu\text{l}$ . The number of metastables was assumed to be approximately twice the number of toluene molecules required to quench 50% of the emission (196).

Another method of estimating the nitrogen metastable population was based upon quenching of the plasma by analyte compounds eluting from the column. The density of molecules that quenched the plasma by 50% was assumed to be approximately equal to one-half the nitrogen metastable density (196). This was also the point where the slope of the sensitivity curves show negative deviation due to self-absorption/post-filter effects.

### Effect of Additive Gases

The effect of adding noble gases to an active nitrogen plasma has not been studied adequately. It is known that argon and helium enhance the first positive system of nitrogen, but no studies of their effect on a second positive nitrogen afterglow system have been reported.

The effects of adding argon and helium to the second positive system were studied by observing the intensities of nitrogen emission at 6 wavelengths for 6 mixtures and for pure nitrogen. The  $N_2$ :He mixtures used were 25:75, 50:50, and 75:25. The  $N_2$ :Ar mixtures used were 90:10, 50:50 and 25:75. The gases were allowed to mix before flowing through the dielectric discharge generator. All measurements were taken with 7 kV applied to the discharge and at a pressure of 1 torr.

Temperature measurements were taken of four argon-nitrogen mixtures using the experimental technique discussed previously under temperature determination.

In addition, the emission intensity of a helium-nitrogen afterglow at 337.1nm was observed at different dielectric discharge voltages (5.0-9.0 kV) and compared to the pure nitrogen afterglow.

### Detection Methods

#### Benzene, Iodine and Naphthalene

The gas-phase spectra of benzene, iodine and naphthalene were obtained.

Pure benzene was introduced continuously into the plasma by the same method described for the introduction of iron carbonyl. The benzene spectrum was obtained with 7 kV supplied to the discharge, 700V across the PMT, 100 $\mu$ m slits and an electrometer gain of  $10^8 \text{ VA}^{-1}$ .

Iodine was introduced by placing crystals in a platinum gauze "cage". This "cage" was attached to a glass rod that was sealed onto a 14/20 female ground glass joint stopper. The iodine spectrum was obtained with 100 $\mu$ m slits and a gain of  $10^9 \text{VA}^{-1}$ . The discharge generator was operated at 7kV and the PMT at 750V.

The naphthalene luminescence spectrum was obtained by continuously introducing naphthalene vapor through the alternate sample port shown in Fig. 3-3. Naphthalene crystals were placed in the sample tube and heated with heating tape. The spectrum was obtained with 80 $\mu$ m slights and a gain of  $10^9 \text{VA}^{-1}$ . The discharge generator was operated at 7kV and the PMT at 750V.

### Polynuclear Aromatic Hydrocarbons

#### Introduction

The detection of polynuclear aromatic hydrocarbons (PAH's) has become an extremely active area of research. This is primarily due to the carcinogenic (240,241) and mutagenic (242-244) properties of this class of compounds. The detrimental effects of PAH's on human health are a matter of international concern (245) especially since the increasing dependence on fossil fuel is releasing increasing amounts of PAH's into the environment (246). Extensive investigations have been carried out to elucidate the role of the numerous impurities and components in PAH mixtures (243). This investigation is necessary to assess the potential health hazards of PAH's and to develop preventive measures (245). PAH's have disseminated throughout the environment; they have been detected in coal-tar, pitch, crude oils, rubber tires, mineral shale, soot, etc. (245). More importantly, PAH's have been detected in substances to which the public has daily contact, such as tobacco smoke, car exhaust, and smoked foods (245).

Accurate and reliable methods for the detection of PAH's are needed. These methods must be both sensitive and selective. Several have been published and extensively reviewed by Hutzinger et al. (243), Sawicki (244), and Shaad (247). Methods include column chromatography (248), thin layer and paper chromatography (243), high performance liquid chromatography (249), ultraviolet spectroscopy (250) and gas-liquid chromatography (247). A few techniques that have been published recently are GC/MS of high molecular weight PAH's in coal tar (259), constant energy synchronous luminescence (252), two photon photoionization (253), and capillary GC of PAH's in vertebrate fish (254). Fluorescence techniques have been very successful in the detection of PAH's because fluorescence is very sensitive and because PAH's constitute an almost ideal class of fluorophors (255). PAH's have large molar absorptivities ( $>10^4 \text{ mL}^{-1} \text{ cm}^{-1}$ ) with maximum absorptions in the near ultraviolet or visible (246). They also have large quantum yields ( $\geq 0.2$ ) and long fluorescent lifetimes (tens to hundreds of nanoseconds (255)).

The research presented here explores the feasibility of using an active nitrogen afterglow as an excitation source for PAH compounds. As demonstrated by its success as an excitation source for metal detection, an active nitrogen afterglow combines gentle excitation with low spectral background.

#### Single channel detection

The PAH's and hydrocarbons and their sources used in this study are listed in Table 4-1. Solutions of the PAH's and hydrocarbons were prepared using scrupulously clean glassware. All glassware was soaked overnight in laboratory cleaning solution, rinsed 5 times with house

Table 4-1 Compounds and Their Sources

Gases	
Argon, Helium, Nitrogen, Hydrogen	Airco, Inc. Montvale, NJ, 07645
Nitric Oxide (99.0%)	Curtis Matheson, Inc. East Rutherford, NJ, 07073
Metals	
Fe(CO) <sub>5</sub>	Aldrich Chemical Co., Milwaukee, WI, 53233
Non-Metals	
Benzene, p-Xylene	Mallinckrodt, Inc., Paris, KY, 40361
Hexane	Burdick and Jackson Laboratories Inc., Muskegon, MI, 49442
Iodine	Fisher Scientific, Co., Fair Lawn, NJ, 07410
Napthalene, Toluene	Eastman Kodak, Rochester, NY, 14650
PAH's	
1,12-benzoperylene, 1,2-benzopyrene, 3,4-benzopyrene, perylene	Aldrich Chemical Co., Milwaukee, WI, 53233
Anthracene, chrysene, 1,2:5,6-dibenzanthracene, naphthacene, pyrene	Eastman Kodak, Rochester, NY, 14650
Coronene	Fluka AG, Buchs, Switzerland
20-methylcholanthrene	K+K Laboratories, Inc. Plainview, NY, 11803



de-ionized water, then 5 times with Barnstead de-ionized water. The glassware was then dried thoroughly overnight at 200° C.

Fifty to one hundred part-per-million (ppm) stock solutions of the PAH's in hexane were prepared and stored in amber bottles at 5° C to minimize photodecomposition. Solutions of lower concentrations were prepared by serial dilution of the stock solution and used immediately. Hydrocarbon solutions were prepared in a similar manner but at higher concentrations.

The hydrocarbon and PAH fluorescence was detected by a 1P28A photomultiplier tube using the experimental set-up diagrammed in Fig. 3-4. The active nitrogen generator was operated at 7.5kV and the PMT at 750V. The nitrogen flow rate was 10 mL/min and the slit width was 250 $\mu$ m. All fluorescence measurements were taken at the most intense peak wavelength that had minimal spectral interference. The injected sample volume was 0.5 $\mu$ L.

#### Multichannel detection

The multichannel detection experimental set-up is diagrammed in Fig. 3-5. The instrumentation used is discussed in Chapter III. Analyte solutions were prepared using the same method outlined in the previous section. Hydrocarbons were separated using an 3% OV-101, Chromosorb W column (Cat. No. SGP-353, Foxboro/Analabs, North Haven, CT, 06473). PAH's were separated on a 1.5% BMBT (liquid crystal) on Chromosorb W HP 100/120 mesh column (Cat. No. GCM-066, Foxboro/Analabs, North Haven, CT, 06473).

Unfortunately, the SIT did not have enough sensitivity in the real-time mode to detect compounds as they eluted from the column. A split-flow device was fabricated so that the sample flow could be divided.

The majority of the sample flow was introduced into the afterglow and the remainder to a flame ionization detector (FID). Hence, the FID was used as a peak detector. Fabrication of the split-flow device was complicated by the fact that an FID operates at 1 atm and the afterglow at 1 torr.

As stated an FID was used as a peak detector. A flame ionization detector (FID) is an extremely sensitive detector of organic compounds. It exhibits almost uniform responses, a wide linear dynamic range, and essential invulnerability to temperature fluctuation and most impurities in the carrier gas (256).

The FID is based on the principle that when organic compounds burn in a flame they ionize to some extent. In addition, when pure hydrogen is burned in air, very few ions are produced. When the carrier gas is eluted from the column through a nozzle, it is mixed with hydrogen and burned. A D.C. voltage is applied across two parallel electrodes placed above the nozzle. When an organic compound is eluted from the column, it is burned and ionized. The ion current produced is amplified by an electrometer and recorded to obtain a chromatogram (256).

The analyte fluorescence was detected with 0.9mm slits and accumulated for 200 cycles (6.55 s). The SIT spectral interval was 62 nm. The monochromator was centered at 380 nm for the PAH's and at 280 nm for the simpler hydrocarbons. All the limits of detection were calculated using 1 $\mu$ L samples. Five microliter samples were used for the mixtures.

A unique method was devised for aligning the reaction chamber with the monochromator and SIT. A small CM 1630 (Chicago Miniature) light bulb was placed in the reaction cell at the sample inlet. The light bulb was supplied by a General Electric, 10V transformer connected to a Variac. Using a very small voltage, a faint light was emitted from the light bulb. The light was used to simulate the sample chemiluminescence so that the system could be aligned precisely to obtain the maximum signal.

## CHAPTER V RESULTS AND DISCUSSION

### Dielectric Discharge

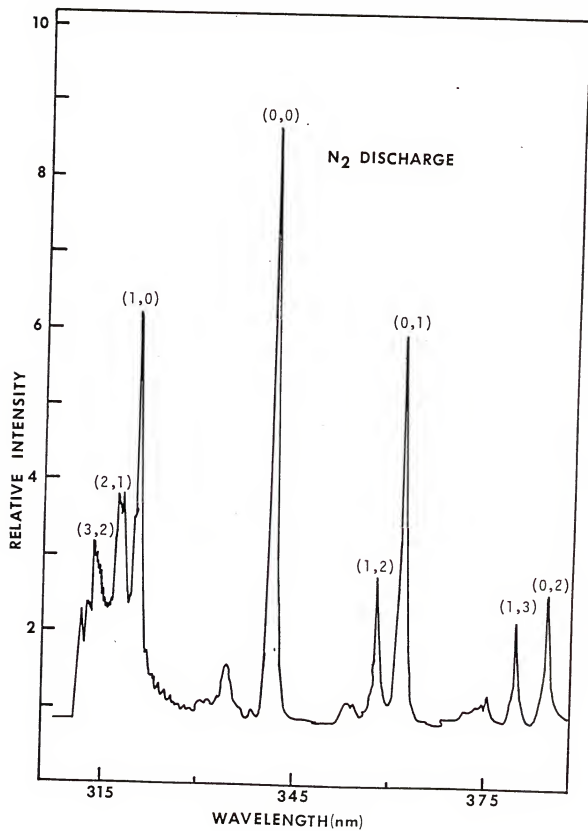
The instrument designs discussed in Chapter III and the experimental procedures outlined in Chapter IV were chosen after numerous alternatives were tried and discarded. Many avenues of experimental research directed towards understanding the discharge mechanism and optimizing the active nitrogen source still remain. This Chapter presents the results of afterglow diagnostic experiments and illustrates the applicability of an active nitrogen excitation source for PAH's and other inorganic and organic species. In addition, the feasibility of using active nitrogen-induced chemiluminescence as a gas-chromatographic detector is demonstrated. Finally, the uses of PMT and SIT detection systems are discussed and compared.

### Discharge Emission

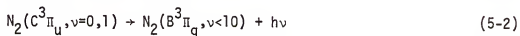
The nitrogen emission detected while looking directly at the discharge source is illustrated by Figure 5-1. The discharge emission is blue with a slight tinge of purple. The emission observed is a result of the second positive ( $2P$ ) emission. No emission was detected  $<250\text{nm}$  or from  $500\text{-}800\text{nm}$ . The prominence of this system, observed as a blue glow, is common to all afterglows at pressures greater than  $0.5$  torr.

The nitrogen  $C^3\Pi_u$  state is formed directly in the discharge region through electron impact excitation of the ground state nitrogen ( $202$ ).

Figure 5-1 Active nitrogen discharge emission spectrum indicating the second positive system of nitrogen. The electronic transition is  $N_2(C^3\Pi_u) \rightarrow N_2(A^3\Sigma_u^+)$ . Vibrational transitions are in parentheses.



The  $N_2(A)$  state is then populated by radiative cascade through the  $N_2(B)$  via the following mechanism:



Borst and Chang (257) have shown that the maximum cross-section for the (0,0) vibrational excitation of the  $N_2(C^3\Pi_u)$  state via electron impact peaks sharply at approximately 15eV. Thus, the average energy of electrons within the discharge is probably 11-15eV since 11eV is required to excite ground state nitrogen to the C level. If the electrons had a lower average energy, then emission from the  $N_2(B) \rightarrow N_2(A)$  would be observed since the cross-section of the B state peaks at approximately 10eV. No emission from the first positive system was observed.

#### Nitrogen Afterglow

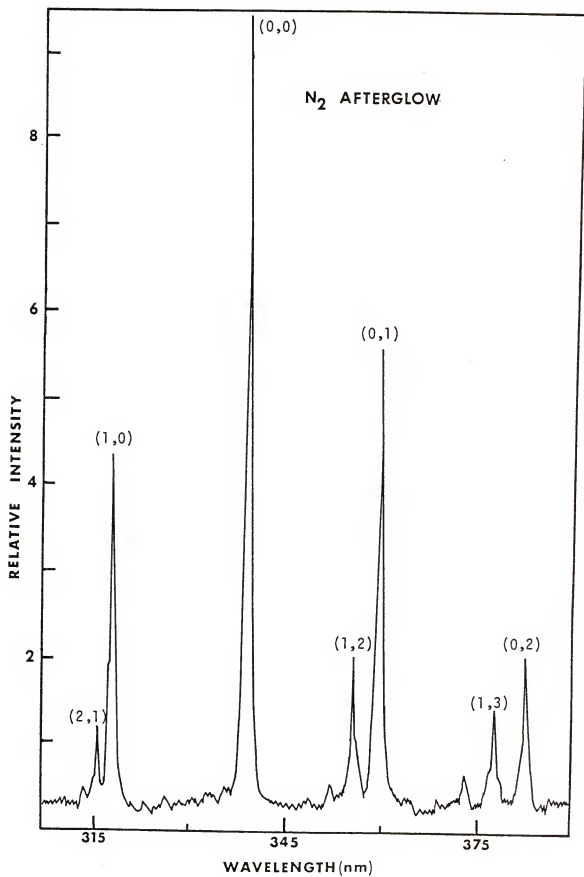
The nitrogen afterglow observed approximately 100ms after the discharge is shown in Figure 5-2. The nitrogen second positive system was again the only one detected when the spectrum was scanned from 200-800nm. The afterglow region was also blue in color, but it had a cloudy, opaque appearance.

The  $N_2(C)$  state has 50ns lifetime. Thus, for the  $N_2(C) \rightarrow N_2(B)$  transition to be seen in the afterglow 100ms past the discharge, the  $N_2(C)$  level must be populated by some reaction in the afterglow.

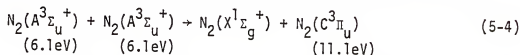
Two possible explanations for the production of the second positive system of nitrogen in the afterglow have been proposed. The first

Figure 5-2 Active nitrogen afterglow spectrum indicating the second positive system of nitrogen. The electronic transition is  $N_2(C^3\Pi_u) \rightarrow N_2(A^3\Sigma_u^+)$ . Vibrational transitions are in parentheses.



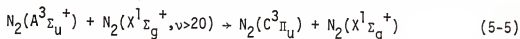


is the result of extensive experiments by Hays et al. (102,159,160) and Stedman and Setser (80). They believe that the  $N_2(C)$  state is populated by triplet-triplet disproportionation energy pooling:



This mechanism has the bulk of experimental evidence behind it. It is important to note that this pooling reaction also populates the  $N_2(C^3\Pi_u)$  and  $N_2(B^3\Pi_g)$  states; emission from the Goldstein-Kaplan system, i.e.,  $N_2(C^3\Pi_u) \rightarrow N_2(B^3\Pi_g)$  and the first positive system, i.e.,  $N_2(B^3\Pi_g) \rightarrow N_2(A^3\Sigma_u^+)$  are absent in the afterglow spectrum of Fig. 5-2. The absence of any first positive emission indicates that the B state is only being populated in the lower vibrational levels ( $v < 6$ ) since emission from these levels is not observed (111). This type of energy pooling will occur only where there are large populations of the metastable  $N_2(A)$  molecules.

A second possible explanation for the population of the  $N_2(C^3\Pi_u)$  has been suggested by Ung (172) who experimented with a similar discharge system. He proposed that the collision of a  $N_2(A)$  state molecule with a vibrationally excited ground state nitrogen ( $v > 20$ )



would be the most probable method of  $N_2(A^3\Sigma_u^+)$  production due to kinetic considerations.

The metastable  $N_2(C^3\Pi_u)$  molecules were probably produced in this system by collision of a  $N_2(A^3\Sigma_u^+)$  with a vibrationally excited ground state molecule ( $v > 20$ ) for two reasons: (1) metastable triplet-triplet disproportionation energy pooling populates the  $N_2(C^3\Pi_u)$ ,  $N_2(C^3\Pi_u)$

and  $N_2(B^3\Pi_g)$  states but no emission from the  $N_2(C^3\Pi_u) \rightarrow N_2(B^3\Pi_g)$  or  $N_2(B^3\Pi_g) \rightarrow N_2(A^3\Sigma_u^+)$  was detected. (2) The  $N_2(A^3\Sigma_u^+)$  state is generally accepted as responsible for excitation of levels requiring  $>4.5\text{eV}$  while excitation of lower energy levels is due to vibrationally excited ground state molecules (190). Also, the second positive afterglow gently excites molecules without fragmentation. Therefore, vibrationally excited ground state molecules may have been present in large enough concentrations to populate the  $N_2(C^3\Pi_u)$  state via Equation (5-5) and participate in excitation of the analyte species.

The dependence of the afterglow emission on the discharge voltage is shown in Fig. 5-3.

As can be seen, increasing the discharge voltage increases the intensity of the afterglow emission. This indicates that the average energy of electrons within the discharge is below  $15\text{eV}$  since excitation of the  $N_2(C^3\Pi_u)$  state by electron impact peaks sharply at  $\sim 15\text{eV}$ .

The intensity of emission at  $337.1\text{ nm}$  from the transition  $N_2(C^3\Pi_u) \rightarrow N_2(B^3\Pi_g)$  as a function of distance from the discharge is shown in Fig. 5-4. As expected, the emission intensity dropped off rapidly with increasing distance from the discharge.

The intensity of emission of the  $N_2$  afterglow at  $337.1\text{ nm}$  as a function of  $N_2$  flow ( $\text{mL/min}$ ) is presented in Fig. 5-5. It is shown that in the range of  $1\text{ mL/min}$  to  $20\text{ mL/min}$ , the nitrogen afterglow emission was independent of the flow rate.

The chemiluminescence of benzene vapor that was continuously introduced into the afterglow as a function of  $N_2$  flow ( $\text{mL/min}$ ) is also presented in Fig. 5-5. At flow rates  $\gtrsim 13\text{ mL/min}$  the chemiluminescence

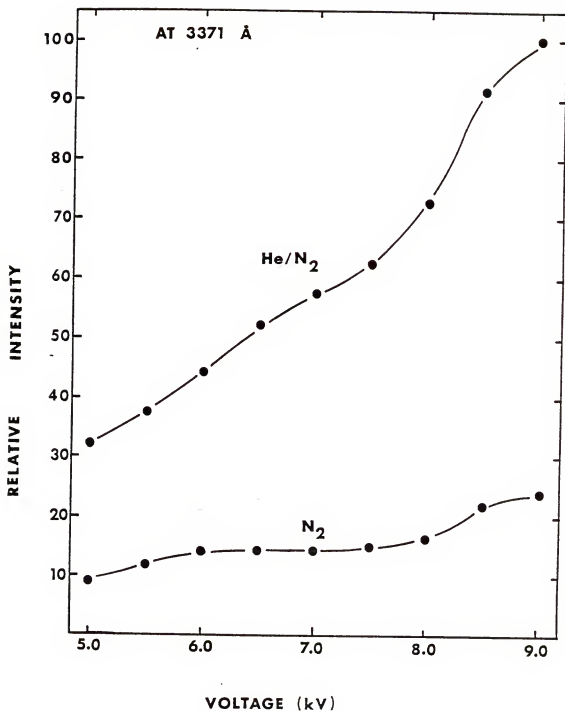
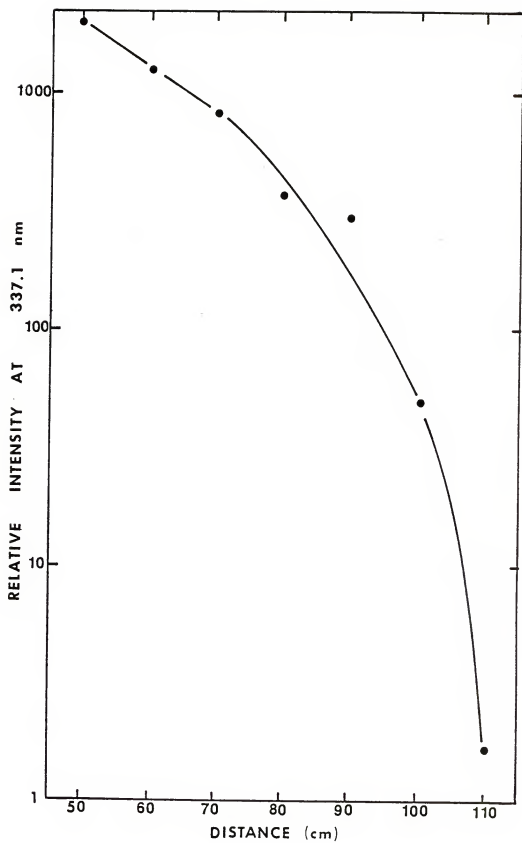


Figure 5-3 Nitrogen emission at 337.1nm in the afterglow for pure nitrogen and for a 50:50 mixture of helium and nitrogen as a function of discharge voltage.

Figure 5-4 Nitrogen emission at 337.1nm in the afterglow as a function of distance from the dielectric discharge active nitrogen generator.



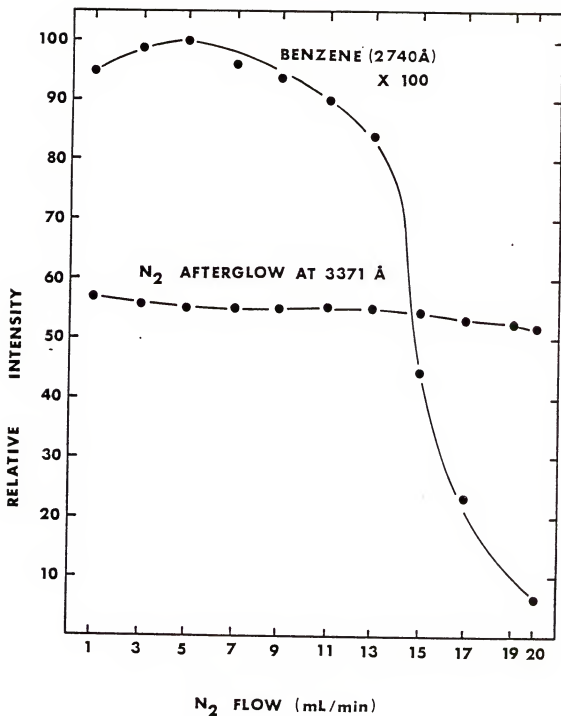


Figure 5-5 Nitrogen emission at 3371 Å in the afterglow as a function of nitrogen flow rate (mL/min). Benzene chemiluminescence at 2740 Å as a function of nitrogen flow rate (mL/min).

signal was still intense because the residence time of a benzene molecule in the reaction chamber was long enough to be excited and chemiluminesce many times. At faster flow rates, >13 mL/min, the residence time of the benzene molecule is not long enough for multiple cycles of excitation followed by chemiluminescence.

The dependence of the discharge and afterglow emission on pressure is presented in Fig. 5-6. It is shown that emission from both the discharge and afterglow was very strongly dependent on pressure. Therefore, it was essential to minimize air leaks in the apparatus to maximize the number of nitrogen metastables and minimize the limits of detection.

#### Temperature results

The discharge and afterglow temperatures were calculated for twelve sets of experimental conditions with varying nitrogen flow rates and applied dielectric discharge voltages. The discharge temperatures are listed in Table 5-1, and the afterglow temperatures are in Table 5-2. These temperatures were found via the two-line method with iron as the thermometric seed. Equation (4-1) was solved to obtain the temperature as a function of the energies, intensities, wavelengths and transition probabilities of the line pairs chosen:

$$T = \frac{0.625 (E' - E)}{\log \frac{I}{I'} + \log \frac{\lambda}{\lambda'} \frac{g'A'}{gA}} \quad (5-6)$$

The temperatures reported were calculated using this equation.

The temperatures of the discharge and afterglow were  $3280 \pm 132\text{K}$  and  $3090 \pm 70\text{K}$ , respectively. The temperatures varied only slightly with the generator voltage and appeared to be independent of the nitrogen flow rate.



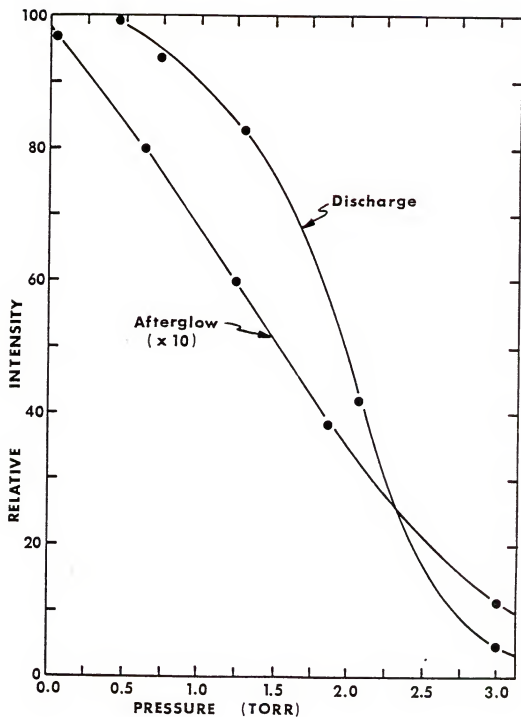


Figure 5-6 Nitrogen emission at 337.1nm in the discharge and afterglow as a function of pressure.

Table 5-1 Temperatures for the Active Nitrogen Discharge  
Calculated Using the Two-Line Method

High Voltage kV	N <sub>2</sub> Flow ml/min	Fe Line Pair			Average Temperature K	Standard Deviation K
		3734-3748 Å K	3820-3825 Å K	3825-3878 Å K		
6	2	3156	3189	3367	3238	114
6	5	3191	3266	3160	3206	55
6	10	3200	3473	3353	3342	137
6	15	3320	3383	3188	3297	100
7	2	3274	3473	3354	3367	100
7	5	3272	3645	3189	3369	243
7	10	3256	3523	3434	3404	136
7	15	3233	3487	3013	3243	237
8	2	3258	3266	3013	3179	144
8	5	3256	3266	3013	3178	144
8	10	3384	3383	3231	3333	88
8	15	3264	3266	3124	3218	81

Table 5-2 Temperatures for the Active Nitrogen Afterglow  
Calculated Using the Two-Line Method

High Voltage kV	N <sub>2</sub> Flow ml/min	Line Pair			Average Temperature K	Standard Deviation K
		3547-3679 K	3734-3748 K	3820-3824 K		
6	2	3049	3074	2911	3011	88
6	5	3049	3062	2919	3011	15
6	10	3095	3129	2931	3051	106
6	15	3202	3007	2996	3068	116
7	2	3056	3128	2986	3057	71
7	5	3109	3173	3093	3125	42
7	10	3188	3130	3063	3127	63
7	15	3167	3060	3073	3100	58
8	2	3077	3130	3077	3095	31
8	5	3197	3159	2986	3114	112
8	10	3243	3153	3077	3158	83
8	15	3182	3134	3083	3133	50

The population of the metastable nitrogen molecules is extremely important in terms of the sensitivity of this excitation source and its linear dynamic range. In a microwave system, the  $N_2(A)$  state is a result of recombination of nitrogen atoms. In addition, the nitrogen A state molecules are constantly being quenched to ground state by the large number of nitrogen atoms present (81,93,99). Thus, the  $N_2(A)$  population is limited by the competitive process of formation and quenching (196). The metastable population has been reported to be on the order of  $5 \times 10^9$  molecules  $cm^{-3}$  (99) and is extremely sensitive to changes in total pressure.

The nitrogen metastable concentration generated by a similar dielectric discharge source has been reported by Dodge (196) to be approximately  $1 \times 10^{17}$  molecules  $cm^{-3}$  at 7 torr.

The first method used to calculate the  $N_2(A)$  concentration for the system involved the injection of increasing amounts of toluene into the plasma. The volume of toluene that reduced the emission at 337.1nm by ~50% was 0.12 $\mu$ L. Since the emission at 337.1nm is due to the  $N_2(C^3\Pi_u) \rightarrow N_2(B^3\Pi_g)$  transition, and the  $N_2(C^3\Pi_u)$  state is populated in the afterglow by metastable energy pooling of the  $N_2(A^3\Sigma_u^+)$  state molecules, the decrease in emission was attributed to a decrease in the  $N_2(A)$  population. A 0.12 $\mu$ L sample of toluene is equivalent to  $1 \times 10^{16}$  molecules  $cm^{-3}$  in the 55  $cm^3$  reaction cell. This suggests that  $2 \times 10^{16}$  molecules  $cm^{-3}$  of metastable nitrogen are present. At 0.5 torr, the total nitrogen concentration is  $9 \times 10^{17}$  molecules  $cm^{-3}$ , approximately 2% of the nitrogen molecules are excited.

A comparable estimate of the nitrogen metastable concentration was obtained by the second method. It was noted that samples of

benzene and toluene 0.5 $\mu$ L slightly quenched the plasma when they eluted from the gas chromatographic column. One microliter samples of 10% benzene in hexane and 10% toluene in hexane did not quench the plasma. These samples correspond to  $6.7 \times 10^{17}$  molecules and  $5.7 \times 10^{17}$  molecules, respectively and were separated from the solvent by 30 s. It can be assumed that the nitrogen metastable concentration was at minimum equal to these analyte concentrations since the plasma was not visibly quenched. This results in a nitrogen A-state concentration of  $1 \times 10^{16}$  molecules  $\text{cm}^{-3}$  for both analytes.

The estimate of metastable concentration for this system is within an order of magnitude of Dodge's reported concentration and is 7 orders of magnitude higher than the metastable concentration produced by a microwave discharge.

#### NO titration

The NO titration performed produced slightly different results than those predicted by Kaufman and Kelso (236). Kaufman and Kelso's titration was of a Lewis-Rayleigh afterglow, while this titration was of a second-positive afterglow. The first color change was masked by the blue glow of the plasma. As the NO flow was increased to 0.9 mL/min, a faint green glow appeared near the walls of the glass tubing. The afterglow was never extinguished since the afterglow was dependent on the nitrogen ( $A^3\Sigma_u^+$ ) state population and not nitrogen atoms. Further addition of NO produced the NO + O continuum observed as an intense, cloudy, green-yellow glow.

The first hint of green glow was observed at 0.9 mL/min of NO. This corresponds to a flow of  $2 \times 10^{19}$  molecules  $\text{cm}^{-3}$  at atmospheric

pressure. Since the nitrogen flow was  $5 \times 10^{20}$  molecules  $\text{cm}^{-3}$  (20 mL/min), the percent of nitrogen atoms was  $<4\%$ . This result was higher than anticipated for this type of plasma although it was the same order of magnitude as Hays' result (102) of 1% nitrogen atoms in a flowing system.

As discussed in Chapter 2, the presence of both argon and helium is known to enhance the Lewis-Raleigh afterglow. In this study, the emission for the following bands was observed for argon/nitrogen, helium/nitrogen and nitrogen afterglows:

$\lambda$ (Å)	$v'$	$v$
3116.7	3,	2
3136.0	2,	1
3159.3	1,	0
3371.3	0,	0
3536.7	1,	2
3576.9	0,	1

The results of this experiment are presented in Figure 5-7. These six bands are major components of the second positive system. Recalling that this system is due to the  $\text{N}_2(\text{C}) \rightarrow \text{N}_2(\text{B})$  transition, and the  $\text{N}_2(\text{C})$  level is populated via metastable energy pooling of the  $\text{N}_2(\text{A})$  states, an increase in intensity of the  $\text{N}_2(\text{C}) \rightarrow \text{N}_2(\text{B})$  emission suggests an increase in the  $\text{N}_2(\text{A})$  metastable population. The plot shows that the addition of argon to the nitrogen plasma quenches a substantial population of A-state metastables. This is probably because argon exhibits an increase in collisional efficiency for the gas-phase deactivation of metastable nitrogen over nitrogen (184,185). This is illustrated by the following reactions and rate constants (186):

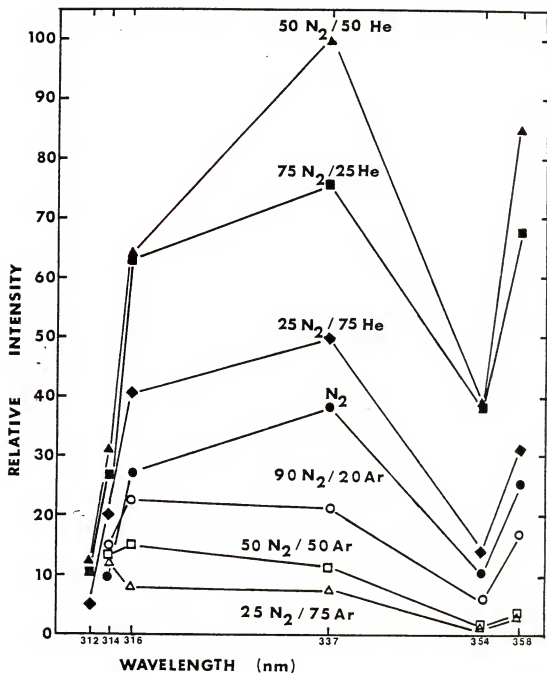


Figure 5-7 Emission from the  $N_2(C^3\Pi_u) \rightarrow N_2(A^3\Sigma_u^+)$  transition at 5 wavelengths for pure  $N_2$  and He/ $N_2$  and Ar/ $N_2$  mixtures.



$$k_{N_2} < 3 \times 10^6 \text{ cm}^3 \text{ mole}^{-1} \text{ s}^{-1}$$



$$k_{Ar} = 1.62 \times 10^8 \text{ cm}^3 \text{ mole}^{-1} \text{ s}^{-1}$$

The addition of helium has the opposite result. A 50:50 mixture of nitrogen:helium shows a 100% increase in 337.1 nm band intensity suggesting a similar increase in metastable population. The 50:50 and 75:25 nitrogen:helium mixtures also show a 100% increase at the other 5 wavelengths. This increase in metastable population could be due to the decrease in quenching ability of helium as compared to nitrogen, but no literature data were available to support this hypothesis.

Temperature measurements were conducted on argon-nitrogen mixtures. The results of these measurements are listed in Table 5-3. As argon is added, the average temperature drops slightly from 3241K to 3178K to 3138K. The drop in temperature coincides with the decrease in second positive emission with additional fractions of argon.

The afterglow intensity of a 50:50 He:N<sub>2</sub> mixture versus discharge voltage is shown in Fig. 5-3. The curve is plotted on the same graph as the pure nitrogen afterglow for easy comparison. As previously shown in Fig. 5-5, the addition of helium increases considerably the afterglow intensity. The helium-nitrogen curve exhibits a similar two-step profile as seen for pure nitrogen. This suggests that the mechanism for populating the N<sub>2</sub>(C) level is not changed by the addition of helium.



Table 5-3 Temperatures for the Active Nitrogen - Argon  
Afterglow Calculated Using the Two-Line Method

% N <sub>2</sub>	% Ar	Fe Line Pair			Average Temperature	Standard Deviation
		3647/3679 Å	3820/3824 Å	3825/3879 Å		
		K	K	K	K	K
25	75	3148	3125	3140	3138	10
50	50	3236	3152	3147	3178	40
75	25	3237	3235	3252	3241	8

### Molecular Species

The active nitrogen-induced gas-phase chemiluminescence spectrum of benzene is shown in Fig. 5-8. The set of benzene bands produced has also been detected in a study of a high-frequency discharge in benzene vapor (258) and via Tesla coil excitation (259). The 76 band heads are observed in five series designated as A, B, C, D and F (260). The vibrational structure of the benzene spectrum has been determined to agree with the selection rules for a forbidden electronic transition  ${}^1A_{1g} \rightarrow {}^1B_{2u}$ . This transition is possible only in the presence of a superposed non-totally symmetrical vibration of the type  $E_g^+$  which distorts the molecule (260,261).

Because a vibrational spectrum of benzene has been observed in the active nitrogen afterglow, the afterglow is shown to be a gentle excitation source. Thus, metastable nitrogen can be used as an excitation source for gas phase molecular fluorescence spectra.

The emission of iodine excited by the second positive afterglow is shown in Fig. 5-9. The fluorescence spectrum of iodine was observed in 1924 by Oldenburg (262). He saw a strong "continuum" with maximum about  $3425 \text{ \AA}$ , some weak bands around  $2700 \text{ \AA}$  and between  $4300\text{--}4900 \text{ \AA}$  and a "continuum" around  $5100 \text{ \AA}$ . This continuum, now designated as the  $\lambda 3416$  continuum, also appears in the absorption spectrum of iodine vapor at high temperatures (260) and in the fluorescence of iodine excited by ultraviolet radiation in the presence of a foreign gas (263). The  $\lambda 3416$  continuum is clearly present in Fig. 5-9 as indicated by the sloping baseline and starred peaks. This continuum is always associated with a band system that involves transitions between the

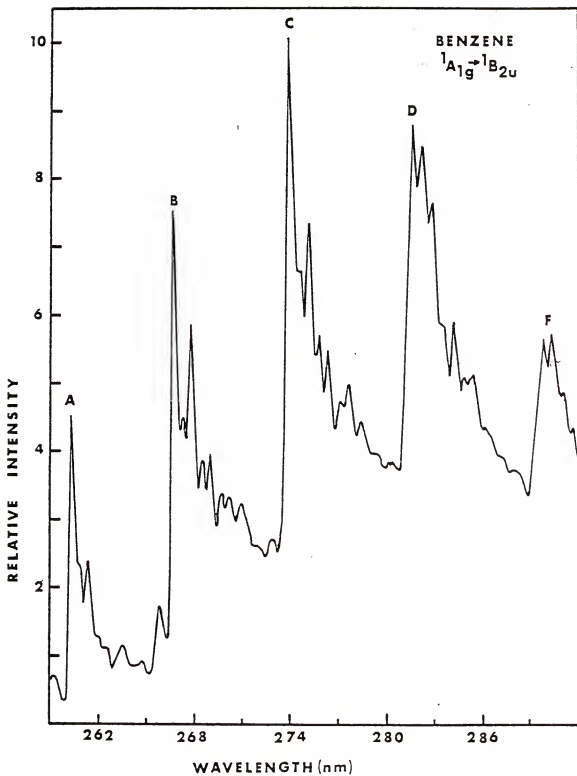


Figure 5-8 Chemiluminescence spectrum of benzene.

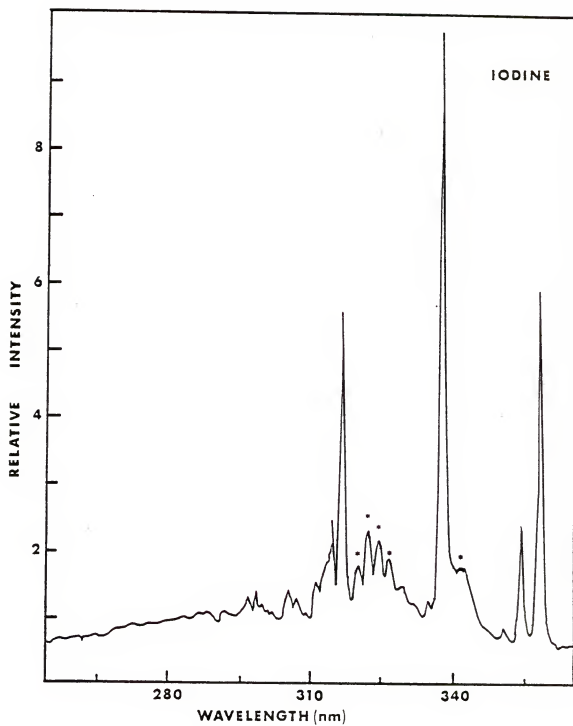


Figure 5-9 Chemiluminescence emission from iodine (starred) and the second positive system of nitrogen.

ground and the D state. It is due to transitions between the vibrational states  $65 \leq v'' \leq 74$  and  $7 \leq v' \leq 17$ . Thus the continuum is simply a region of strongly overlapping bands (264). This type of continuum is common to all halogen spectra (265).

The chemiluminescence spectrum of naphthalene is shown by the solid line in Fig. 5-10. The dotted line is the fluorescence spectrum of naphthalene (266). Comparison of the two spectra shows that the chemiluminescence spectrum is due to fluorescence of the naphthalene molecule and not CN band emission. This provides further proof that the second positive afterglow is a gentle excitation source.

#### Polynuclear Aromatic Hydrocarbons

The fluorescence emission wavelengths, limits of detection, standard deviations and log-log sensitivity curve slopes for all compounds are listed in Table 5-4. The analytical calibration curves are presented in Figures 5-11 to 5-25. The limits of detection for most PAH's are in the tens of nanograms and have a linear dynamic range over 3 orders of magnitude.

The limits of detection for the PAH's were primarily limited by the spectral background. Good limits of detection were obtained for benzene and toluene even though they are poor fluorophors. This is because of minimal afterglow emission at 380 nm. Unfortunately, the second positive system has numerous emission bands in the 350-450 nm region where most PAH's fluoresce. Thus, in many cases, detection of the most intense emission peak of a PAH was masked by the background and the background noise and a second, less intense peak had to be used.

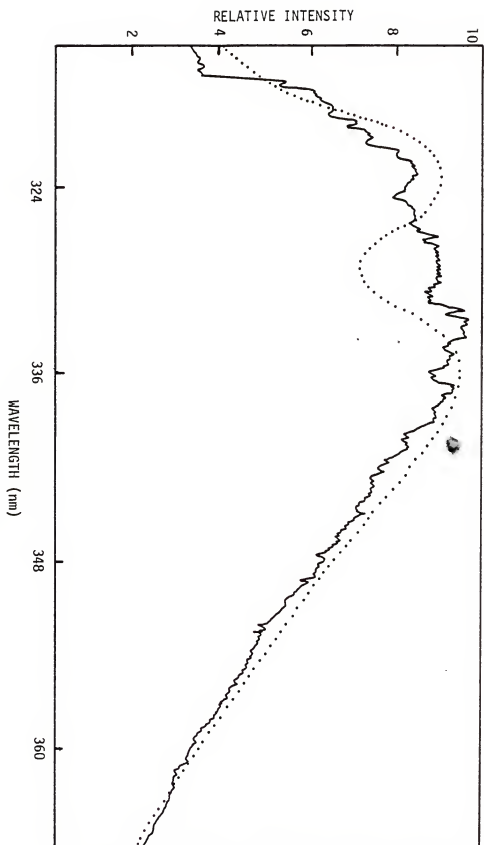


Figure 5-10 Chemiluminescence spectrum (solid line) and fluorescence spectrum (dotted line) of naphthalene.

Table 5-4 Limits of Detection<sup>†</sup> for Several PAH's and Hydrocarbons with PMT Detection

Compound	Wave-length (nm)	Limit of Detection			r <sup>†</sup>
		Amount	Molecules Measured	Molec·cm <sup>-3</sup> in Reaction Chamber	
Anthracene	445.5	0.01ng	$3 \times 10^{10}$	$6 \times 10^8$	0.9991
Benzene	274.2	1 g	$8 \times 10^{15}$	$1 \times 10^{14}$	0.98
3,4-Benzopyrene	402.4	0.05ng	$1 \times 10^{11}$	$2 \times 10^9$	0.995
1,2-Benzopyrene	386.8	0.02ng	$5 \times 10^{10}$	$9 \times 10^8$	0.997
1,12-Benzoperylene	471.5	0.04ng	$9 \times 10^{10}$	$2 \times 10^9$	0.9996
Chrysene	401.5	0.03ng	$8 \times 10^{10}$	$1 \times 10^9$	0.996
Coronene	453.1	0.1ng	$2 \times 10^{11}$	$3 \times 10^9$	0.998
1,2:5,6-Dibenzanthracene	391.7	0.003ng	$6 \times 10^9$	$1 \times 10^8$	0.992
20-Methylcholanthrene	414.7	0.04ng	$9 \times 10^{10}$	$2 \times 10^9$	0.9997
Naphthacene	504.4	0.02ng	$5 \times 10^{10}$	$1 \times 10^9$	0.9990
Naphthalene	330.0	2 g	$9 \times 10^{15}$	$1.7 \times 10^{14}$	0.963
Perylene	436.4	0.04ng	$1 \times 10^{11}$	$2 \times 10^9$	0.99995
Pyrene	373.1	0.04ng	$1 \times 10^{11}$	$2 \times 10^9$	0.998
Toluene	281.0	1 g	$6 \times 10^{15}$	$1 \times 10^{14}$	0.998

<sup>†</sup> The limit of detection equals 3 times the standard deviation of the blank divided by the sensitivity.  
r stands for correlation coefficient.

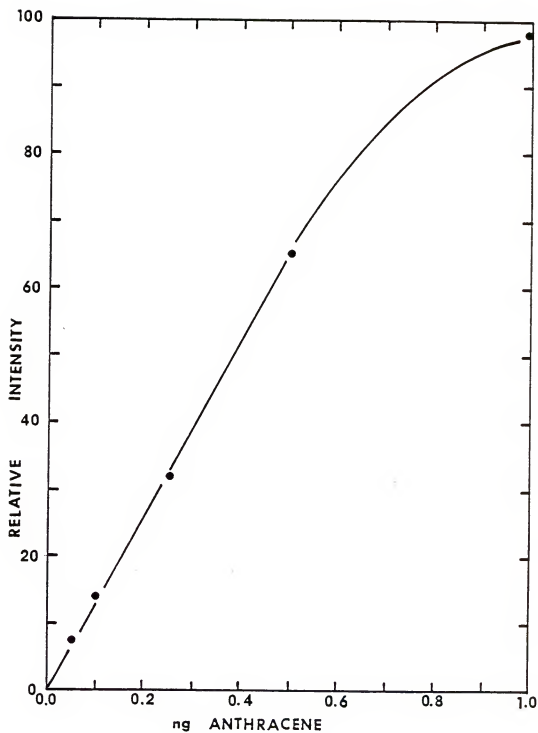


Figure 5-11 Analytical calibration curve of anthracene with single channel detection.



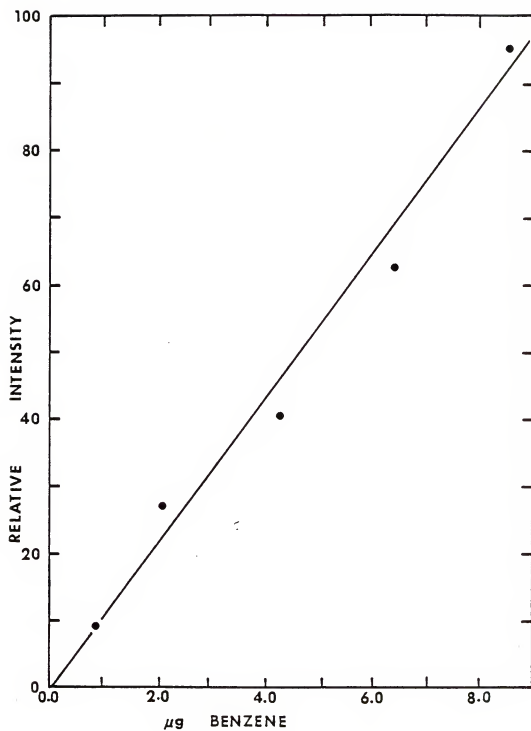


Figure 5-12 Analytical calibration curve of benzene with single channel detection.

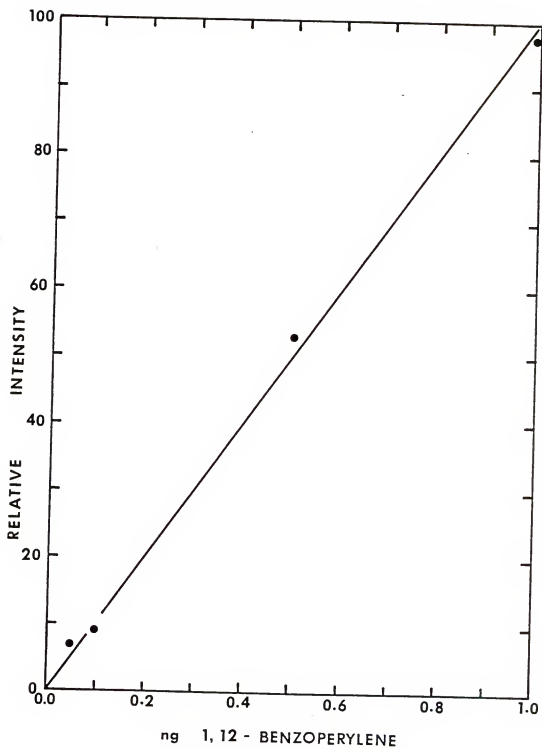


Figure 5-13 Analytical calibration curve of 1,12-benzoperylene with single channel detection.

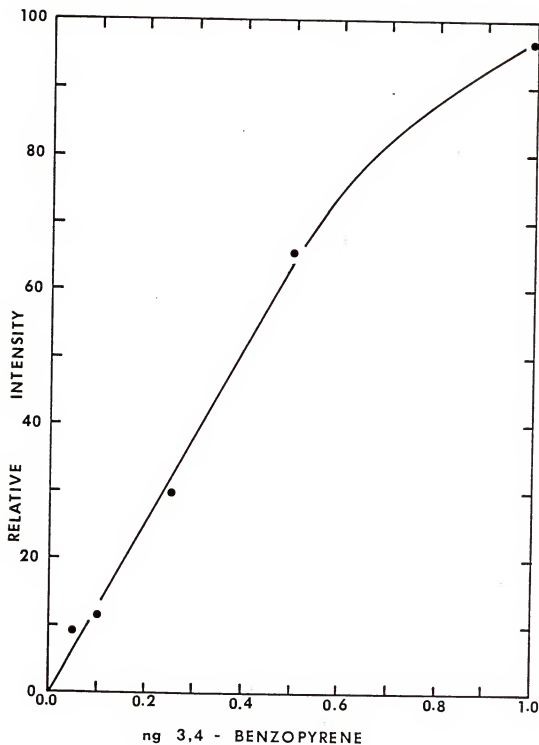


Figure 5-14 Analytical calibration curve of 3,4-benzopyrene with single channel detection.

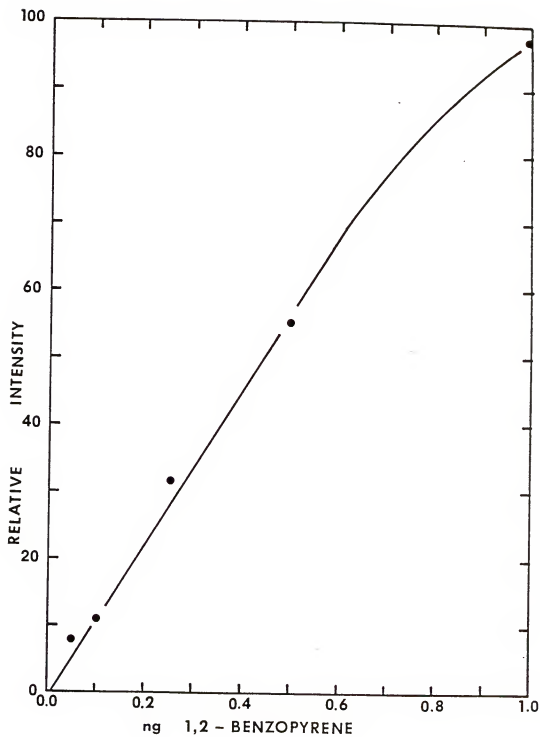


Figure 5-15 Analytical calibration curve of 1,2-benzopyrene with single channel detection.

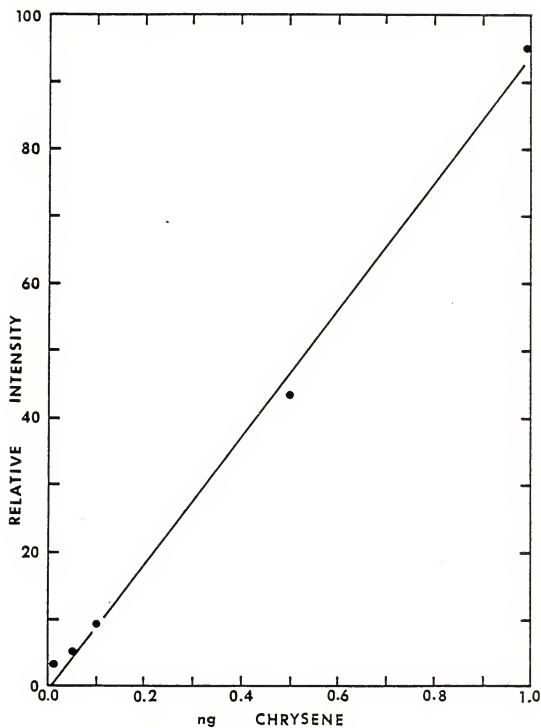


Figure 5-16 Analytical calibration curve of chrysene with single channel detection.

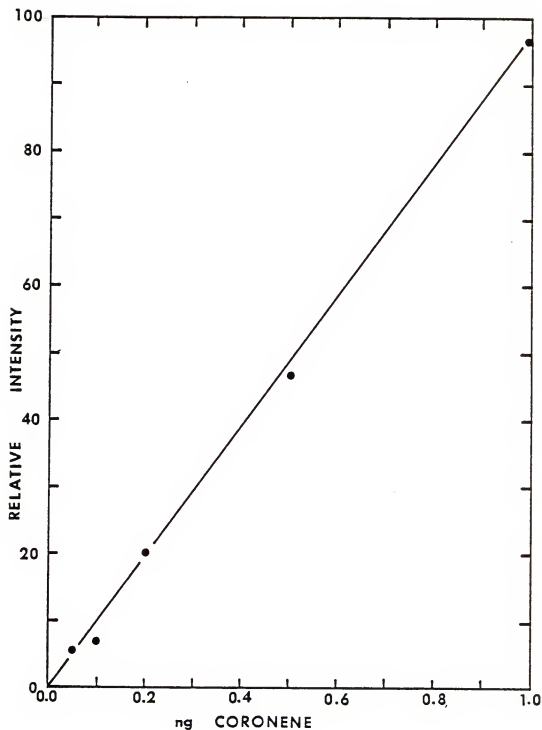


Figure 5-17 Analytical calibration curve of coronene with single channel detection.

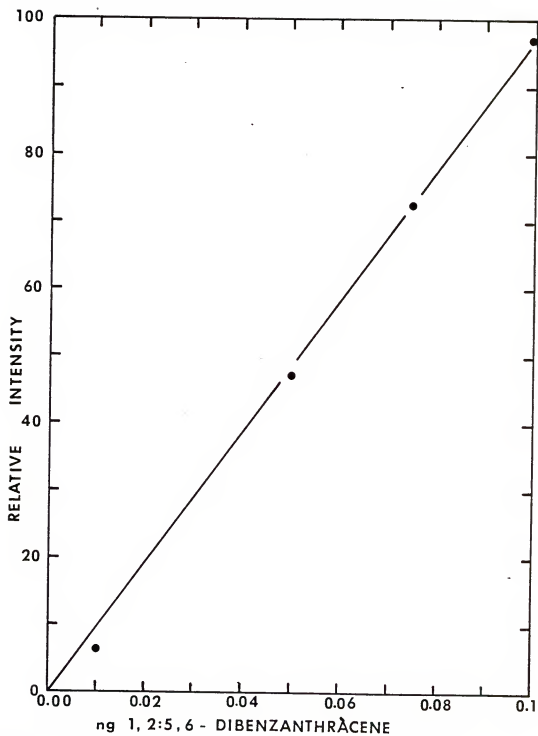


Figure 5-18 Analytical calibration curve of 1,2:5,6-dibenzanthracene with single channel detection.

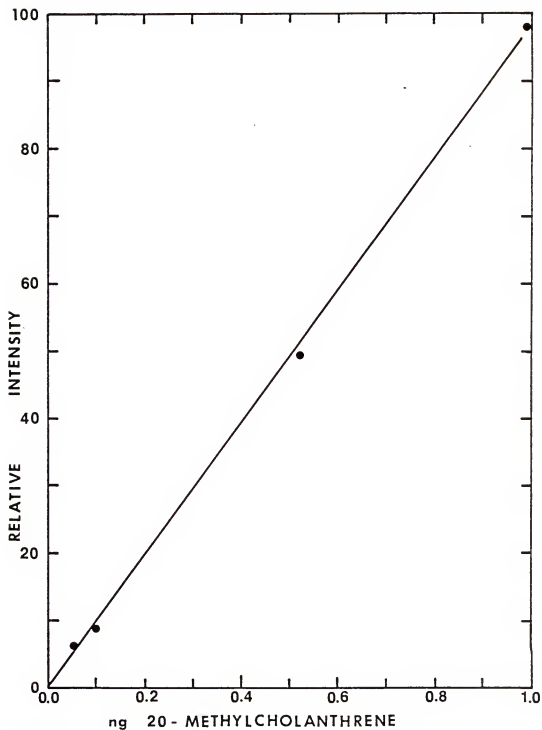


Figure 5-19 Analytical calibration curve of 20-methylcholanthrene with single channel detection.



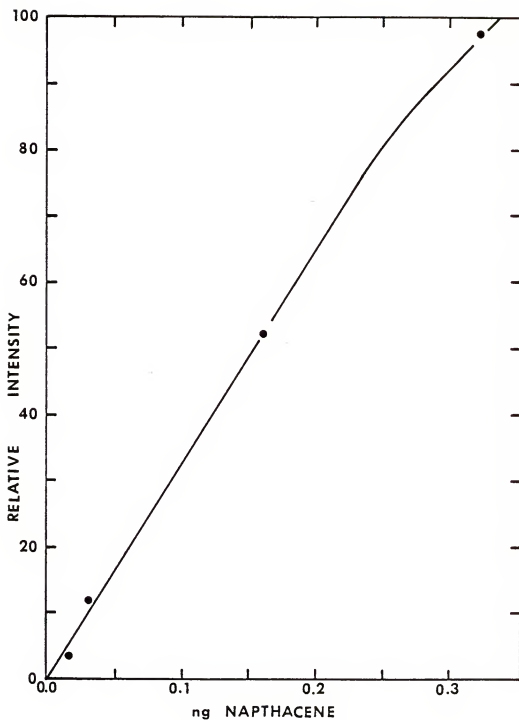


Figure 5-20 Analytical calibration curve of naphthalene with single channel detection.

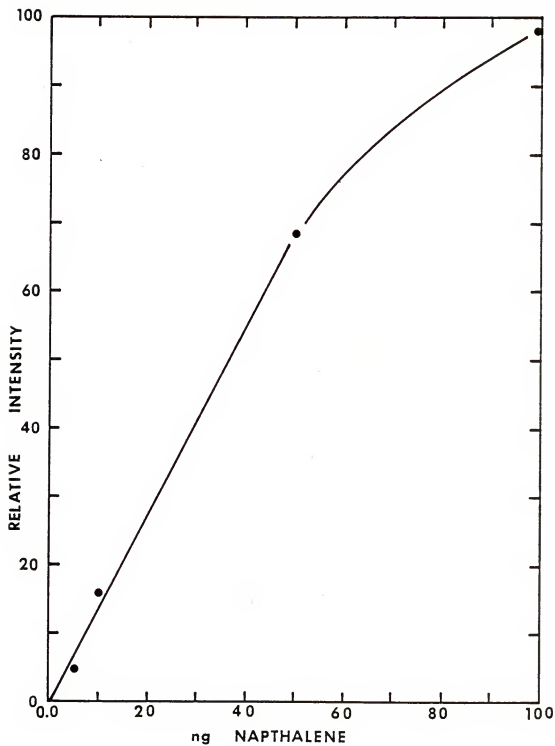


Figure 5-21 Analytical calibration curve of naphthalene with single channel detection.

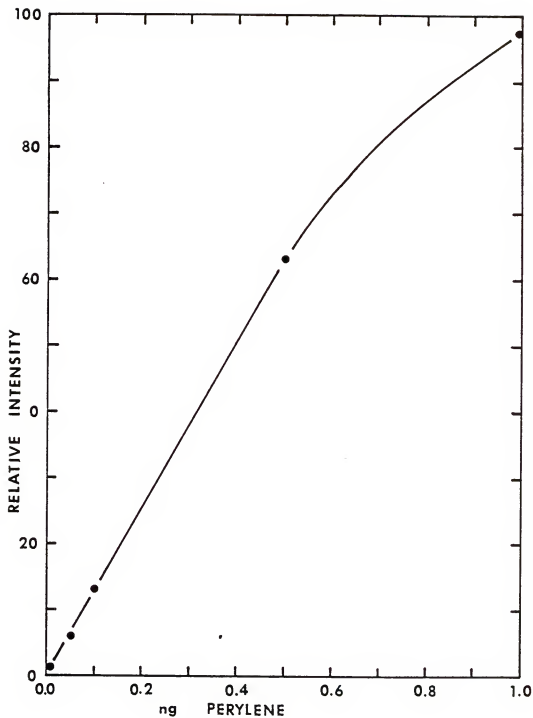


Figure 5-22 Analytical calibration curve of perylene with single channel detection.

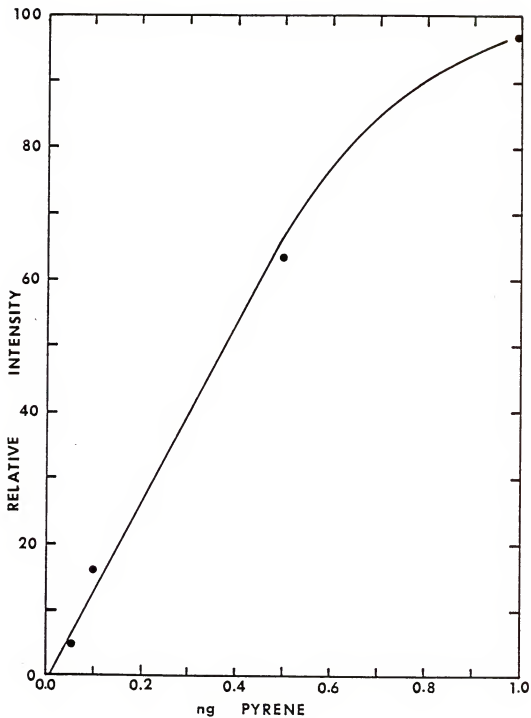


Figure 5-23 Analytical calibration curve of pyrene with single channel detection.

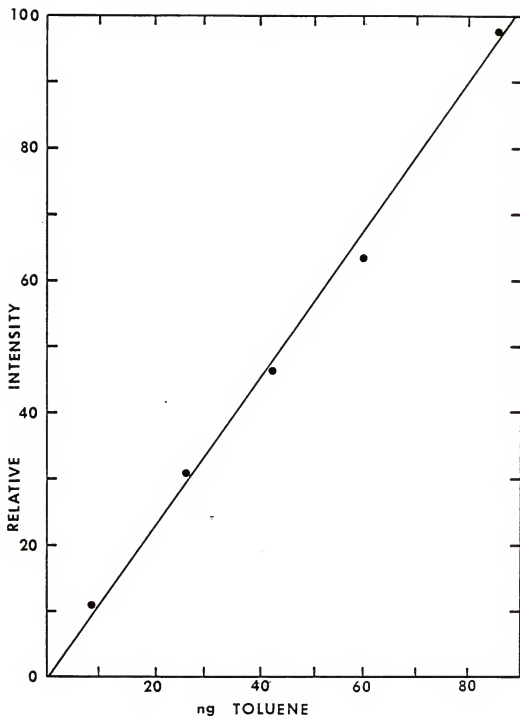


Figure 5-24 Analytical calibration curve of toluene with single channel detection.

The chemiluminescence spectrum of anthracene obtained with the SIT is shown in Fig. 5-26. The fluorescence spectrum of anthracene (266) is superimposed in dotted lines.

The limits of detection obtained utilizing an SIT detector are listed in Table 5-5. The results of the two synthetic mixture analysis are listed in Table 5-6. The linear dynamic range of the hydrocarbons was limited to two orders of magnitude because the addition of larger amounts of analyte to the afterglow began to quench the metastable  $N_2(A)$  population. The maximum concentration of PAH introduced into the afterglow was  $5 \times 10^{16}$  molecules  $cm^{-3}$ . Since the metastable population is  $1 \times 10^{16}$ , no quenching due to sample introduction was observed.

The limits of detection are between 100 and 500 times worse than those obtained for PMT detected samples. This is due to many factors: (1) The spectral interference is worse with the SIT than the PMT. Because the spectral window is 62nm, many nitrogen bands, in addition to analyte chemiluminescence are accumulated when integrating with the OMA. In contrast, when detecting with the PMT, the entrance slit width to the monochromator can be decreased to minimize detection of  $N_2$  band emission. (2) The method of sample introduction was different for the two methods. With the PMT system, the sample was directly introduced into the afterglow. For the SIT system, the sample was introduced as it eluted from a gas chromatographic column. In the SIT system, the PAH's eluted from the column over a minimum of 30 s. Hence, the signal was spread out over the nitrogen background, and the signal to noise ratio is reduced. This is especially evident for compounds such as 1,2-benzopyrene and 3,4-benzopyrene. These

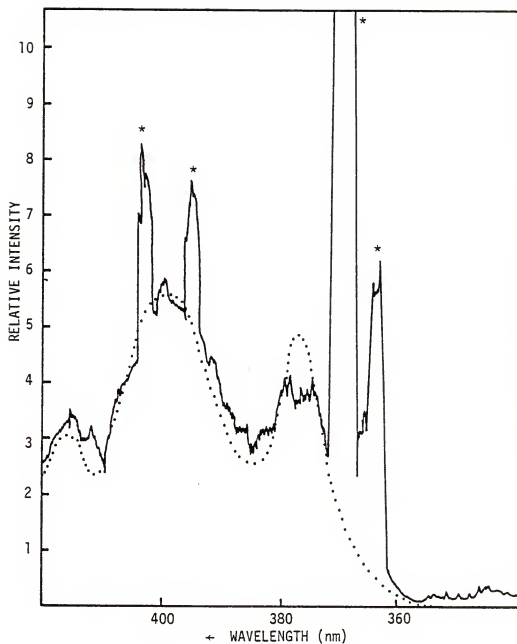


Figure 5-26 Chemiluminescence spectrum (dotted line) and fluorescence spectrum (solid line) of anthracene. The starred peaks are nitrogen bands from the  $N_2(C^3\Pi_u) \rightarrow N_2(A^3\Sigma_u^+)$  transition.

Table 5-5 Limits of Detection for Several PAH's and Hydrocarbons with PMT and SIT Detection.

Compound	SIT		PMT	
	$\lambda$ (nm) <sup>†</sup>	LOD	$\lambda$ (nm)	LOD
Benzene	280	1 $\mu$ g	274.2	1 $\mu$ g
Toluene	280	1 $\mu$ g	281.0	2 $\mu$ g
p-Xylene	280	1 $\mu$ g	-	-
Anthracene	380	5ng	445	0.01ng
Chrysene	380	3ng	401.5	0.03ng
Pyrene	380	20ng	373.1	0.04ng

<sup>†</sup>The SIT has a spectral window of 62 nm. The wavelength region was chosen to include the maximum fluorescence of all 3 compounds.



Table 5-6 Results of a Hydrocarbon and a PAH Mixture Separated on a Gas Chromatograph with SIT Detection

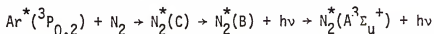
	Compound	True Amount ( $\mu\text{g}$ )	Calculated ( $\mu\text{g}$ )
Hydrocarbon Mixture	Benzene	70	72
	Toluene	69	66
	p-Xylene	69	68
PAH Mixture	Anthracene	0.24	0.20
	Chrysene	0.21	0.19
	Pyrene	0.39	0.34

samples eluted over 3-4 min and no fluorescence signal could be detected. (3) The residence time of the analyte species in the reaction chamber was reduced in the GC/SIT system, because the nitrogen flow rate into the reaction chamber was doubled to 20 mL/min. The nitrogen flow rate into the discharge was 10 mL/min and the nitrogen carrier gas flow introduced into the afterglow (after division by the split-flow device) was ~10 mL/min. (4) The SIT is inherently less sensitive than the PMT.

## CHAPTER VI CONCLUSIONS

The second positive nitrogen afterglow has been demonstrated to be a gentle molecular excitation source. Excellent limits of detection are presented for several small hydrocarbons that fluoresce around 280 nm. The ability of the active nitrogen system to detect these compounds as they elute from a gas chromatographic column has been investigated. The limits of detection for numerous polyaromatic hydrocarbons are presented. These LOD's were limited by spectral interferences in the 350-450 nm region and the sample introduction method. Detection by a photomultiplier tube was shown to be more sensitive; however, the silicon intensified target still offers more selectivity.

Several avenues can be explored to improve the limits of detection. The results of the NO titration revealed a small population of nitrogen atoms. Nitrogen atoms rapidly quench nitrogen A-state molecules which limits the sensitivity of the plasma. Active nitrogen can be produced free of nitrogen atoms by mixing nitrogen molecules with metastable argon. The reaction is as follows:



The possibility of using this active nitrogen source should be examined.

Another method of increasing the metastable population and possibly improving limits of detection is to mix helium with the nitrogen before passing through the active nitrogen discharge generator. This should increase the metastable population, but the effect on the spectral background needs to be studied.

## REFERENCES

1. E.N. Harvey, *A History of Luminescence* (American Philosophical Society, Philadelphia, PA, 1957).
2. J. Lee, in *Chemiluminescence and Bioluminescence*, J. Lee, D.M. Hercules and M.J. Cormeir, Eds. (Plenum Press, New York, NY, 1973).
3. G.G. Guilbault, *Practical Fluorescence; Theory, Method and Techniques* (Marcel Dekker, New York, NY, 1973).
4. W.R. Seitz and M.P. Neary, *Anal. Chem.* 46, 188A (1974).
5. M.M. Rauhut, *Kirk-Othmer Encycl. Chem. Technol.*, 3rd Ed., 5, 416, 1979.
6. M.G. Evans, H. Eyring and J.F. Kincaid, *J. Chem. Phys.* 6, 349 (1938).
7. A. Fontijn, in *Chemiluminescence and Bioluminescence*, J. Lee, D.M. Hercules and M.J. Cormeir, Eds. (Plenum Press, New York, NY, 1973).
8. H.O. Albrecht, *Z. Phys. Chem.* 136, 321 (1928).
9. K. Gleu and W. Petsch, *Angew Chem.* 48, 57 (1935).
10. J.R. Totler, *Photochem. Photobiol.* 3, 231 (1964).
11. U. Isacsson and G. Wettermark, *Anal. Chim. Acta* 68, 339 (1974).
12. *Gmelins Handbuch der Anorganischen Chemie. Si. Teil B*, 8. Aufl., 1959, p. 591.
13. H. Kantsky, *Kolloid-Z.*, 102, 2 (1943).
14. L.I. Dubovenko and E. Ya Khotinets, *Zh. Anal. Khim* 26, 784 (1971).
15. A.K. Babko, A.V. Terletskaia and L.I. Dubovenko, *J. Anal. Chem. USSR* 23, 809 (1968).
16. W.R. Seitz and D.M. Hercules, in *Chemiluminescence and Bioluminescence*, J. Lee, D.M. Hercules and M.J. Cormeir, Eds. (Plenum Press, New York, NY, 1973).
17. L.I. Dubovenko and E. Ya Khotinets, *Zh. Anal. Khim* 26, 784 (1971).

18. L.I. Dubovenko and Chan Ti Huu, Ukr. Khim Zh. 35, 637 (1969).
19. A.K. Babko and N.M. Lukovskaya, Zavod Lab. 29, 404 (1963).
20. W.R. Seitz, W.W. Suydam and D.M. Hercules, Anal. Chem. 44, 957 (1972).
21. A.K. Babko and N.M. Lukovskaya, J. Anal. Chem. USSR. 17, 47 (1962).
22. I.E. Kalnichenko and O.M. Grishchenko, Ukr. Khim. Zh. 36, 610 (1970).
23. W.R. Seitz and D.M. Hercules, Anal. Chem. 44, 2143 (1972).
24. L.I. Dubovenko and T.A. Bogoslovskaya, Ukr. Khim Zh. 37, 1057 (1971).
25. L.I. Dubovenko and A.P. Tovmasyan, J. Anal. Chem. USSR. 25, 812 (1970).
26. L.I. Dubovenko and A.P. Tovmasyan, Ukr. Khim. Zh. 37, 943 (1971).
27. I.E. Kalinichenko, Ukr. Khim Zh. 35, 755 (1969).
28. J. Bognar and L. Sipos, Mikrochim. Ichnoanal. Aeta. 5-6, 1066 (1963).
29. L.I. Dubovenko and L.D. Guz, Ukr. Khim. Zh. 36, 1264 (1970).
30. L.I. Dubovenko and Chan T. Huu, Ukr. Khim. Zh. 35, 957 (1969).
31. L.I. Dubovenko and A.P. Tovmasyan, Ukr. Khim. Zh. 37, 845 (1971).
32. A.K. Babko and N.M. Lukovskaya, J. Anal. Chem. USSR. 20, 1153 (1965).
33. A.K. Babko, L.I. Dubovenko and L.S. Mikhailova, Metody Anal. Khim. Reakt. Prep. No. 13, 139 (1969).
34. A.A. Ponomarenko and L.M. Amelina, J. Gen. Chem. USSR. 35, 750 (1965).
35. A.A. Ponomarenko and L.M. Amelina, J. Gen. Chem. USSR. 35, 2252 (1965).
36. H.A. Neufeld, C.J. Conklin and R.D. Towner, Anal. Biochem. 12, 303 (1965).
37. J. Goldenson, Anal. Chem. 26, 877 (1957).
38. K. Weber, J. Matkovic and M. Busljeta, Acta Pharm. Jugosl. 19, 47 (1969).
39. K. Weber and J. Matkovic, Arch. Toxikol. 21, 38 (1965).
40. A.A. Ponomarenko and B.I. Popov, J. Anal. Chem. USSR. 19, 1300 (1964).

41. N.M. Lukovskaya and M.I. Gerasimenko, J. Anal. Chem. USSR, 26, 1462 (1971).
42. S.S. Brody and J.E. Chaney, J. Gas Chromatogr. 4, 42 (1966).
43. R.K. Stevens, J.D. Mulik, A.E. O'Keefe and K.J. Krost, Anal. Chem. 43, 827 (1971).
44. A.D. Snyder and G.M. Wooten, *Final Report*, Environmental Protection Agency, Research Triangle Park, NC, Contract No. CPA-22-69-8, NTIS PB-188-103, 1969.
45. A.P. D'Silva, G.W. Rice and V.A. Fassel, Appl. Spectrosc. 34, 578 (1980).
46. R.K. Stevens and J.A. Hodgeson, New Instrument for Measurement of Gaseous Pollutants, presented at the *Int. Air Pollution Control and Noise Abatement Conf.*, Jönköping, Sweden, 1971.
47. J.A. Hodgeson, K.A. Rehme, B.E. Martin and R.K. Stevens, Measurements for Atmospheric Oxides of Nitrogen and Ammonia by Chemiluminescence, 1972 *Air Pollution Control Association Meeting*, Miami, Fla., 1972, Paper No. 72-12.
48. A. Fontijn, A.J. Sabadell and R.J. Ronco, Anal. Chem. 42, 575 (1970).
49. J.A. Hodgeson, J.P. Bell, K.A. Behem, K.J. Krost and R.K. Stevens, Application of a Chemiluminescence Detector for the Measurements of Total Oxides of Nitrogen and Ammonia in the Atmosphere, *Joint Conference on Sensing of Environmental Pollutants*, American Institute of Aeronautics and Astronautics, New York, NY, 1971, Paper No. 71-1067.
50. A.K. Babko, L.I. Pubovenko and L.S. Mikhailova, *Metody Anal. Khim. Reakt. Prep. No. 13*, 139 (1969).
51. K.J. Krost, J.A. Hodgeson and R.K. Stevens, *Publication Preprint*, Environmental Protection Agency, Research Triangle Park, NC, 1972.
52. M.G. Evans and M. Polanyi, Trans. Faraday Soc. 35, 178, 192, 195 (1939).
53. G.W. Nederbragt, A. Van der Horst and J. Van Duijn, Nature 206, 87 (1965).
54. R.K. Stevens and J.A. Hodgeson, Anal. Chem. 45, 443A (1973).
55. A.N. Wright and C.A. Winkler, *Active Nitrogen* (Academic Press, New York, NY, 1968).
56. Lavoisier, Memoirs, 2, 211 (1972), in *The Electrochemistry of Gases and Other Dielectrics*, G. Glocker and S.C. Lind, Eds. (Wiley, New York, NY, 1939).

57. M. Berthelot, Compt. Rend. 67, 1141 (1869).
58. M. Berthelot, Compt. Rend. 82, 1283 (1876).
59. M.A. Morren, Ann. Chem. Phys. 4, 293 (1865).
60. E. Warburg, Arch. Sci. Phys. Nat. (3)12, 504 (1884).
61. E.P. Lewis, Ann. Physik (4)2, 459 (1900).
62. E.P. Lewis, Astrophys. J. 12, 8 (1900).
63. E.P. Lewis, Phys. Rev. 18, 125 (1904).
64. R.J. Strutt, Proc. Roy. Soc. 85A, 219 (1911).
65. R.J. Strutt and A. Fowler, Proc. Roy. Soc. 86A, 105 (1912).
66. R.J. Strutt, Proc. Roy. Soc. 86A, 56 (1912).
67. R.J. Strutt, Proc. Roy. Soc. 88A, 539 (1913).
68. H. Spöner, Z. Physik. 34, 622 (1925).
69. M.F. Golde, Proc. Roy. Soc. 330A, 121 (1972).
70. S. Byron, J. Chem. Phys. 44, 1378 (1966).
71. S.K. Mitra, *Active Nitrogen - A New Theory* (Assoc. Cult. Sci., Calcutta, India, 1945).
72. A. Fontijn, in *Progress in Reaction Kinetics*, K.R. Jennings and R.B. Cundall, Eds. (Plenum Press, New York, NY, 1975).
73. E.C. Zipf, Can. J. Chem. 47, 1863 (1969).
74. P.G. Wilkinson and R.S. Mulliken, J. Chem. Phys. 31, 674 (1959).
75. B. Stevens, *Collisional Activation in Gases* (Pergamon Press, Oxford, 1966).
76. H.H. Bromer and F. Spieweck, Planetary Space Sci. 15, 689 (1967).
77. C. Moore, *Atomic Energy Levels*, Circular 467 (National Bureau of Standards, Washington, DC).
78. R.H. Garstung, *The Airglow and the Aurorae*, E.B. Armstrong and A. Dalgarno, Eds. (Pergamon Press, New York, NY, 1956), p. 324.
79. K.T. Compton and J.C. Boyce, Phys. Rev. 33, 145 (1929).
80. D.H. Stedman and D.W. Setser, J. Chem. Phys. 50, 2256 (1969).
81. D.E. Schemansky, J. Chem. Phys. 51, 689 (1969).
82. D.E. Schemansky, N.P. Carleton, J. Chem. Phys. 51, 682 (1969).

83. B. Brocklehurst and K.R. Jennings, *Prog. React. Kin.* 4, 1 (1967).
84. M. Jeunehomme, *J. Chem. Phys.* 45, 1805 (1966).
85. W. Brennen and E.C. Shane, *Chem. Phys. Lett.* 2, 143 (1968).
86. D.E. Shemansky, *J. Chem. Phys.* 51, 5487 (1969).
87. L.F. Phillips, *Can. J. Chem.* 41, 723 (1963).
88. J. Anketell and R.W. Nicholls, *Rep. Prog. Phys.* 33, 269 (1970).
89. M.F. Golde and B.A. Thrush, *Rep. Prog. Phys.* 36, 1285 (1973).
90. J. Berkowitz, W.A. Chupka and G.B. Kistiakowsky, *J. Chem. Phys.* 25, 457 (1956).
91. I.M. Campbell, B.A. Thrush, *Proc. Roy. Soc.* 296A, 201 (1964).
92. J.A. Meyer, D.W. Setser and W.G. Clark, *J. Phys. Chem.* 76, 1 (1972).
93. B.A. Thrush, A.H. Wild, *J. Chem. Soc. Faraday II* 68, 2023 (1972).
94. W. Brennen, *J. Chem. Phys.* 52, 4910 (1970).
95. N. Jonathan and R. Petty, *J. Chem. Phys.* 50, 3804 (1969).
96. R.A. Back and J.Y.P. Mui, *J. Phys. Chem.* 66, 1362 (1962).
97. R.A. Young, *J. Chem. Phys.* 60, 5050 (1974).
98. W. Brennen, *J. Phys. Chem.* 75, 1552 (1971).
99. R.R. Baker, *Can. J. Chem.* 49, 1671 (1971).
100. C.R. Stanley, *Proc. Phys. Soc. (London)* 67, 821 (1954).
101. E.C. Shane, *Chem. Phys. Lett.* 4, 31 (1969).
102. G.N. Hays and N.J. Oskam, *J. Chem. Phys.* 59, 1507 (1973).
103. E.J. Stone and E.C. Zipf, *J. Chem. Phys.* 58, 4278 (1973).
104. Y. Tanaka, F.R. Innes, A.S. Jursa and M. Nakamura, *J. Chem. Phys.* 42, 1183 (1965).
105. S.J. Lusasik and J.E. Young, *J. Chem. Phys.* 27, 1149 (1957).
106. R.E. March and H.I. Schiff, *Can. J. Chem.* 45, 189 (1967).
107. R.A. Young and R.L. Sharpless, *J. Chem. Phys.* 39, 1071 (1963).
108. R.G. Gann, F. Kaufman and M.A. Biondi, *Chem. Phys. Lett.* 16, 380 (1972).



109. J. Kaplan, Phys. Rev. 42, 807 (1932).
110. G.E. Beale and H.P. Broida, J. Chem. Phys. 31, 1030 (1959).
111. O. Oldenberg, J. Opt. Soc. Amer. 61, 1092 (1971).
112. Y. Tanaka and A.S. Jursa, J. Opt. Soc. Am. 51, 1239 (1961).
113. A.B. Drag and K.C. Clark, J. Chem. Phys. 39, 799 (1963).
114. R.A. Young, J. Chem. Phys. 36, 2854 (1962).
115. P.K. Carroll and H.E. Tubacilava, Proc. Phys. Soc. 76, 337 (1960).
116. G.B. Kistikowsky and P. Warneck, J. Chem. Phys. 27, 1417 (1957).
117. K.D. Bayes and G.B. Kistiakowsky, J. Chem. Phys. 29, 949 (1958).
118. G. Herzberg, Astrophys. J. 89, 288 (1939).
119. J.F. Noxon, J. Chem. Phys. 36, 926 (1962).
120. D.H. Stedman and D.W. Setser, Chem. Phys. Lett. 2, 542 (1968).
121. L. Vegard, Nature 125, 14 (1930).
122. J. Kaplan, Phys. Rev. 45, 675 (1934).
123. H. Hamada, Phil. Mag. (2)23, 25 (1937).
124. R.W.B. Pearse and A.G. Gaydon, *The Identification of Molecular Spectra* (Chapman and Hall, London, 1963).
125. P.G. Wilkinson, Astrophys. J. 126, 1 (1957).
126. P.G. Wilkinson and R.S. Mulliken, Astrophys. J. 126, 10 (1954).
127. R.S. Mulliken, in *The Threshold of Space*, M. Zelikoff, Ed. (Pergamon Press, Oxford, 1957), p. 169.
128. A. Lofthus, Can. J. Phys. 34, 780 (1956).
129. T. Lyman, Astrophys. J. 33, 98 (1911).
130. R.T. Birge and J.J. Hopfield, Astrophys. J. 68, 257 (1928).
131. Y. Tanaka, A. Jursa and F.J. LeBlanc, in *The Threshold of Space*, M. Zelikoff, Ed. (Pergamon Press, Oxford, 1957), p. 169.
132. Y. Tanaka, A. Jursa, F.J. LeBlanc and E.C.Y. Inn, Planetary Space Sci. 1, 7 (1959).

133. A. Lofthus, in *The Molecular Spectrum of Nitrogen*, Spectroscopic Rept. No. 2 (Dept. of Physics, University of Oslo, Blindern, Norway, 1960).
134. H.G. Heard, *Nature* 200, 667 (1963).
135. H.G. Heard, *Bull. Am. Phys. Soc.* 9, 65 (1964).
136. P. Lindau, *Z. Physik.* 25, 247; 26, 343; 30, 187 (1924).
137. R. Mecke and P. Lindau, *Z. Physik* 25, 277 (1924).
138. E. Huthén and G. Johansson, *Z. Physik* 26, 308 (1924).
139. J. Kaplan, *Phys. Rev.* 37, 1406 (1931).
140. G. Herzberg, *Ergeb. Exakt. Naturw.* 10, 207 (1931).
141. G. Büntenbender and G. Herzberg, *Ann. Physik* (5)21, 577 (1935).
142. D.R. Bates, *Proc. Roy. Soc.* 196A, 217 (1949).
143. C.T. Elvey, *Astrophys. J.* 111, 423 (1950).
144. M.K. Vainu Bappu, *Astrophys. J.* 111, 201 (1950).
145. L. Wallace, *J. Atmospheric Terrest. Phys.* 17, 46 (1959).
146. J.W. Chamberlain and A.B. Meinel, in *The Earth as a Planet*, G. Kuiper, Ed. (Univ. of Chicago Press, Chicago, IL, 1954), p. 514.
147. R.W. Nicholls, *Phys. Rev.* 77, 421 (1950).
148. L. Herman, G. Lucas, and R. Herman, *Spectrochim. Acta* 11, 325 (1957).
149. N. Ya. Dodonova, *Zh. Fiz. Khim.* 40, 969 (1966).
150. Y. Tanaka, *J. Opt. Soc. Am.* 45, 663 (1955).
151. B.K. Chin, G.R. Cook and R.A. Becker, *J. Quant. Spectrosc. Radiat. Transfer* 7, 323 (1967).
152. L. Herman, R. Lunt and E. Tuff, *Proc. 3rd Internat. Conf. Phys. Electron Qt. Collisions* (London, 1963), Abstract 4A5.
153. A.G. Engelhardt, A.V. Phelps and C.G. Risk, *Bull. Am. Phys. Soc.* 9, 187 (1964).
154. D.T. Stewart and E. Gabathuler, *Proc. Phys. Soc. (London)* 72, 287 (1958).

155. S.M. Kishko and M.I.U. Kuchinka, Opt. Spectry. (USSR) 6, 378 (1959).
156. G.J. Schulz, Phys. Rev. 116, 1141 (1959).
157. D.C. Tyte, Proc. Phys. Soc. (London) 80, 1347 (1962).
158. E.C. Zipf, Bull. Am. Phys. Soc. 13, 219 (1968).
159. G.N. Hays, C.J. Tracy, A.R. de Monchy and H.J. Oskam, Chem. Phys. Lett. 14, 352 (1972).
160. G.N. Hays and H.J. Oskam, J. Chem. Phys. 59, 6088 (1973).
161. H.U. Shemansky and A.L. Broadfoot, J. Quant. Spectrosc. Radiat. Transfer 11, 1385 (1971).
162. L.F. Phillips, Can. J. Chem. 43, 369 (1965).
163. M.F. Golde and B.A. Thrush, Proc. Roy. Soc. London 330A, 97 (1972).
164. M.F. Golde and B.A. Thrush, Proc. Roy. Soc. London 330A, 109 (1972).
165. A.B. Cellar and P.M. Wood, Trans. Faraday Soc. 67, 272 (1971).
166. J.A. Meyer, D.W. Setser and D.H. Stedman, J. Phys. Chem. 74, 2238 (1970).
167. R.A. Young and G.A. St. John, in *Chemical Reactions in Electrical Discharges*, Advances in Chemistry Series 80, R.F. Gould, Ed. (American Chemical Society, Washington, 1969).
168. D.E. Shemansky, J. Chem. Phys. 64, 565 (1976).
169. I.M. Campbell and B.A. Thrush, Proc. Chem. Soc. 410 (1964).
170. B. Brocklehurst, Trans. Faraday Soc. 60, 2151 (1964).
171. M. Dufay, M. Druetta and M. Eidelsberg, Compt. Rend. 260, 1901 (1965).
172. A.Y.M. Ung, Chem. Phys. Lett. 32, 193 (1975).
173. N.W. Finkelstein, J. Chim. Phys. 49, 196 (1952).
174. E. Goldstein, Z. Physik 6, 14 (1905).
175. J. Kaplan, Phys. Rev. 46, 534 (1934).
176. J. Kaplan, Phys. Rev. 47, 193 (1935).
177. H. Hamada, Nature 134, 851 (1934).
178. K.C. Clark and A.E. Belon, J. Atmospheric Terrest. Phys. 16, 205 (1959).

179. O. Oldenberg, Phys. Rev. 87, 786 (1952).
180. C.W. Ufford and R.M. Gilmor, Astrophys. J. 111, 580 (1950).
181. H.H. Landolt and R. Bornstein, *Zahlenwerte und Funktion - Atom und Molekularphysik*, Part 1 (Springer, Berlin, 1950).
182. L. Herman and R. Herman, Nature 191, 346 (1961).
183. R.L. Brown, J. Chem. Phys. 52, 4604 (1950).
184. J.E. Morgan, L.F. Phillips and H.I. Shiff, Discuss. Faraday Soc. 33, 118 (1962).
185. J.E. Morgan and H.I. Shiff, Can. J. Chem. 41, 903 (1963).
186. C. Kenty, J. Chem. Phys. 23, 1555 (1955).
187. C. Kenty, Phys. Rev. 93, 651 (1954).
188. C. Kenty, Report 20th Ann. M.I.T. Conf. Phys. Electron, p. 192 (1960).
189. W.R. Brennen and G.B. Kistiakowsky, J. Chem. Phys. 44, 2695 (1966).
190. H.C. Na and T.M. Niemczyk, Anal. Chem. 54, 1839 (1982).
191. S. Rosenwaks and H.P. Broida, J. Chem. Phys. 51, 2764 (1969).
192. R.J. Oldman and H.P. Broida, J. Chem. Phys. 51, 2764 (1969).
193. C. Kenty, J. Chem. Phys. 35, 2267 (1961).
194. G.A. Capelle, D.G. Sutton, Appl. Phys. Lett. 30, 407 (1977).
195. C.J. Duthler and H.P. Broida, J. Chem. Phys. 59, 1967 (1973).
196. W.B. Dodge and R.O. Allen, Anal. Chem. 53, 1279 (1981).
197. H. Hamada, Phil. Mag. 23, 25 (1937).
198. J.E. Bedinger, E.R. Manring and S.N. Ghosh, J. Geophys. Res. 63, 19 (1958).
199. J.E. Melzer, Anal. Chem. 52, 348 (1980).
200. L.F. Phillips, Can. J. Chem. 41, 2060 (1963).
201. G.A. Capelle and D.G. Sutton, Rev. Sci. Instrum. 49, 1124 (1978).
202. W.B. Dodge, Thesis, Univ. of Virginia, 1980.
203. H.C. Na and T.M. Niemczyk, Anal. Chem. 55, 1240 (1983).

204. T. Takeuchi, M. Yanagisawa and M. Suzuki, *Talanta* 19, 465 (1972).
205. W.G. Schrenk and R.T. Everson, *Appl. Spectrosc.* 29, 41 (1975).
206. T. Maruta and T. Takeuchi, *Anal. Chim. Acta* 62, 253 (1972).
207. D.G. Sutton, J.E. Melzer and G.A. Capelle, *Anal. Chem.* 50, 1247 (1978).
208. D.G. Sutton, K.R. Westburg and J.E. Melzer, *Anal. Chem.* 51, 1399 (1979).
209. G.W. Rice, A.P. D'Silva and V.A. Fassel, *Anal. Chem.* accepted for publication, 53 1519 (1981).
210. G.W. Rice, J.J. Richard, A.P. D'Silva and V.A. Fassel, *Anal. Chem.*, accepted for publication.
211. J.E. Melzer, *Appl. Spectrosc.* 34, 434 (1980).
212. D.R. Safranry, P. Harteck and R.R. Reeves, Jr., *J. Chem. Phys.* 41, 1161 (1964).
213. Lord Rayleigh, *Proc. Roy. Soc.* 151A, 567 (1935).
214. Y. Talmi, *Anal. Chem.* 47, 658A (1975).
215. R.P. Cooney, T. Vo-Dinh and J.D. Winefordner, *Anal. Chim. Acta* 89, 9 (1977).
216. T.C. O'Haver and J.D. Winefordner, *J. Chem. Ed.* 46, 214 (1969).
217. J.D. Winefordner, J.J. Fitzgerald and N. Omenetto, *Appl. Spectrosc.* 29, 269 (1975).
218. Y. Talmi, *Anal. Chem.* 47, 699A (1975).
219. G. Horluck and E.G. Coddington, *Anal. Chem.* 46, 133 (1974).
220. T.E. Cook, H.L. Pardue and R.E. Santino, *Anal. Chem.* 48, 451 (1976).
221. T.A. Nieman, F.J. Holler and C.G. Enke, *Anal. Chem.* 48, 899 (1976).
222. R.E. Deny, W.G. Nahna, G.A. Titus and W.R. Reynolds, *J. Chromatogr. Sci.* 14, 195 (1976).
223. T. Vo-Dinh, D.J. Johnson and J.D. Winefordner, *Spectrochim. Acta* 33A, 341 (1977).
224. R.P. Cooney, T. Vo-Dinh, J.D. Winefordner, *Anal. Chim. Acta* 89, 9 (1977).
225. *Operating and Service Manual, Optical Multichannel Analyser, Model 1205A* (Princeton Applied Research, Princeton, NJ).

226. L.S. Ornstein and H. Brinkmann, K. Acad. Amsterdam 34, 489 (1931).
227. L.S. Ornstein and H. Brinkman, Physica 1, 797 (1934).
228. G.F. Kirkbright, M.K. Peters and T.S. West, Talanta 15, 663 (1968).
229. P. Gartaganis and C.A. Winkler, Can. J. Chem. 34, 1457 (1936).
230. B. Dunford, H.G.V. Evans and C.A. Winkler, Can. J. Chem. 34, 1074 (1956).
231. H.G.V. Evans, G.R. Freeman and C.A. Winkler, Can. J. Chem. 34, 1271 (1956).
232. H.G.V. Evans and C.A. Winkler, Can. J. Chem. 34, 1217 (1956).
233. G.V. Verbecke and C.A. Winkler, J. Chem. Phys. 64, 319 (1960).
234. J.T. Herron, J. Phys. Chem. 69, 2736 (1965).
235. G.B. Kistiakowsky and G.G. Volpi, J. Chem. Phys. 27, 1141 (1957).
236. F. Kaufman and J.R. Kelson, J. Chem. Phys. 27, 1209 (1957).
237. J.T. Herron, J.L. Franklin, P. Bradt and V.H. Diebeler, J. Chem. Phys. 29, 230 (1958).
238. P. Harteck, R.R. Reeves and G. Manella, J. Chem. Phys. 29, 608 (1958).
239. Y. Tanaka, J. Chem. Phys. 22, 2045 (1954).
240. P. Shubik, Proc. Nat. Acad. Sci. USA 69, 1052 (1972).
241. H.W. Gerade, *Toxicology and Biochemistry of Aromatic Hydrocarbons* (Elsevier, Amsterdam, 1960).
242. E.C. Miller and J.A. Miller, *Chemical Mutagens*, A. Hollaender, Ed. (Plenum Press, New York, NY, 1971), Vol. 1, p. 105.
243. O. Hutzinger, S. Safe and M. Zander, Analabs Inc. Res. Notes 13 (1973).
244. E. Savicki, Chemist-Analyst 53, 24 (1964).
245. G.M. Janini, K. Johnston and W.L. Zielinski, Anal. Chem. 47, 670 (1975).
246. J.H. Richardson, in *Modern Fluorescence Spectroscopy*, E.L. Wehry, Ed. (Plenum Press, New York, NY, 1981).
247. R. Shaad, Chromatogr. Rev. 13, 61 (1970).
248. E. Sawicki, R.C. Corey, A.E. Dooley, J.B. Gisclard, J.L. Monkman, R.E. Neligan and L.A. Ripperton, Health Lab Sci. 1, 31 (1970).

249. N.F. Ives and L. Guiffrid, J. Assoc. Offic. Anal. Chem. 55, 757 (1972).
250. E. Clas, Spectrochim. Acta 4, 116 (1950).
251. T. Ronanowski, W. Funcke, I. Grossman, J. Konig and E. Balfanz, Anal. Chem. 55, 1030 (1983).
252. E.L. Inman, Jr. and J.D. Winefordner, Anal. Chem. 54, 1018 (1982).
253. E. Voigtman and J.D. Winefordner, Anal. Chem. 54, 1834 (1982).
254. D.L. Vassilaros, P.W. Stoker, G.M. Booth and M.L. Lee, Anal. Chem. 54, 106 (1982).
255. Birks, J.B., *Photophysics of Aromatic Molecules* (Wiley - Interscience, New York, NY, 1970).
256. *Flame Ionization Detector FID-6 for Gas Chromatograph GC-6A* (Shimadzu Seisakusho LTD., Kyoto, Japan).
257. R.K. Asundi and M.R. Padhye, Nature 156, 368 (1963).
258. J.B. Austin and I.A. Black, Phys. Rev. 35, 452 (1930).
259. H. Sponer, G. Nordheim, A.L. Sklar and E. Teller, J. Chem. Phys. 7, 207 (1939).
260. A.L. Sklar, J. Chem. Phys. 5, 669 (1937).
261. A.E. Elliot, Proc. Roy. Soc. 174A, 273 (1940).
262. O. Oldenburg, Z. Phys. 25, 136 (1924).
263. L. Mathieson and L.G. Rees, J. Chem. Phys. 25, 753 (1956).
264. R.S. Mulliken, Phys. Rev. 46, 144 (1934).
265. A.R. Jurgensen, Thesis, Univ. of Florida, 1981.
266. R. Loevinger, W.E. Bush, in *Vacuum Equipment and Techniques*, A. Guthrie and R.K. Wakerling, Eds. (McGraw-Hill, New York, NY, 1949), Chapters 1 and 2.
267. S. Dushman, in *Scientific Foundations of Vacuum Techniques*, J.M. Lafferty, Ed. (Wiley, New York, NY, 1962), pp. 80-110.

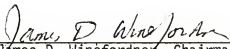
#### BIOGRAPHICAL SKETCH

Heather Andrews Jurgensen was born on May 2, 1958, in Long Beach, California. She attended Pascagoula High School, Pascagoula, Mississippi. Ms. Jurgensen obtained her B.S. in chemistry in 1978 and her M.S. in electrical engineering in 1980 from Louisiana State University, Baton Rouge, Louisiana. She was awarded her Ph.D. with a specialization in analytical chemistry in 1983 from the University of Florida.


Ms. Jurgensen is married to Arthur Robert Jurgensen. They have two children, Michael, age 4, and Melanie, age 1.



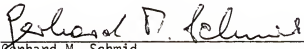
I certify that I have read this study and that in my opinion it conforms to acceptable standards of scholarly presentation and is fully adequate, in scope and quality, as a dissertation for the degree of Doctor of Philosophy.

  
James D. Winefordner, Chairman  
Professor of Chemistry


I certify that I have read this study and that in my opinion it conforms to acceptable standards of scholarly presentation and is fully adequate, in scope and quality, as a dissertation for the degree of Doctor of Philosophy.

  
John G. Dorsey  
Assistant Professor of Chemistry

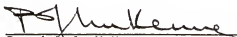
I certify that I have read this study and that in my opinion it conforms to acceptable standards of scholarly presentation and is fully adequate, in scope and quality, as a dissertation for the degree of Doctor of Philosophy.

  
Gerhard M. Schmid  
Associate Professor of Chemistry

I certify that I have read this study and that in my opinion it conforms to acceptable standards of scholarly presentation and is fully adequate, in scope and quality, as a dissertation for the degree of Doctor of Philosophy.

  
Richard A. Yost  
Assistant Professor of Chemistry

I certify that I have read this study and that in my opinion it conforms to acceptable standards of scholarly presentation and is fully adequate, in scope and quality, as a dissertation for the degree of Doctor of Philosophy.



Patrick J. McKenna  
Associate Professor of Mathematics

This dissertation was submitted to the Graduate Faculty of the Department of Chemistry in the College of Liberal Arts & Sciences and to the Graduate Council and was accepted as partial fulfillment of the requirements for the degree of Doctor of Philosophy.

December 1983

---

Dean for Graduate Studies and Research